The Real-Time Characterisation of Dry Machine Element Contacts Using Ultrasonic Reflectometry

Henry Peter Brunskill

Thesis submitted for the Degree of Doctor of Philosophy

Department of Mechanical Engineering

The University of Sheffield

December 2013

ACKNOWLEDGEMENTS

I would like to express my sincerest gratitude to my supervisor Roger Lewis. His support and friendship has facilitated the work presented here and numerous other projects. It has been a real pleasure and I aim to continue to have a thriving working relationship with him in the future. I would also like to thank Rob Dwyer-Joyce for his guidance. He introduced me to the field of Tribology at the early stages of my engineering studies and this has been one of the greatest gifts I have ever received. I feel I have found my true calling and his vast knowledge and enthusiasm for the subject has made me the passionate tribologist that I am today.

Thanks to Robin Mills and Dave Butcher for their seemingly endless amount of knowledge, patience and willingness to go out of their way to help me and teach me some of the most valuable skills I have learned throughout my studies. Í would like to acknowledge the help and support I have received from all of the members of The Leonardo Centre for Tribology, especially Tom Slatter and Matt Marshall. It has been a pleasure being part of such a wonderful research group and I am thankful for some of the friendships I have made.

I must mention Phil Harper as I have benefitted so much from his help, guidance and friendship. Thanks to Andy Hunter and the rest of the team at Tribosonics Ltd. It has been a real pleasure working with them and I have learned so much pondering over scribbles on the whiteboard. Thanks to Upul Fernando at GE Wellstream International Ltd. and Matthias Stark for their help with the industrial applications.

A special thanks to all of my family and friends for putting up with me. Thanks to Marie-anne for getting me through my undergraduate studies and setting me straight and thanks to Hannah for making my PhD so immensely enjoyable. Thanks to Team Eric, 33 and to my Crowborough compadres for their friendship, help and support.

To my mother and my brother, I love you so much that words cannot begin to describe. Finally I dedicate this work to my father Peter John Brunskill. I know you have been with me every step of the way and to you I owe my eternal gratitude.

TABLE OF CONTENTS

NOMENCLATURE

a	Area, m^2
c	Acoustic velocity, m/s
D	Diameter, m
d	Distance, m
E	Elastic (Young's) modulus, Pa
E_0	Reduced elastic modulus, dimensionless
F	Nominal, measured friction during sliding, N,
FL	Full length from the back wall echo, metres, m or time, t
F_s	Focal spot size (diameter), m
f	Frequency of ultrasound, Hz
f_c,	Centre frequency, f_c,
h	Thickness, m
K	Interfacial stiffness, GPa μ/m
N	Near field distance, m
P_{nom}	Nominal contact pressure, Pa
p_m	Mean contact pressure, Pa
p_0	Maximum contact pressure, Pa
R	Reflection coefficient, dimensionless
R_0	Reduced radius of contact, m
$R_{1,2}$	Radius of curvature of two contacting parts, m
R_a	Centre-line average surface roughness, m
RL	Reference reflection length, metres, m or time, t
r	Radius, m

L	Length, m
M	Frequency dip count, dimensionless
P	Normal force, N
T	Temperature, K
t	Time, s
TL	Temperature compensated length, metres, m or time, t
u	Deflection, m
V_w,	volumetric wear, m^3
v	Velocity, m/s
$v_{1,2}$	Poisson's ratios of the two materials, dimensionless
W	Load, N
x	Coordinate along the length of the surface
Z	Height of measured surface, m
z	Acoustic impedance of medium, $Kgm^2s \times 10^6$
α	Thermal expansion coefficient, dimensionless
θ_1	Incident wave angle, ^{o}
θ_2	Refracted wave angle, ^{o}
λ	Wavelength, m
μ	Coefficient of friction, dimensionless
ρ	Density, kg/m^3
σ	Stress, Pa
ω	Angular frequency of pulse, radians

LIST OF ACRONYMS

ADC	Analogue-to-digital converter
ASTM	American Society for Testing and Materials
BNC	Bayonet Neill-Concelman
FE	Finite Element
FFT	Fast Fourier transform
GDP	Gros domestic product
LVDT	Linear variable differential transformer
MMCX	Micro-miniature coaxial
NDT	Non-destructive testing
PCI	Peripheral component interconnect
PRF	Pulse repatition frequency
PTFE	Polytetrafluoroethylene
PVDF	Polyvinylidene fluoride
PZT	Lead zirconium titanate
RF	Radio frequency
RMS	Root mean square
SMA	SubMiniature version A
SMB	SubMiniature version B
UPR	Ultrasonic Pulser/Reciever
UT	Ultrasonic

LIST OF FIGURES

LIST OF TABLES

1 INTRODUCTION

1.1 Statement of the Problem

Studies estimate that as much as one third of all purposefully produced energy is lost to friction and wear. For example friction at the interface between a piston ring and liner in an internal combustion engine is one of the major influential factors of operating efficiency, [Mang *et al.* 2010]. The estimated potential savings that could be made from the correct use of tribological knowledge are substantial and have been estimated as an average of 1.6 % GDP. Tribology is defined as the science of interacting surfaces of different components in relative motion. For two components to be in contact they must be physically touching, and if two solids are touching, the contact is by definition inaccessible. How can one develop an understanding about a contact if it is inaccessible? One way scientists have overcome this challenge to use transparent materials; something that has been done with varying degrees of success in the laboratory, but this approach is rarely feasible in real life applications. Some of these interfacial relationships can be characterised using post processing techniques which are inherently difficult to achieve in real-time with real components in a dynamic situation. Mathematical models have been developed to predict these events with varying degrees of success, but all require assumptions to be made and some form of validation to be carried out. A non-invasive measurement technique is required to really understand these interfaces without disturbing them.

1.2 Seeing with Our Ears

The concept seems fundamentally flawed, but by using sound, it is possible to visualise things in places that our sight could never access. Sound is not particular as to the opacity of a material enabling it to probe deep into solid matter and partially reflect when it experiences a change in material properties. It is these reflections that can be sensed and used to form a multi-dimensional image of the area in which the sound is being reflected from. Bats and dolphins successfully utilise this technique and it is termed ‘echolocation’. The medical industry use this method as a diagnostic imaging technique for visualising subcutaneous body structures such as muscles and

internal organs. The most common medical use is obstetric sonography, which is when sound is used to create an image of an unborn foetus in the womb [Novelline, 1997]. This process of actively creating an inaudible sound wave and sensing the reflected signal is known as ultrasonic reflectometry and is widely used in engineering in the field of non-destructive testing. If a sound wave travelling through a material reaches a point of different material properties, the wave will be partially reflected. The most common use for this in engineering is to detect cracks and imperfections.

This aim of this work is to utilise ultrasonic reflectometry to measure and monitor tribological contacts in real-time. By using permanently embedded sensors, modern digitising techniques and detection algorithms, it is possible to detect the most miniscule of changes in the reflected sound wave that can not only lead to the imaging of the interface between machine element components, but can give us quantifiable measurements of various important parameters.

1.3 The Use of Ultrasonic Reflectometry in Tribology

A substantial amount of work has been carried out investigating the use of ultrasound to measure lubricant films, see Dwyer-Joyce *et al.* [2003] and Reddyhoff *et al.* [2005]. The technique has been successfully applied to numerous engineering applications including journal bearings, [Dwyer-Joyce *et al.* 2004a], theoretical mixed lubrication contacts, [Dwyer-Joyce *et* al. 2011], rolling element bearings, [Dwyer-Joyce *et al.* 2004b; Reddyhoff *et al.* 2004], and combustion engine piston ring and liner, [Dwyer-Joyce *et al.* 2013]. Kendal and Tabor [1971] first used ultrasound to investigate dry contacts. They determined that the transmission of ultrasound was a function of the interfacial stiffness. This work has been continued and numerous static ultrasonic contact measurements have been carried out using a scanning system to investigate machine element interfaces, such as Marshall *et al.* [2010] investigating the contact between bolted plates, interference fits [Marshall, 2004] and the static contact pressure and area between a railroad vehicle wheel and rail [Marshall *et al.* 2006]. These studies proved successful in the analysis of dry static contacts, but in order to apply these methods to industrial use, dynamic contact

measurements must be achieved. In achieving dynamic contact measurements, it will allow multiple conditions to be changed and the resultant behaviour to be monitored in real-time.

Lubrication is used to separate dynamic sliding contacts, but if this fluid film breaks down, wear is often the result. Ultrasonic reflectometry has been used to measure thickness of components so it is proposed that it is possible to measure wear using the same method. Birring and Kwun [1989] conducted an investigation into the measurement of wear using ultrasound and discovered the substantial affect that temperature has on the measurement. Ahn & Kim [2001] also investigated this concept and established the ability to assess the severity of the worn surface. They also established the qualitive relationship between FFT echo-amplitude and the roughness of the wear face. No temperature effects were considered.

The work presented in this thesis will develop the techniques needed to investigate dynamic contact conditions and wear rates using a mix of fundamental and applied studies.

1.4 Outline of Thesis

Chapter 1 of this document gives the reader the fundamental knowledge of engineering surfaces and their behaviour when they are brought into contact with one another. This information is beneficial as it supports the experimental work which is covered in the later chapters. Analytical models are introduced that can predict the behaviour of materials as they interact with one another. Other contact and wear measurement techniques are described and critiqued. The second chapter is a reference of the relevant fundamental theory of ultrasound that have been utilised in order to achieve the measurement techniques used in the latter chapters. The third chapter describes the physical equipment that enables the ultrasonic measurements to be taken. This includes a number of test rigs and instruments that have been developed by the author to achieve the required measurements.

The first applied study in Chapter 4 investigates the use of ultrasound to measure wear in-situ in real-time using a pin-on-disk test configuration. The method is critiqued and conclusions are drawn. In Chapter 5, a second method of measuring wear is hypothesised which uses the frequency content of the reflected wave to measure wear. Experiments are undertaken to test the method. Again the process is critiqued and conclusions are drawn. Industrial applications of both methods are discussed.

A lower speed dynamic contact is investigated in Chapter 6. A metal-to-metal swaged seal arrangement is characterised in terms of contact pressure and area as it is a critical tribosystem that experiences minimal wear but very high contact pressures spread over a relatively substantial area. In Chapter 7, the measurement technique is applied to a number of rolling contacts to assess its viability to characterise a railroad vehicle wheel and rail in contact. Discussions are made and conclusions are drawn in Chapter 8.

1.5 Engineering Surfaces

All real engineering surfaces are imperfect, and even if they may appear smooth, they are inherently rough consisting of peaks (known as asperities), troughs (valleys) and waves. These features become evident when the surface is inspected on a microscopic scale and have great influence on contact conditions and wear behaviour.

There are many ways to characterise the surface topography of a component but it is widely recognised that there is no single numerical parameter that can be used to describe it completely. R_a or the centre-line average value of roughness is commonly used and can be calculated from Equation 1-1.

$$R_a = \frac{1}{L}\int_0^L |z|\, dx \qquad 1\text{-}1$$

If a mean line is drawn so that the material above is equal to that of the voids below, *z* is the height of the surface measured from the mean line. *x* is the coordinate along the length of the surface and *L* is the measurement length. This can be seen in Figure 1-1 below from Williams [2005]. This method of categorising surface roughness does not consider the shape of the asperities which often influence a tribosystem.

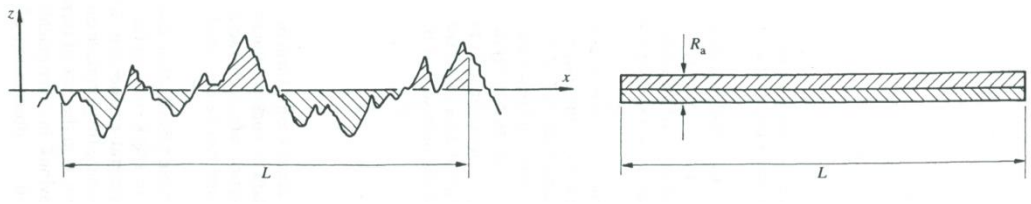

Figure 1-1. A diagram showing the method of calculating R_a, from Williams [2005].

The R_a values are critical factors determining the tribological behaviour at an interface. Some example R_a values from various manufacturing processes can be seen in Figure 1-2 from Degarmo *et al.* [2011].

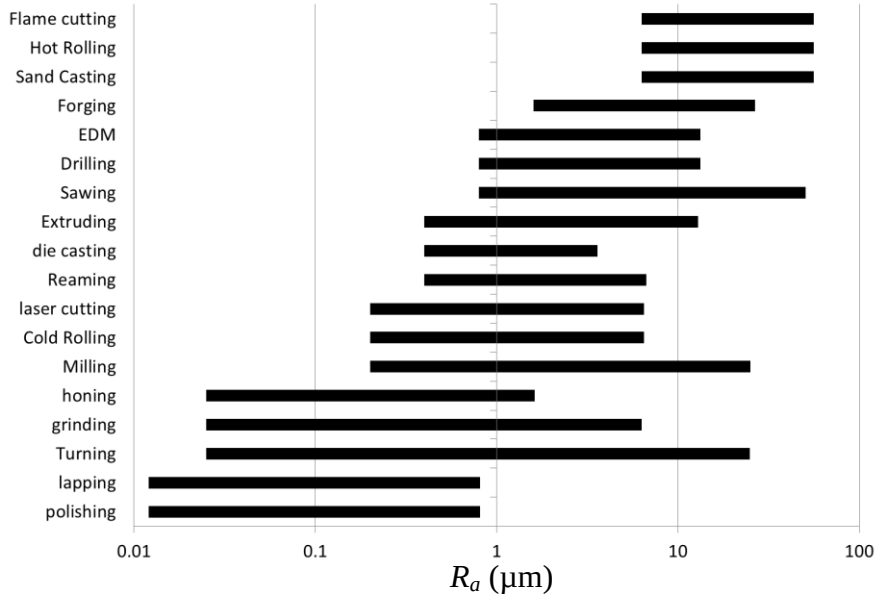

Figure 1-2. Example Ra values from various manufacturing processes, from Degarmo et al. [2003].

Other definitions of surface roughness include R_{max}; the measurement of maximum peak-to-valley calculated from 5 adjoining sample lengths, R_q; the root mean squared (RMS) roughness, R_t; the separation of the highest peak and lowest valley and R_z; the average of single R_t values over five adjoining sample lengths.

1.6 Contact Analysis

When two surfaces are loaded together, deformation will always occur to some extent as the surface features of the two materials are pressed together and the localised asperities begin to conform to one another. This can happen on both a macro scale, for example when using a centre punch there will be obvious visible deformation of the material. This also happens on a micro scale, for example when placing a pencil carefully on a table this will cause displacement on an atomic level. When two surfaces come into contact, it is only the asperity peaks, described in the previous section, that engage with one another, so the actual or real area of contact is far smaller than the apparent area of contact. Leonardo da Vinci documented that the areas in contact have no effect on friction and this was popularised by Guillaume Amonton in his second law; that the force of friction is independent of the apparent area of contact, [Williams, 2005]. The micro-deformation is due to the point loading of the asperities as they experience large contact stresses as seen in from Equation 1-2.

$$\sigma = \frac{F}{A} \qquad 1\text{-}2$$

where σ is stress, F is force and A is area. This stress causes the asperities each to deform and this can be entirely elastic, which is when the material returns to its previous shape after loading. More commonly there is a mixture of elastic and plastic deformation, which is when the shape of the material is permanently altered after reaching its elastic limit. As deformation occurs, more asperities come into contact until the load is spread across enough material to prevent further distortion and equilibrium is reached. This results in an increase in the real area of contact.

Often occurring at the same time as this micro-deformation is the macro scale deformation which is when the apparent shape and apparent area of contact change due to high stresses. This behaviour is usually attributed to non-conformal contacts such as two spheres or two parallel cylinders see Figure 1-3.

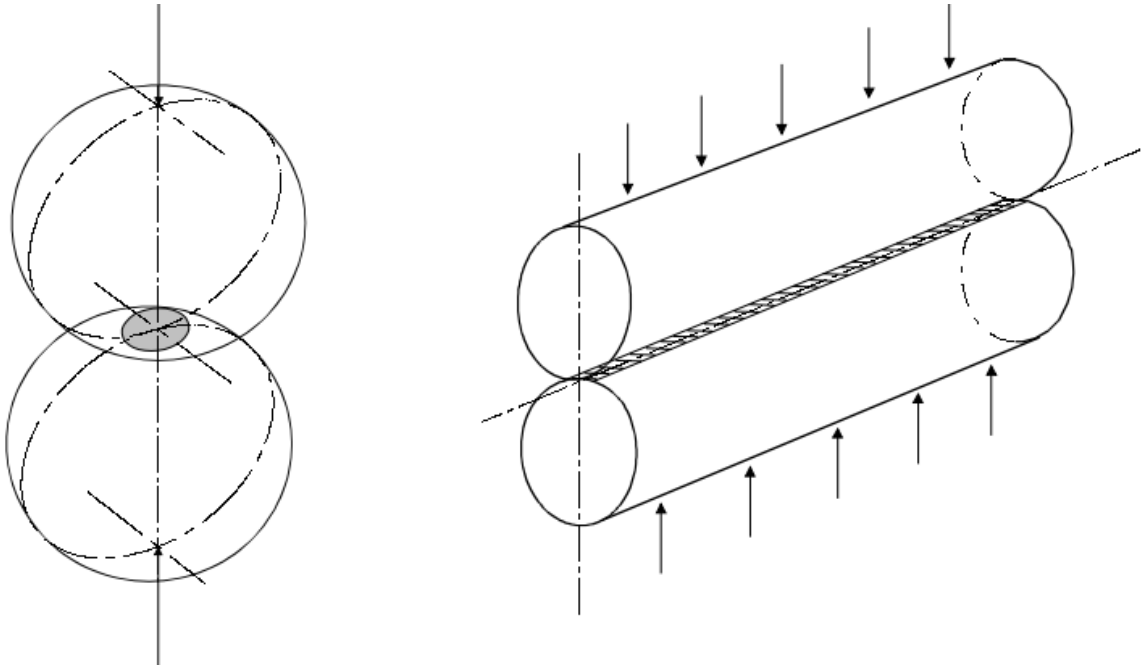

(a) (b)

Figure 1-3. Two spheres loaded together resulting in a circular contact (a) and two cylinders loaded together resulting in a line contact (b), from Williams [2005].

Heinrich Hertz described a method to calculate these contact areas in 1881, known as Hertz' theory of elastic contact. The theory assumes that the size of the contact is small compared to the size of the curved bodies, the contact is smooth and frictionless and that the deformation is elastic [Bhushan *et al*, 2000]. The model has been successfully applied to relate contact area, a, to contact force, W which is dependent on the reduced elastic modulus E_0 and the relative or reduced radius of contact R_0, [Timoshenko & Goodier, 1951]. Equation 1-3 can be used to calculate the contact area for two loaded spheres.

$$a = \left(\frac{3WR_0}{4E_0}\right)^{\frac{1}{3}} \qquad 1\text{-}3$$

The reduced elastic modulus can be found from Equation 1-4.

$$\frac{1}{E_0} = \frac{1}{2}\left(\frac{1-{v_1}^2}{E_1} + \frac{1-{v_2}^2}{E_2}\right) \quad \text{1-4}$$

where E_1 and E_2 are the elastic (Young's) modulus of material 1 and 2 respectively and v_1 and v_2 are Poisson's ratio of material 1 and 2 respectively. The relative or reduced radius of curvature can be found from Equation 1-5.

$$\frac{1}{R_0} = \frac{1}{R_1} + \frac{1}{R_2} \quad \text{1-5}$$

where R_1 and R_2 are the radius of curvature of material 1 and 2 respectively. For a flat surface, the radius should be set to infinity. Equation 1-6 can be used to calculate Hertzian stress in a circular point contact; for example, the contact between a ball-on-flat where p_m is the mean contact pressure and p_0 is the maximum contact pressure, w is the normal load, a is the contact area.

$$p_m = \frac{2p_0}{3} = \frac{W}{\pi a^2} \quad \text{1-6}$$

Comparisons can be drawn between a ball-on-flat contact and the contact between the microscopic asperities, so much of the contact theory holds true for both macro and micro contacting conditions.

For more complex shapes, second degree polynomials must be employed to represent bodies in the vicinity of the contact, [Rovira *et al.* 2012]. Numerical Hertzian modelling is a useful method and if the assumptions are reasonable for the particular application, a suitable analytical solution can often be found. In reality, the assumptions can be substantial and often lead to extensive inaccuracies in the results. One limiting factor is that the model assumes purely elastic deformation. Several

models have been developed that consider elasto-plastic deformation, for example Change *et al.* [1987] and Polycarpou & Etsion [1999]. These and some other models are described by Jackson & Green [2005]. Finite element analysis software is a powerful tool to carry out complex contact models, but great care must be taken to control the input parameters. A common term used to describe this dependency is 'rubbish in, rubbish out'.

There are a number of assumptions with the aforementioned contact models that have to be made to simplify the calculations. Some examples include assuming that the contacting bodies are frictionless and that the contacts are continuous and are not made up of sharp edges. These assumptions are quite bold and are often a significant cause of inaccuracy. Due to these potential errors, models therefore require validation of some form and this is often achieved through experimentation.

Contact modelling is of fundamental importance across a wide range of industries as it can help engineers optimise design to reduce stresses and component damage, minimise maintenance, maximise grip, ensure safe operation and increase understanding of component interaction.

1.6.1 Contact Measurement Techniques

Numerous methods exist to measure the contact conditions of interacting surfaces. These can vary from the simplest solution to the most complex network of automated sensing devices. Take for example 'engineer's blue', a non-drying blue coloured oil based substance that is commonly used throughout the engineering world. When one is told to 'blue it up', the surface of one object is painted blue and contact is made with the mating element. The paint is transferred at the points of contact and these are then clearly visible when the materials are separated, [Chapman, 1964]. This provides accurate contact position information, but no information regarding the contact pressure distribution. This is only a more advanced version of the first recorded contact measurements being taken by applying a moist chalk to one surface, [Johnson & Marston, 1894].

Many argue that by introducing a third body you are inherently changing the tribological conditions and potentially changing the resultant contact shape. An example would be that the engineers blue could lower the friction coefficient of the interface and the component could slip resulting in a different contact position. A slightly more advanced method is to use pressure sensitive film. This is a thin laminate film that can be placed between contacting surfaces that when compressed, the film changes colour relative to the magnitude of the pressure applied. As before, the introduction of a third body inherently changes the contact conditions but in this case, adding a relatively thick film can lead to a larger contact area being measured than the actual size. These methods are only effective in static conditions thus limiting the application, [Pau *et al.* 2001]. Dynamic measurements on a rolling contact have been obtained using a modified rail section with a grid of small holes passing low pressure air through the surface of the railhead. As the wheel moves over the rail, some of the holes will stop the flow of air and by monitoring this, it is possible to derive low resolution contact area evolution data, [Poole, 1987]. Some information can be extracted by measuring the capacitance across the interface as this is proportional to the contact conditions, [Chiang *et al*. 2011]. However, the requirement for electrical isolation means that this method is usually confined to the laboratory.

Strain gauges and load cells are commonly used to measure loads and displacements and this can greatly increase the understanding of a tribosystem. Mukesh *et al*, [2013] have developed a technique using strain gauges that involves measuring the movement of the inner surface of a piston ring that can infer the lubricant film thickness of the piston/liner contact. They cannot, however, give direct information regarding contact shape or wear characteristics, although they are very useful to measure frictional forces. Photoelastic stress measurements such as those carried out in the 1950's by Hetenyi & McDonald [1958] can be a powerful tool in the measurement of resultant stress distributions from contacts but are largely defined to laboratory conditions.

1.7 Friction and Wear

Amontons law states that the friction force F between a pair of loaded sliding surfaces is proportional to the normal load P that they carry: in other words, the tangential force F required to slide a metal block along a surface is proportional to the weight of the block, [Williams, 2005]. For a pair of materials, the relationship is termed the coefficient of friction, μ.

$$F = \mu P \qquad 1\text{-}7$$

Wear is the progressive damage involving material loss which occurs on the surface of a component as a result of its motion relative to the adjacent working parts as defined by Williams, [2005]. Wear is synonymous with dry dynamic contact conditions and it is notorious for being very difficult to predict due to the large number of influential parameters. There are numerous different types of wear that are classified by the different mechanisms in which materials are removed. These have been defined clearly in numerous texts such as Hutchings *et al.*, [1992] and Williams [2005]. Bhushan *et al.* [2011] states that these numerous different mechanisms can be grouped into four first order classifications; adhesive wear, abrasive wear, wear caused by surface fatigue, and wear due to tribochemical reactions when different oxide layers are developed during sliding.

These different mechanisms often occur concurrently and are often quantified in terms of wear rate, which is the material lost in terms of sliding distance or time. Moving components brought into contact with one another for the first time experience an initial running in period when the two surfaces conform to one another on a microscopic level. During this initial breaking-in period, the components usually experience high levels of wear. As the surfaces become smoother, the wear rate decreases and often settles to somewhat of a steady state. This state is maintained until either an external parameter is introduced to the tribosystem or until fatigue processes in the materials lead to a rapid increase in material loss often leading to catastrophic wear and seizure. Figure 1-4 shows the typical wear behaviour over the life of a component, [Williams, 2005].

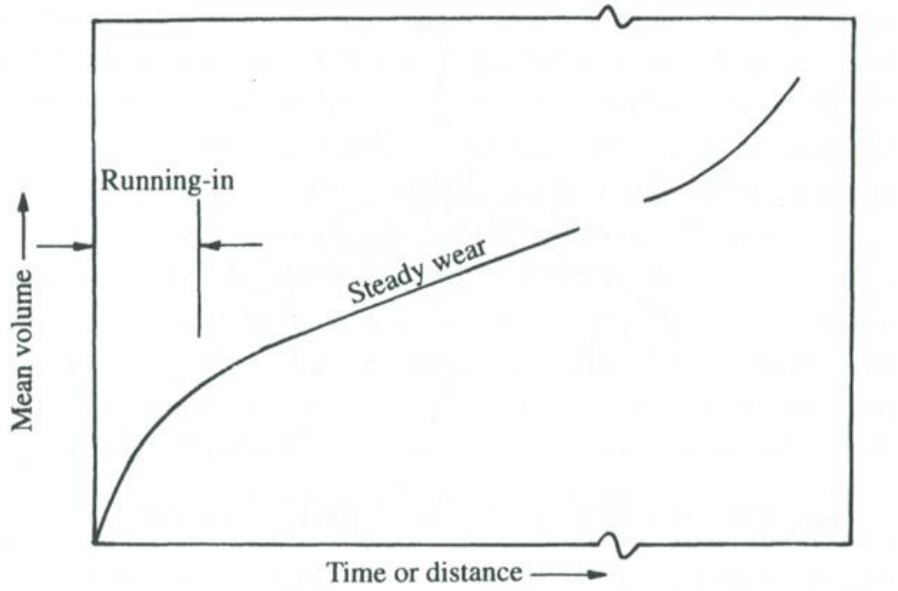

Figure 1-4. The trend of wear rate over the life of a component, from Williams [2005].

As a component experiences wear, energy is released in the form of heat known as surface conjunction temperatures and flash temperatures that for a steel on steel contact can be approximately 200-250 ºC. This can affect the behaviour of the tribosystem by localised melting and alteration of the molecular structure, see Stackiowack & Batchelor [2005].

1.7.1 Wear Measurement Techniques

The traditional method to understand wear behaviours is to conduct laboratory based experiments with similar materials and representative contact conditions. Analysis of wear then takes place post experiment. The traditional method of quantifying wear is the mass-loss measurement, the procedure of measuring the mass before and after the test and reporting the overall mass removed. This method has been successfully used for many applications, although not always feasible when material transfer takes place or when testing porous materials in lubricated environments. The understanding of wear behaviour is paramount to material selection and machine element design.

Another post-test measurement method is surface profilometry. This is the procedure of ‘measuring the surface of a material’, usually using optical or stylus based method. These tools are very useful to characterise surface detail and deep grooves, but cannot measure wear of some geometries such as a pin, as the entire contacting face will wear down with no datum point for reference. In some cases, i.e. wear on a ball; it is possible to estimate wear from geometrical wear scars. The drawback is that none of these methods actually give a value for wear rate, only absolute wear post-test. It is possible to intermittently halt the test, remove specimen and take measurements, but this can interfere with the experiment.

Eddy current, linear potentiometers and laser displacement sensors are all devices that are used to measure position and displacement. By mounting a sensor on a fixed position measuring the displacement of the moving wearing component, it is possible measure a change in component thickness and thus infer a measurement of wear. Some tribometers have this feature fitted as standard or as an optional extra, for example the Plint TE99 Universal Wear Testing machine has the option of having a transducer to measure the vertical movement of the pin relative to the fixed datum during the test. In the product literature, this is described as ‘giving an indication of wear’, but factors such as to thermal expansion, wear debris and the transfer of material can also lead to displacement. These displacement systems measure the net wear of both components.

1.8 Aims

The aim of this work was to investigate the application of ultrasonic reflectometry to analyse dry dynamic tribological contacts in real-time, in-situ, by monitoring the reflected sound waves from the surface of interest. It has been established that the contact pressure at an interface is a critical parameter to understand because often if this is kept within the design tolerances, failure should not occur. The work aims to show how it is possible to measure this important parameter in real-time on actual engineering components. If the contact pressure is too large, the lubrication fails or a sacrificial component is used, the result will be wear. This work also aimed to describe two new methods of measuring wear again in real-time on real machine

element components. By describing the important aspects of both the hardware that creates the sound wave and the theory that transforms a reflected pressure wave into a mechanical unit, the reader will have a complete understanding of the new measurement methods introduced with enough information to replicate the work in any measurement or monitoring application. To achieve this, the following objectives have been defined:

- To provide a clear definition of the problem
- To explain why measurement and monitoring is important and the limitations of current techniques
- To describe the fundamentals of ultrasonic wave theory
- To introduce the theory behind the proposed technique of ultrasonic wear measurement
- To explain the ultrasonic contact pressure measurement technique
- To provide a review of appropriate hardware solutions for ultrasonic measurements
- To introduce the new hardware devices that have been developed for this work
- To describe the important aspects learned about the use of permanently embedded ultrasonic monitoring
- To carry out wear tests to prove the hypothesised ultrasonic wear measurement concepts
- To carry out contact pressure measurements on a sliding contact condition
- To carry out contact pressure measurements on a rolling contact condition
- Conclude on the findings

1.9 Objectives

By describing the important aspects of both the hardware that creates the sound wave and the theory that transforms a reflected pressure wave into a mechanical unit, the reader will have a full understanding of the new measurement methods introduced. This leads onto the authors' main objective; to provide a reference text for anyone wishing to carry out dry dynamic tribological contact measurements using ultrasonic reflectometry in terms of the contact distribution and wear. This includes all necessary information regarding the appropriate hardware selection options, pitfalls and tips for permanent sensor installation, signal processing techniques, the things to consider when measuring of a long period of time and various calibration procedures that have been developed whilst conducting this research. The new methods introduced in this text will provide the foundations that will lead to new discoveries in the field and other applications that fall beyond the scope of this work.

2 ULTRASONIC THEORY

Ultrasound is the name given to sound waves of a frequency higher than those audible by the human ear. This varies from person to person but 20 kHz is understood to be the lower end of the ultrasonic scale, [Kräutkramer & Kräutkramer, 1969]. Sound waves in this range are created naturally in mechanical equipment and by monitoring these acoustic emissions with passive sensors, information about the running conditions of the system can be extracted. This work is not concerned with naturally occurring sound in the ultrasonic range, rather the case when an ultrasonic wave is purposefully introduced and the behaviour of this wave monitored. The sound wave penetrates through a material and when it reaches a change in material properties, part of the sound wave is reflected.

The reflection/transmission signature can be analysed revealing sub-surface details. This is called ultrasonic reflectometry and is the basic principle facilitating the work in this document. The most well-known application of ultrasonic reflectometry is its use in medical sonography to produce pictures of foetuses in the womb, [Novelline, 1997]. The non-destructive nature of ultrasonic testing allows it to be used in-situ and because it does not permanently alter the article being inspected, it is a highly-valuable non-destructive technique that can save both money and time in product evaluation, troubleshooting, and research, [Cartz, 1995].

2.1 Wave Propagation

Sound is a travelling wave which is an oscillation of pressure propagating through a host medium. The host medium is made up of particles held together by elastic forces. Assuming the body is not stressed beyond its elastic limit, these forces can be analogised as springs and the particles as individual masses. As one particle is displaced (oscillated), this force is transmitted onto the adjacent particle and so on, [Kräutkramer & Kräutkramer, 1969]. Due to the elasticity of the bonds, a delay is introduced resulting in a phase lag, thus creating zones of both expansion and compression which propagate through the medium.

Details of new and exciting modes of wave motion are constantly being reported. All kinds of wave particle velocity motion (e.g. a guided wave made up of a Lamb wave and a surface wave) are just superpositions of the traditional longitudinal or compression waves and transverse or shear waves, [Rose, 2004].

2.1.1 Longitudinal Waves

In longitudinal waves, the particles oscillate in the same plane as the direction of wave propagation. This can be seen in Figure 2-1 adapted from Kräutkramer & Kräutkramer [1969].

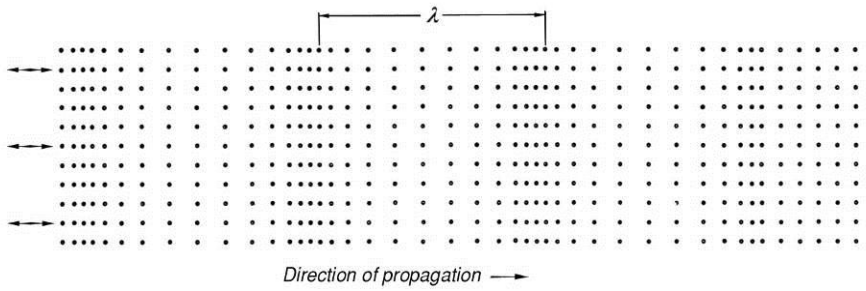

Figure 2-1. Instantaneous picture of a longitudinal wave, from Kräutkramer & Kräutkramer [1969].

This represents an instantaneous picture of a section of a body through which a longitudinal wave is propagating. Parts of the body can be seen to be in compression whilst adjacent parts are in tension and the distance between cycles is the wavelength, λ. The waves will travel at a constant velocity with uniform intervals towards the right. This represents a longitudinal elastic wave. These are also known as pressure or compression waves.

2.1.2 Transverse or Shear Waves

Transverse waves, also known as shear waves are the second type of elastic body waves that support sound wave propagation through solid media. The motion of the particles is perpendicular to the direction of wave propagation, a diagram of which

can be seen in Figure 2-2 from Kräutkramer & Kräutkramer [1969]. Shear waves can be created directly using an ultrasonic shear transducer, but are also created from angle beam transducers and refraction due to dissimilar materials as discussed further in Section 2.1.8.

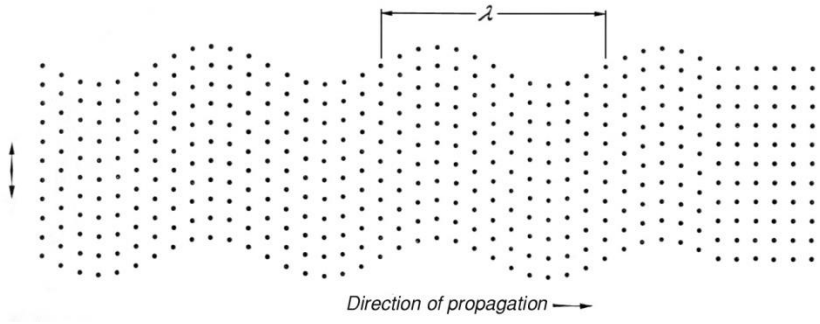

Figure 2-2. An instantanious picture of a transverse or shear wave, from Kräutkramer& Kräutkramer [1969].

2.1.3 Wave Velocity or 'The Speed of Sound'

If one is asked to quote the speed of sound, many will respond with an approximate answer of around 340 m/s. This is actually a trick question as the speed at which a disturbance propagates is entirely dependent on the host medium, and the answer most people will quote will be the speed of sound in air. The rate at which the waves propagate through a medium is determined by the elastic forces between particles. The wave therefore will travel different speeds through different materials and this is also dependant on the wave type. Bulk longitudinal wave velocity, c, is generally thought of as being proportional to the square root of the elastic modulus, E, over density, ρ, shown in Equation 2-1.

$$c = \sqrt{\frac{E}{\rho}} \qquad 2\text{-}1$$

Likewise bulk shear wave velocity is proportional to the square root of the shear modulus *G* over velocity, [Rose, 2004]. The speed of sound in an ideal gas can be found using the adiabatic index, the molar gas constant and the temperature.

The sound velocities for standard materials are readily available in reference tables, but *c* can also be obtained by a simple time-of-flight measurement discussed in Section 2.2.1. This is the process of measuring the time taken for a sonic pressure wave to propagate through a known distance.

The wave velocity, *c*, is also related to frequency, f, and acoustic wavelength, λ, by the following relationship:

$$c = f\lambda \qquad 2\text{-}2$$

If the speed that sound travels through a material is known, it is possible to calculate the thickness of said material from the speed, distance and time relationship using an ultrasonic pulse. This is known as a time-of-flight measurement and is the basis of many of the numerous ultrasonic thickness gauges available on the market today. This is discussed in detail in Section 2.2.1.

2.1.4 Acoustic Impedance

The acoustic impedance is a measure of the acoustic pressure generated by the oscillatory movement of the particles within the host medium. The acoustic impedance, *z*, is defined as the multiple of density, ρ, and sound velocity, *c*, as seen in Equation 2-3.

$$z = \rho c \qquad 2\text{-}3$$

The units of acoustic impedance are pressure per velocity per area: commonly referred to as rayls per square metre.

The reflection coefficient, *R*, is the term given to the proportion of the wave reflected at an interface. For an atomically perfect interface between two dissimilar materials, *R* is defined as:

$$R = \frac{z_1 - z_2}{z_1 + z_2} \qquad 2\text{-}4$$

where z_1 and z_2 are the acoustic impedances of the upper and lower materials respectively. This relationship describes the maximum possible proportion of sound that can be transferred between two materials at an interface. David & Cheeke [2002] have created a list of acoustic impedance values for common engineering solids and fluids can be seen in Table 2-1 and Table 2-2.

Medium	**Longitudinal Velocity (km/s)**	**Shear Velocity (km/s)**	**Density (g/m^3)**	**Acoustic Impedance (MR/m^2)**
Acrylic, Plexiglas MI-7	2.61		1.18	3.08
Aluminium	6.42	3.04	2.7	17.33
Bacon P68	4	2.17	1.9	8.25
Bearing babbit	2.3	N/A	10.1	23.2
Brass - yellow	4.7	2.1	8.64	40.6
Concrete	3.1	N/A	2.6	8
Copper, rolled	5.01	2.27	8.93	44.6
Epoxy glue, EPX1	2.44	N/A	1.1	2.68
Glass - Pyrex	5.64	3.28	2.24	13.1
Gold - hard drawn	3.24	1.2	19.7	63.8
Inconel	5.7	3	8.28	47.2
Iron	5.9	3.2	7.69	46.4
Iron - cast	4.6	2.6	7.22	33.2
Lead	2.2	0.7	11.2	24.6
Molybdenum	6.3	3.4	10	63.1
Neoprene	1.6	1.31	2.1	N/A
Nylon, 6/6	2.6	1.1	1.12	2.9
PVDF	2.3	N/A	1.79	4.2
Silicon carbide	13.06	7.27	3.217	42
Steel - mild	5.9	3.2	7.8	46
Tin	3.3	1.7	7.3	24.2
Titanium	6.1	3.1	4.48	27.3

Table 2-1. A table showing the relevant acoustic and material properties of some commonly used engineering materials, from David & Cheeke [2002].

Medium	Longitudinal Velocity (km/s)	Density (g/m^3)	Acoustic Impedance (MR/m^2)
Air - dry at 0°C	0.33145	1.293	0.0004286
Alcohol, isopropyl, 2-Propanol, at 20°C	1.17	0.786	0.92
Diesel	1.25	0.832	N/A
Gasoline/Petrol	1.25	0.803	1
Honey, Sue Bee Orange	2.03	1.42	2.89
Oil - SAE 30	1.7	0.88	1.5
Sonotrack couplant	1.62	1.04	1.68
Water - liquid at 25°C	1.4967	0.998	1.494
Water - sea, at 25°C	1.531	1.025	1.569

Table 2-2. A table showing the relevant acoustic and material properties of some commonly used engineering fluids, from David & Cheeke [2002].

From Equation 2-4, when a sound wave travels from a solid, such as steel, to a gas (air), 99.998 % of the energy of the sound wave will be reflected at the interface. It is this premise that is the foundation of ultrasonic crack detection.

2.1.5 Attenuation in Solids

Ultrasonic attenuation is the term given to the reduction in magnitude of a sound wave as it travels through the host medium. Many of the methods used in this body of work rely on the measurement of sound wave magnitude to obtain results. It is for this reason that attenuation has to be considered in detail as its effects will influence the results. This is especially true when a single measurement of sound wave magnitude is used as a comparative reference over a longer period of time.

In an ideal material, the sound pressure reflected at an interface would only reduce in magnitude due to the spreading of the sound wave explained by Huygens's principle, see Section 2.1.7. Real polycrystalline solids are made up of many crystals of varying size and orientation. This introduces discontinuity of elastic moduli at grain boundaries thus resulting in reflections at these boundaries due to a variance in acoustic impedance. The magnitude of this affect is dependent on the grain size, the wavelength, and the degree of anisotropy, [Blitz, 1963]. This effect, along with reflections caused by micro-cracks in the material, is generally referred to as scattering.

The wave magnitude is reduced due to the conversion of sound energy to heat; this process is known as absorption. Absorption occurs from intermolecular action, molecular rearrangement, thermal conduction and viscosity. In most cases, energy in molecules is made up of translational, rotational and vibrational energy. As a sound wave passes through a material, the molecules transfer this energy via translational energy. As a result of molecular collisions, part of this energy is converted into internal energy, rotational and possibly vibrational energy, before equilibrium between the three states is gradually restored, [Vigoureux, 1950b]. This intermolecular action is the primary reason for absorption in solids.

From Equation 2-2, it can be concluded that the higher the frequency, the shorter the wavelength. Attenuation increases approximately as the square of frequency. It is for this reason that that high frequency signals cannot be transmitted long distances through highly attenuative materials, [Vigoureux, 1950]. This is one of the main factors that prohibit the use of ultrasound as a measurement tool in some applications such as rubber components. Figure 2-3 is a time domain waveform plot known as an A-Scan, showing the magnitude of consecutive ultrasonic reflections decreasing with time from the first reflection. The initial excitation wave has been removed from the graph.

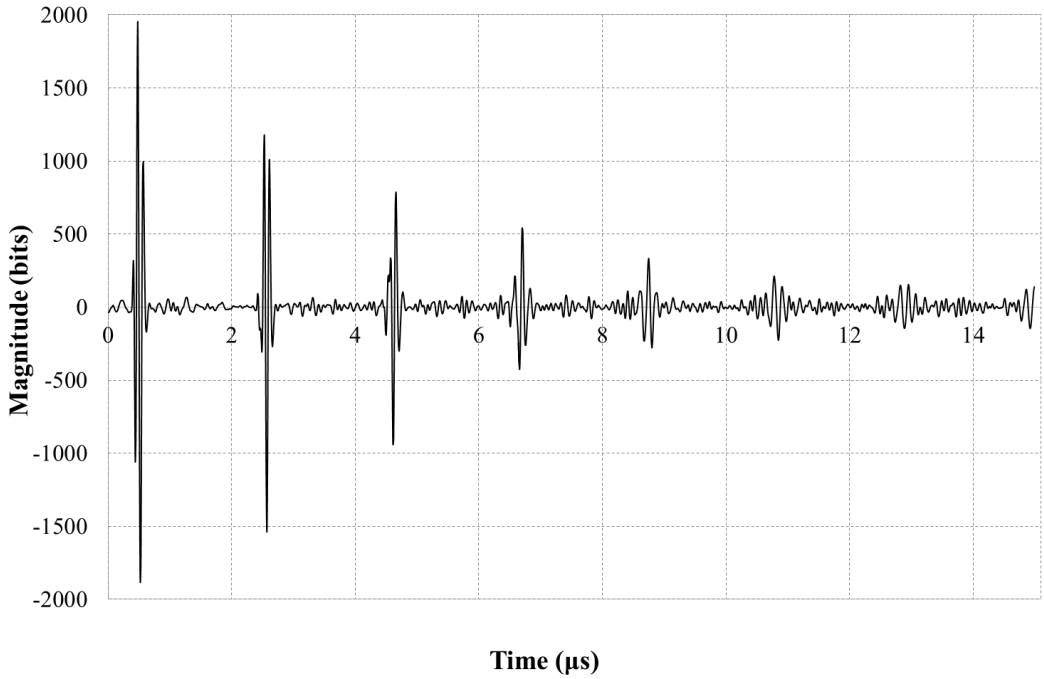

Figure 2-3. A diagram showing the magnitude of consecutive ultrasonic reflections decreasing over time.

2.1.6 Near-Field Affect

The sound wave generated by the transducer does not emanate from a single discrete point, but rather the entire active face of the element as described in Huygens principle, see Section 2.1.7. The wave interference or diffraction effect results in fluctuations in signal amplitudes as they go through a series of peaks and troughs near the face of the element culminating in a final peak in amplitude as shown in Figure 2-4, from NDT Resource Centre [2012]. These fluctuations are caused by constructive and destructive interference of the multiple waves which originate from the transducer face.

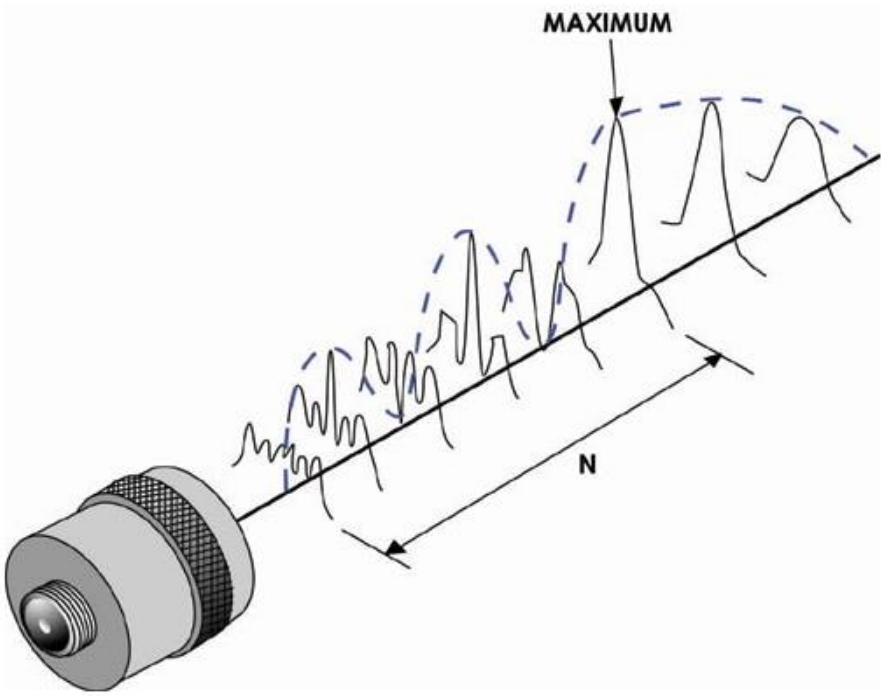

Figure 2-4. A diagram showing the cross sectional profile of a transducer beam showing the near field effect, from NDT Resource Centre [2012].

This area is known as the near field range and measurements in this range can be problematic and considerations must be made when designing the measurement configuration. As the sound wave propagates further through the host medium, the wave becomes more stable and uniform. The near field distance, *N*, is a function of element size; diameter *D*, frequency, *f*, and the sound velocity of the host medium, *c*, and can be calculated from Equation 2-5 from NDT Resource Centre [2012].

$$N = \frac{D^2 f}{4c} \qquad 2\text{-}5$$

For a common ultrasonic sensor arrangement using a 10 MHz transducer with a 7 mm diameter element, the near field length in steel is 20 mm.

2.1.7 Huygens Principle and the Measurement Window

For a theoretical point source of acoustic energy, radiation is emitted equally in all directions with a spherical wave front, [Blitz, 1963]. Figure 2-5 shows an energy source of finite length to represent an ultrasonic transducer. The front face has been divided into 8 nodes on which spherical wave fronts have been drawn at three stages of propagation with respect to time.

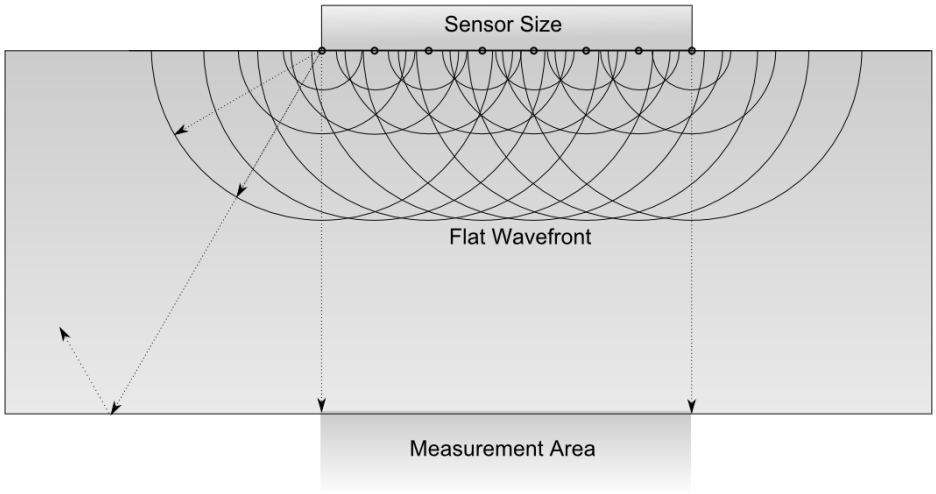

Figure 2-5. The 2D ultrasonic wave propagation in a solid body modelled as a linear array of points located on the face of the source.

If the number of nodes increases, the resultant wave front tends towards a flat line that is equal to the length of the emitting body. As this flat propagating wave front meets a parallel interface, it will be reflected perpendicularly directly back to the sensor. Either side of the emitting body, the wave front is curved, the radius of curvature increasing with time-of-flight. Arrows have been drawn to show the direction of sound wave propagation. It can be seen that either side of the emitting body, the energy is reflected elsewhere and will therefore not be detected by the sensor.

In reality, as the wave energy strikes the interface outside of the ‘measurement area’, a new series of spherical waveforms are generated scattering energy in all directions, shown in the diagram Figure 2-6. It can be seen that some of this energy will theoretically be reflected back to the sensor. The diagram also shows how the sideways travelling wave energy can meet other incident interfaces that can result in erroneous echoes which will appear as a second echo in the time domain plot.

Robin Mills from The University of Sheffield devised a method of measuring the energy profile of a sound wave at an interface. This was achieved by exciting a transducer, causing a sound wave to travel through a section of material and using a traversing secondary receiving sensor attached to a finite point, measuring the magnitude of the wave at discrete points across the interface. The measured profile of a 6.2 mm 10 MHz transducer pulsing through a 5 mm block of EN24 steel can be seen in Figure 2-6. It shows that there is very little in the way of beam spread in this particular arrangement. From Equation 2.1.6, we can see that the measurement is in the near-field region. The amount of beam spread will be a function of frequency, the lower the frequency, the greater the spread.

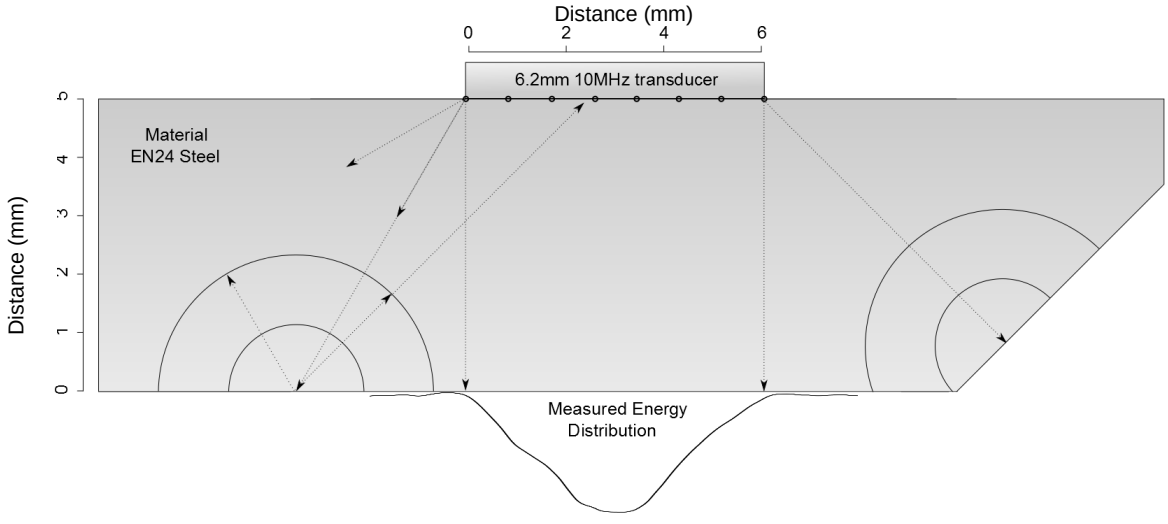

Figure 2-6. A diagram showing the new spherical wave fronts being generated at an interface.

The assumption can therefore be made that as long as the two surfaces are parallel, the area that is sensed by the transducer or the ‘measurement window’ is the same size as the active element. This also shows that the magnitude of the energy is not linear across the face of the element and is larger in the centre. If the measurement window contains partial contact, the result is often an increase in the reflected amplitude, resulting in a reflection coefficient greater than one. Previous work has not been able to explain this phenomenon so the results when this happens have thus far been ignored.

2.1.8 Snell’s Law

Ultrasonic wave paths follow many of the same laws of reflection and refraction seen with light. When an oblique wave reaches an interface of dissimilar materials, the wave is partially reflected and partially transferred. The speed of the wave will change as it reaches the new material. This differing acoustic velocity causes the beam to ‘bend’. A schematic diagram can be seen in Figure 2-7 showing a bending beam. If Huygens theory is applied to this concept, the concept is easier to explain. This has been achieved by annotating the wavelength of the path and the spherical wavelets. It can be seen that as the wavelength’s change between the dissimilar materials, the resultant wave-front will change direction.

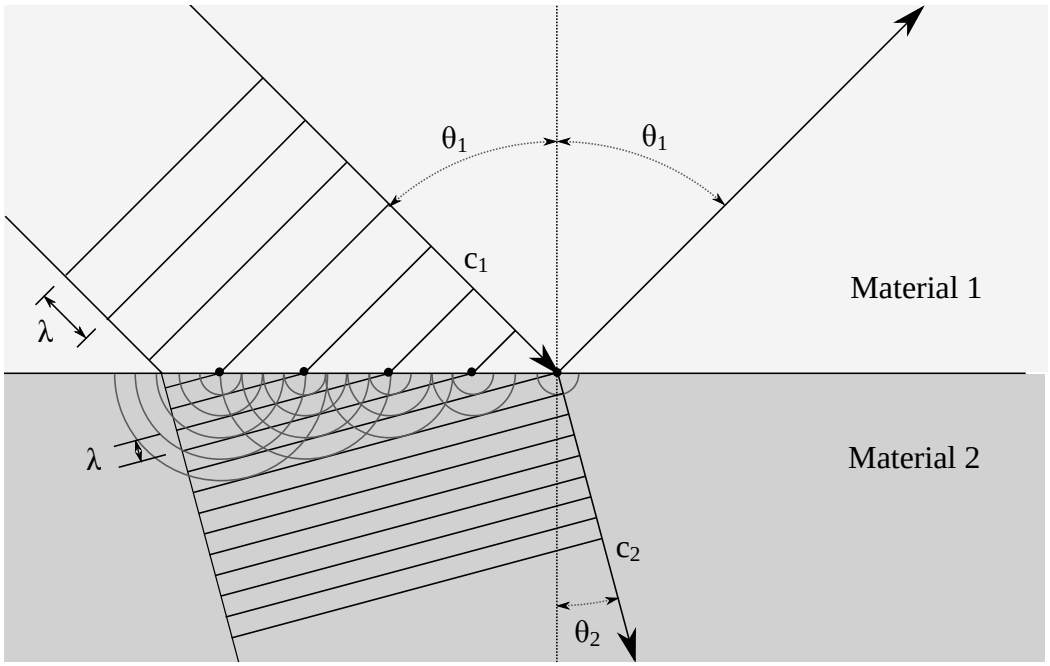

Figure 2-7. A schematic diagram showing a bending beam due to Snell's laws of refraction.

Snell's Law states that the ratio of sound velocities of material 1 and 2 (c_1 and c_2) is equal to the ratio of the sine's of the incident wave (θ_1) and the refracted wave (θ_2) as shown in Equation 2-6.

$$\frac{c_1}{c_2} = \frac{sin\theta_1}{sin\theta_2} \qquad 2\text{-}6$$

This relationship is particularly important when using immersion transducers as discussed in Section 3.3.5 as it affects the focal length of the beam.

A further point to note is that when a wave hits an interface at an angle, the energy in the wave can cause the particles to move in the transverse plane resulting in a shear wave being generated. This is known as mode conversion. More information can be found in Rose [2004] but it is important to note as it can be the reason for unexpected reflections in the measured signal.

2.1.9 Acoustoelastic Effect

The acoustoelastic effect is the term given to the effect that stress has on a sound wave travelling through solid media. The velocity in which a sound wave travels is governed by the elasticity of the material and the elasticity is altered by stress. If the material is in tension, the sound propagation is slower and if the material is in compression, the wave propagates faster, see Toupin & Bernstein [1961] and Tverdokhlebov [1983].

2.2 Ultrasonic Thickness Measurement

The ultrasonic time-of-flight measurement is commonly used in ultrasonic thickness gauging. Other methods also exist for measuring thin layers that will also be discussed.

2.2.1 Time-of-Flight Measurement

If both the speed, *c*, that sound travels through a host medium and the time, *t*, that the journey takes is known, it stands to reason that the distance, *d*, can be established from the relationship between speed, distance and time, shown in Equation 2-7. The distance, *d*, that the sound wave travels is twice the thickness of the material as it has to travel there and back. This is the premise behind ultrasonic thickness gauging.

$$c = \frac{d}{t} \qquad 2\text{-}7$$

Equation 2-7 implies that material sound velocity is a constant material parameter that can be either looked up from material tables or measured directly. A list of the speeds that sound travels through common materials can be found in Table 2-1.

There are numerous ways to extract time information from an A-Scan. The analogue sing-around and pulse-overlap methods have been traditionally used with varying degrees of success; more information can be found in Mason & Thurston [1976]. With digitised waveforms, a number of options are available to calculate the time-of-flight. The zero-crossing time-of-flight cross correlation measurement is evaluated as the distance between the zero crossing points of two successive echoes. A few data points either side of the zero crossing point are fitted by a linear function, then the zero crossing point is calculated as the intersection of the linear function and the horizontal zero line as shown in Figure 2-8, from Thompson & Chimenti [1995]. This increases measurement accuracy as it is not as dependant on the digitising clock speed as discussed in Section 3.2.1.

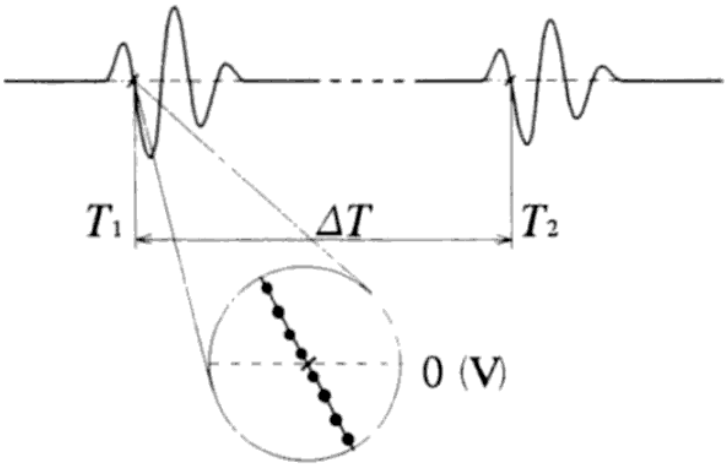

Figure 2-8. A diagram showing the zero-crossing method, from Thompson & Chimenti [1995].

With this method, it is important to capture at least two consecutive reflections and use the distance between the two reflections to calculate the time-of-flight. It is important to use the same zero crossing point in each reflection. It is not suitable to use the excitation pulse or 'initial bang' because the waveform is not of similar shape. In many ultrasonic applications, the same transducer that generates the sound-wave also receives the signal after it is reflected from an interface, this is known as pulse-echo mode. If this is the case, it is vital to remember that the time-of-flight refers to the path of material in which the ultrasound travels which is twice the thickness of the material so the sound has to travel there and back. Figure 2-9 shows two consecutive echoes from a 10 mm thick block of steel corresponding to 3.4 µs.

This would be the expected time-domain response from the instrumented block seen in Figure 2-5

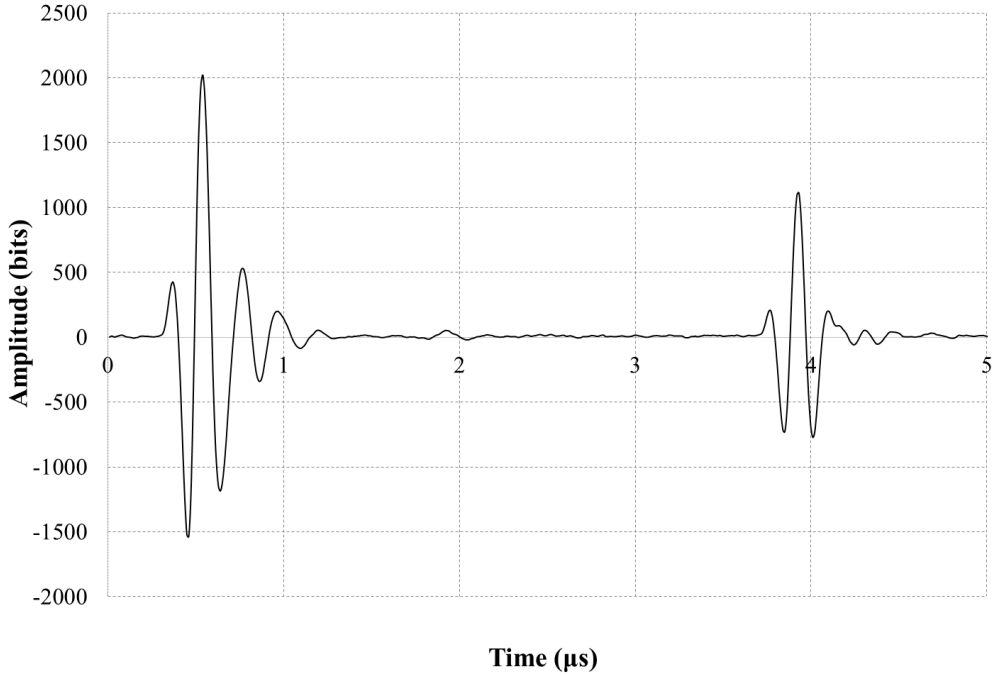

Figure 2-9. The time-domain plot showing two echoes from a 10 mm thick block of steel.

To increase robustness of the measurement, multiple zero-crossings measurements can be extracted from each reflection and the different measurements compared in as they all should give the result. There are arguments against using this method as in some applications; there can be substantial system noise at the zero crossing that can affect the results.

The zero-crossing method is only applicable for non-dispersive media. Another method uses a Hilbert transform and an appropriate parabolic interpolation on the echo, then taking the peak value for the time-of-flight datum Kažys **[**1996]. This is commonly used with air-coupled transducers as the method effectively eliminates the noise in the received signal reportedly accurate to within 1 mm at a distance of 1 m, [Namas & Dogruel, 2008]. Other cross correlation methods exist including cubic spline, [Svilainis & Dumbrava, 2008] and parabolic interpolation, [Queiros *et al,* 2006].

2.2.2 Resonant Dip Technique

When measuring thin materials, the two pulse echoes can become so close to one another that they begin to overlap. If this occurs, it can be difficult to differentiate each reflection in the time domain and thus it becomes impossible to perform a zero crossing measurement.

To demonstrate this, a 5 MHz commercial ultrasonic transducer was used to pulse a sound wave through a series of steel test blocks of different thicknesses. Figure 2-10 (a), (b), (c), and (d) are time domain A-Scans showing two subsequent reflections for steel blocks of thickness 10 mm, 5 mm, 1.5 mm and 0.9 mm respectively. Plots (b), (d), (f) and (h) are frequency domain plots obtained by taking a Fast Fourier transform (FFT) of the adjacent A-Scan time-domain windows.

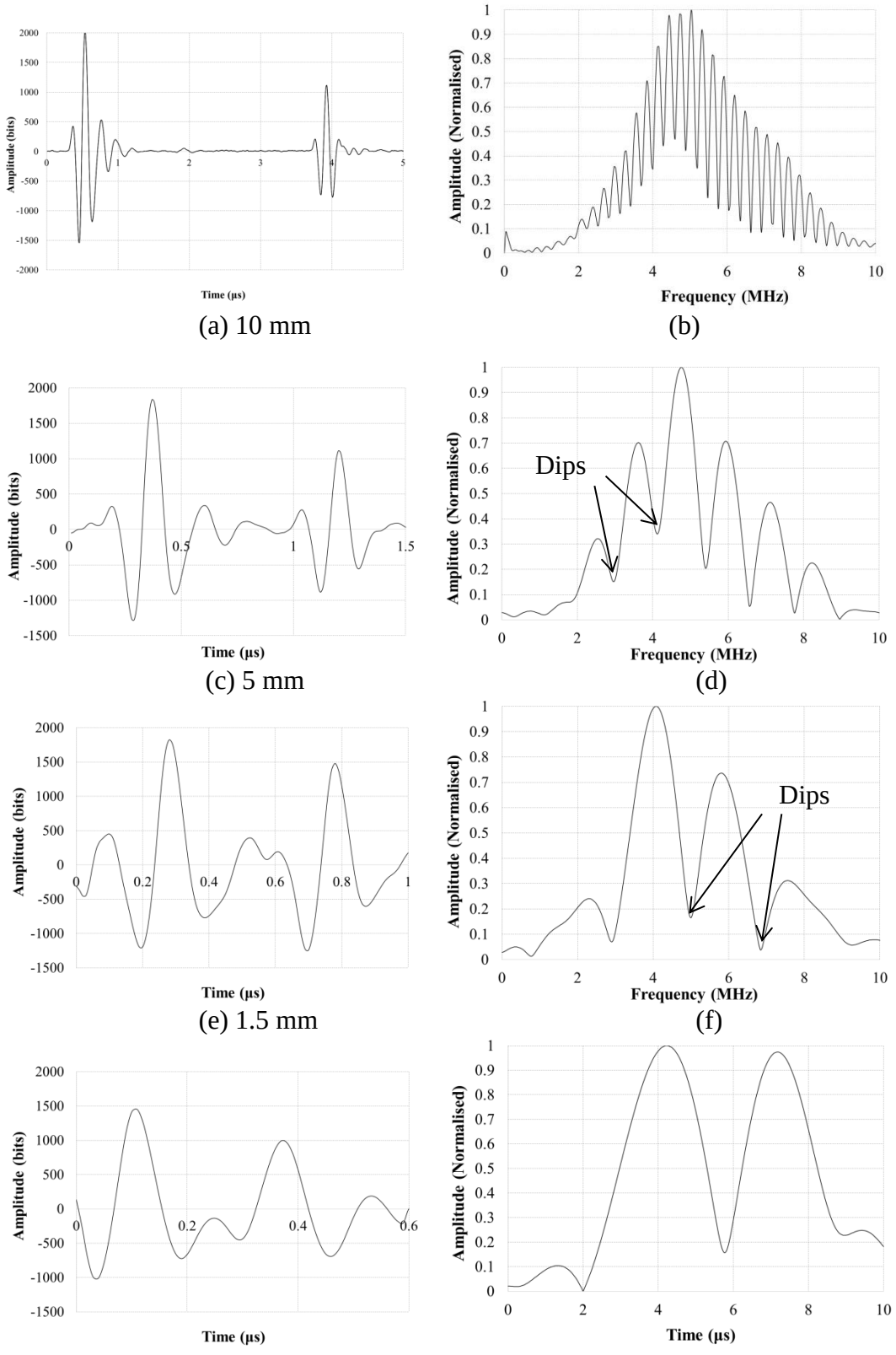

Figure 2-10. (a), (c), (e), and (g) are time domain A-Scans showing two subsequent reflections for steel blocks of thickness 10 mm, 5 mm, 1.5 mm and 0.9 mm respectively. (b), (d), (f) and (h) and frequency domain plots of the adjacent A-Scans.

With the 1.5 mm and 0.9 mm material, it can be seen that the waveforms overlap and it becomes difficult to take a zero crossing on each echo. If both echoes are viewed in the frequency domain, it can be seen that destructive interference occurs in the form of 'resonant dips', labelled in Figure 2-10 (b), (d), (f) and (h). These are destructive interferences that occur due to their being an odd integral number of half wavelengths between the two pulses, while constructive interference occurs at an integral number of wavelengths, [Silk, 1984]. This distance is a function of material thickness, *h,* and the dips occur when the thickness is a multiple of the wavelength, λ. It can be seen that the thicker the material, the smaller the gap between the dips. The relationship between material thickness, *h,* and frequency, *f,* is shown in Equation 2-8;

$$h = \frac{cm}{2f} \qquad 2\text{-}8$$

where *c* is the acoustic velocity and *m* is the dip count starting from 1. Difficulties can arise when obtaining the dip count but it is possible to take the differential of two dips and the formula then becomes;

$$h = \frac{c}{2\Delta f} \qquad 2\text{-}9$$

This method has been used to measure lubricant films in a number of publications, see Dwyer Joyce [2005] and Zhang *e al.* [2005]. The author has applied this method to the thickness measurement of solid structures.

2.3 Using Ultrasound to Measure Contact Pressure

2.3.1 The Spring Model

Engineering surfaces have an inherent surface roughness irrespective of how smooth they may appear as discussed in Section 1.5. As two solid surfaces are pressed together, the asperity peaks come into contact with one another and many microscopic air gaps are formed. The actual area of contact is very small relative to the apparent area. Assuming the asperities undergo elastic deformation, the interface can be analogised as a series of springs with stiffness, K per unit area, where an increase in nominal contact pressure, P_{nom}, results in a unit increase in deflection, u, of the two materials, described by Equation 2-10.

$$K = \frac{dP_{nom}}{du} \qquad 2\text{-}10$$

Figure 2-11 (a) shows the real engineering surface interface and (b) is the system analogised as a series of springs. The surface topography of the left image is that of ground EN24 steel R_a =0.47 μm with the scale shown on the diagram for visualisation purposes.

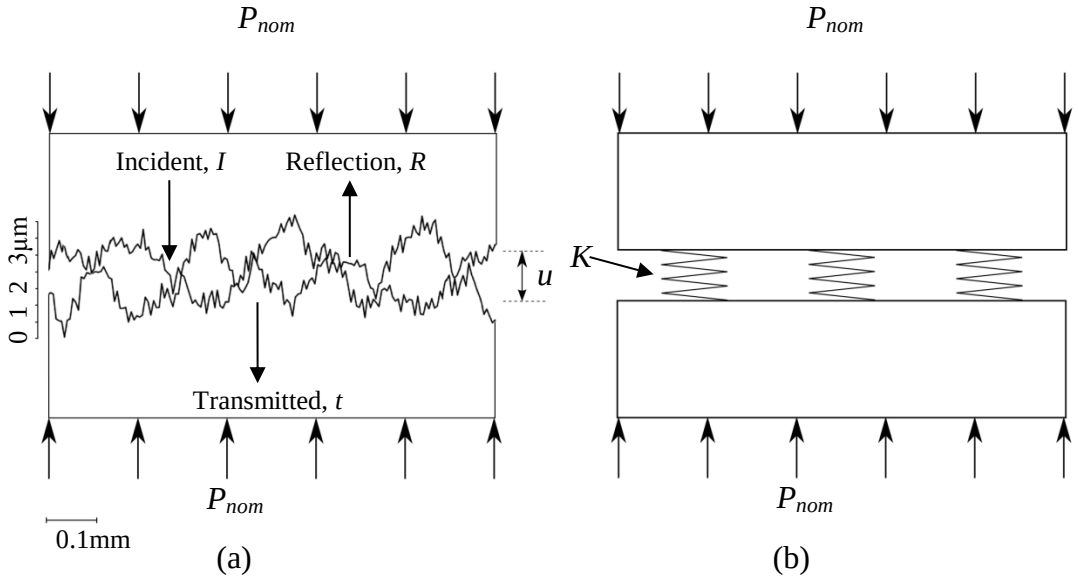

Figure 2-11. (a) is a diagram showing to scale the surface asperities coming into contact and (b) how the interface behaves as a series of springs of stiffness K.

As discussed in Section 2.1.4, an ultrasonic wave travels well through dense material, but does not propagate through materials of sparse particle density, such as air. and is therefore reflected back due to its low acoustic impedance, [Tattersall, 1973]. Figure 2-11 (a) shows two real engineering surfaces lightly loaded together. When an ultrasonic wave strikes this interface, almost 100 % of the wave will be reflected. As the nominal load P_{nom} is increased, the number of asperities in contact increases and for identical materials, 100 % of the wave will be transmitted at these contact points. For dissimilar materials, the proportion of wave that is transmitted is governed by Equation 2-4. As the load is increased, the interfacial stiffness increases resulting in an increase in ultrasonic transmission and a reduction in the measured reflection coefficient. There is still 100 % of the wave being reflected where there are air gaps, only they now make up a smaller proportion of the measured window. Kendall & Tabor [1971] discovered that if the length of the ultrasonic wave is long in comparison with the air gaps, the whole interface behaves as a single reflector therefore the ultrasonic reflection is dependent upon the spring behaviour of the interface. The reflection coefficient R can be defined in terms the interfacial stiffness, K (GPa μ/m) from the relationship;

$$|R| = \sqrt{\frac{(\omega z_1 z_2)^2 + K^2(z_1 - z_2)^2}{(\omega z_1 z_2)^2 + K^2(z_1 + z_2)^2}} \qquad 2\text{-}11$$

where ω is the angular frequency of the wave ($\omega = 2\pi f$) and z the acoustic impedance of materials 1 and 2 for the upper and lower materials respectively. Equation 2-11 is known as the quasi-static spring model of reflection [Marshall *et al.* 2004]. If similar materials are used, this equation reduces to:

$$|R| = \frac{1}{\sqrt{1 + (2K/\omega z)^2}} \qquad 2\text{-}12$$

In practice, the reflection coefficient, R, is obtained from ultrasonic measurements and from this, the interfacial stiffness can be calculated.

2.3.2 Air Referencing to Obtain Reflection Coefficient

In order to calculate the proportion of the magnitude wave reflected from an interface (the reflection coefficient, *R)*, a reference measurement of (assumed) 100 % reflection from a solid-air interface must be taken prior to contact. The phase of the wave is not considered when using this technique. When contact occurs, some of the wave will be transmitted and the magnitude of the reflected wave will decrease. A division of the measured reflected wave by the reference reflection results in a value of *R*, accounting for any mismatch in acoustic impedance of the materials. This division can take place in the time or frequency domain. Numerous external factors can influence the referencing process as discussed in Section 3.9.

2.3.3 Frequency Independence of Measurement

The interfacial stiffness values, *K*, are independent to frequency, *f*. By plotting *K* against *f*, the result should be a flat line through the usable frequency range as Equation 2-1 contains a frequency term. This is often used as a checking procedure to ensure the process has been completed. This can be seen in Figure 2-12, from Dwyer-Joyce [2005].

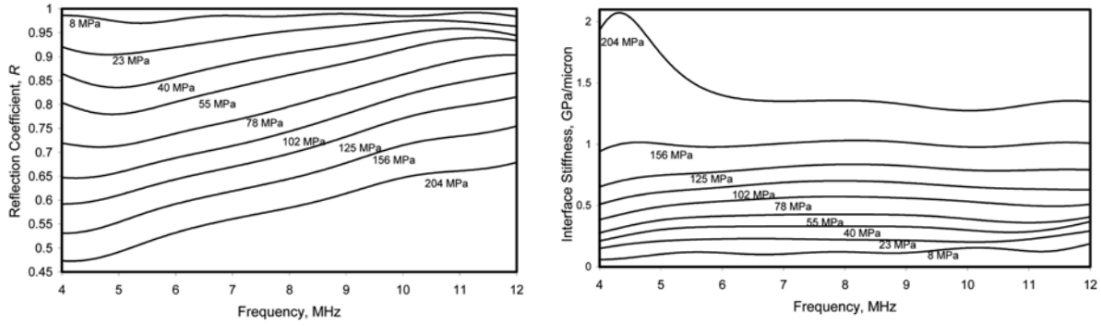

Figure 2-12. (a) a plot of frequency against reflection coefficient, R, showing how R is frequency dependant and (b), a plot of intrerfacial stiffness, K, against frequency showing how K is frequency independent, from Dwyer-Joyce [2005].

2.3.4 The Relationship between Interfacial Stiffness and Contact Pressure

The work of Kendal & Tabor [1971] clearly determined that the reflection coefficient, *R*, is not dependant on the real area of contact, *A*, but rather the interfacial stiffness of an interface which is determined by both the diameter of the asperities in contact and the asperity distribution. It is therefore impossible to determine an analytical relationship between *R* and *A* without an in-depth knowledge of the surface topographies of the contact.

Interfacial stiffness measurements are, however, a good indication of areas of conformity and can be used to infer contact pressure distribution. This alone can be an extremely useful tribological tool, but far more useful than this is the ability to extract contact pressure distribution from the reflection coefficient. Dwyer-Joyce *et al.* [2001] determined that the relationship between contact pressure and interfacial stiffness can be approximated as linear for low contact pressures (MPa).

2.3.5 Calibration

By performing a calibration procedure with like for like materials and surface topographies, it is possible to obtain contact pressure from measuring *R*. A known load is applied to a known contact area and from this, a linear relationship can be determined between the interfacial stiffness and the contact pressure that holds true for that particular contact pair. This calibration procedure takes places in a loading frame, the load and therefore known contact pressure is applied using a hydraulic actuator. The ultrasonic sensor is mounted above. This can be seen in Figure 2-13, from Marshall *et al.* [2005].

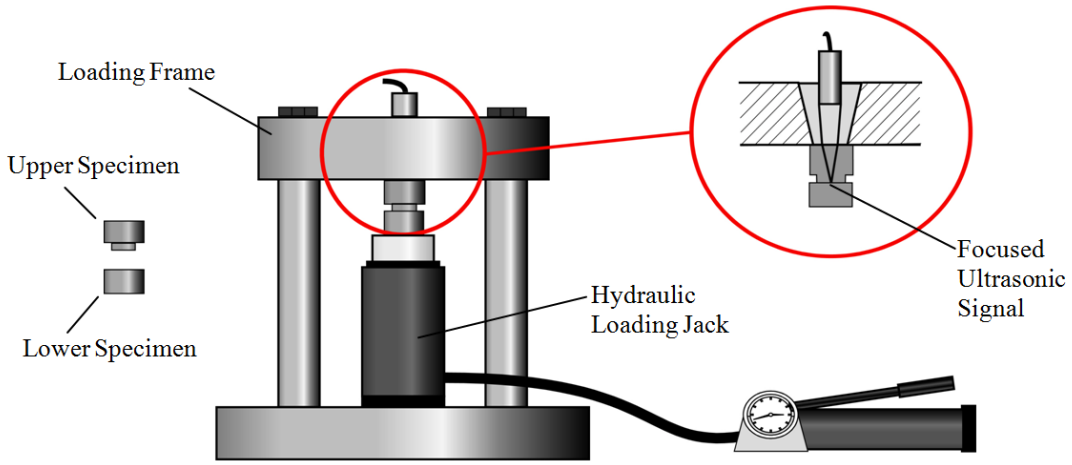

Figure 2-13. Diagram of the calibration specimens and loading equipment, from Marshall et al. [2005].

An example loading relationship for two polished EN24 steel specimens can be seen in Figure 2-14, Marshall *et al* [2005].

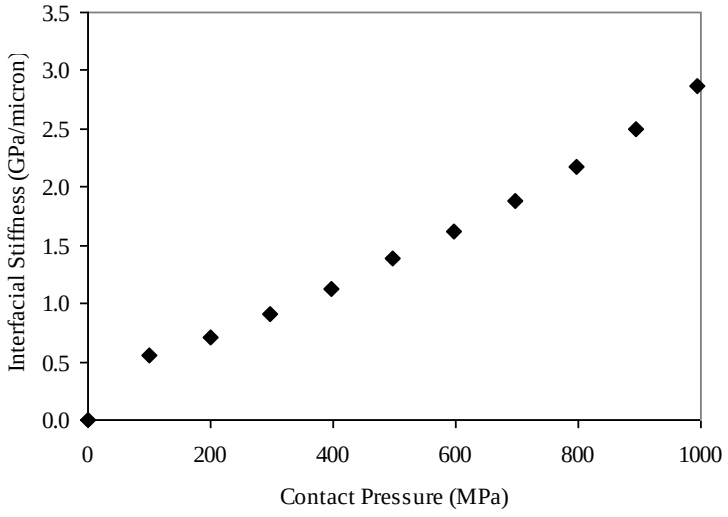

Figure 2-14. An example calibration curve relating interfacial stiffness to contact pressure, from Marshall et al. [2005].

This calibration process has allowed numerous authors to characterise contacts using ultrasonic reflectometry. Pau *et al.* [2001] have proven ultrasound as a tool for measuring the contact pressure at the wheel/rail interface with great success. Rovira *et al.* [2012] have shown excellent relationships between ultrasonic contact

measurements of the wheel/rail interface and analytical models based on Hertz model. Stancu-Niederkorn *et al.* [2000], investigated the use of ultrasound as a measurement tool of the real area of contact of metal forming. They carried out a large body of work successfully using ultrasound to characterise the contact pressure distribution of bolted joints [Marshall *et al*. 2010] and interference fits [Marshall *et al*. 2004].

2.4 Dynamic Issues

As previously discussed, even when surfaces seem to be smoothly sliding against one another, the asperity contacts are constantly breaking apart and re-forming together. During a dry sliding condition, the asperity interfaces are getting ripped apart and a result of this is vibration, juddering and chattering. There is a higher initial requirement to start sliding than there is to continue sliding, hence the static coefficient of friction is higher than the dynamic coefficient of friction. These dynamic conditions are too hostile for a contact pressure to be obtained as the interface is changing so much, it can no longer be analogised as a spring and therefore the spring model cannot be applied. Work was carried out to investigate a sliding contact by Kendall & Tabor [1971], although this work was never officially published. Hodgson [2002] carried out some interfacial stiffness measurements of numerous materials. Of those tested, it was PTFE and Copper sliding on Steel that proved to be successful as these contact pairs did not experience much wear. The results indicate that the contact stiffness drops by as much as 80 % once sliding occurs, this is due to the time dependence of asperity contacts. In some material combinations, the results showed an increase in contact stiffness with sliding. This was explained via a phenomenon known as junction growth which is a combination of both compressive and shear stress acting upon the asperity contacts.

Due to the high rate at which the ultrasonic measurements can be made (up to 200 KHz depending on thickness and path length), it is possible to detect a single moment of contact separation due to vibration as the measured reflection coefficient will momentarily revert to one. This ability to measure vibration and contact separation is a powerful tool in the characterisation of dynamic interfaces.

The ultrasonic measurement is in most cases highly affected by temperature as this affects the coupling between the transducer and the interface (see Section 3.4) and the acoustic properties of the material. This can be controlled in laboratory based static measurements but can be problematic with dynamic tribological tests as they often generate heat. There are numerous methods to factor for this, discussed in detail in Section 2.4.

3 ULTRASONIC APPARATUS

Due to the increasing demand for high quality products and asset protection, non-destructive testing (NDT) ultrasonic equipment is becoming more and more commercially available. With all exploratory work, it is crucial that the hardware used is optimised for each measurement application and there is no one device that suits all applications. This ranges from the hardware requirements such as transducer selection and portability, to the hardware settings such as excitation pulse rise time and filters.

This Section will serve as a reference, enabling the appropriate selection and assembly of a complete ultrasonic system based on specific requirements. Figure 3-1 is a flow diagram showing the fundamentals of the ultrasonic measurement process.

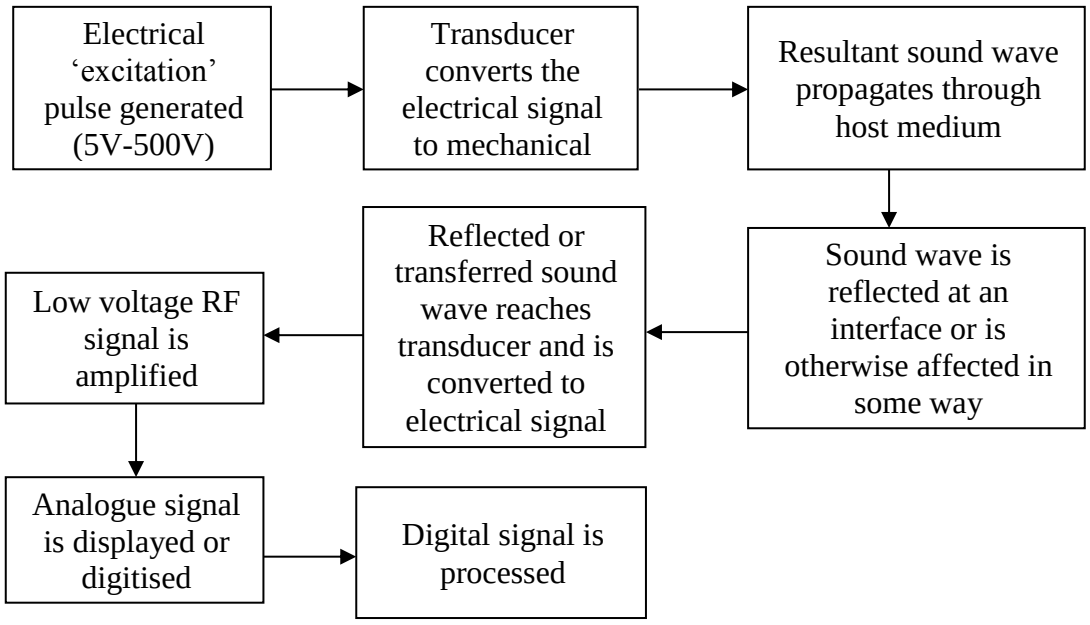

Figure 3-1. A flow diagram showing the fundamentals of the ultrasonic measurement process.

From this flow diagram, it can be seen that the ultrasonic measurement requires five crucial elements, a pulse generator, a transducer, an amplifier, a digitiser and a device to process the signal, most commonly a PC. A further important factor is the interconnecting cables that have not been included in the diagram. The pulser and the

amplifier usually come as a single device known as an ultrasonic pulser/receiver or UPR, which both sends the signal to, and receives the response from the transducer. The transducers are usually piezoelectric and the digitiser is an analogue to digital converter. The timing of the pulser and digitiser have to be in sync with one another so usually the pulser will act as a master and have a trigger output signal that sends a square wave pulse at the same time as the transducer is excited. This signal is then input into the digitiser which has a trigger/sync input so that it can display the echo waveform in the correct time. This is a far more stable option than triggering off the RF echo signal.

3.1 Pulser/Receiver

The ultrasonic pulser/receiver (UPR) is the backbone of any ultrasonic system and appropriate hardware selection is crucial. Numerous pulser/receivers exist on the market catering for a wide variety of applications and budget. The device is responsible for generating the excitation pulse and amplifying the received signal as described in the flow diagram Figure 3-1. These devices usually have the ability to pulse and receive from the same transducer, known as pulse-echo configuration, or to pulse one element and receive on the other, known as pitch-catch. Pulse-echo configuration requires the UPR to have a switch near the transducer connection that can direct the low voltage received RF signal to the amplifier. Photographs of some different UPR's can be seen in Figure 3-2 below.

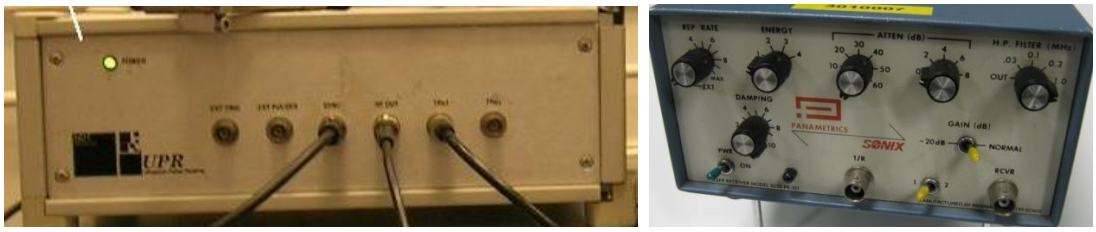

Figure 3-2. Examples of some UPR's.

3.1.1 Excitation pulses

The shape of the excitation pulse is a governing factor of the vibrational response of the transducer that determines the shape of the resultant sound wave. The optimum excitation pulse shape will be dependent on the transducer characteristics. The recommended voltage should always be checked from the manufacturer's guidelines. As a rule of thumb, the applied voltage should not exceed 50 V/mm as shown in Figure 3-3.

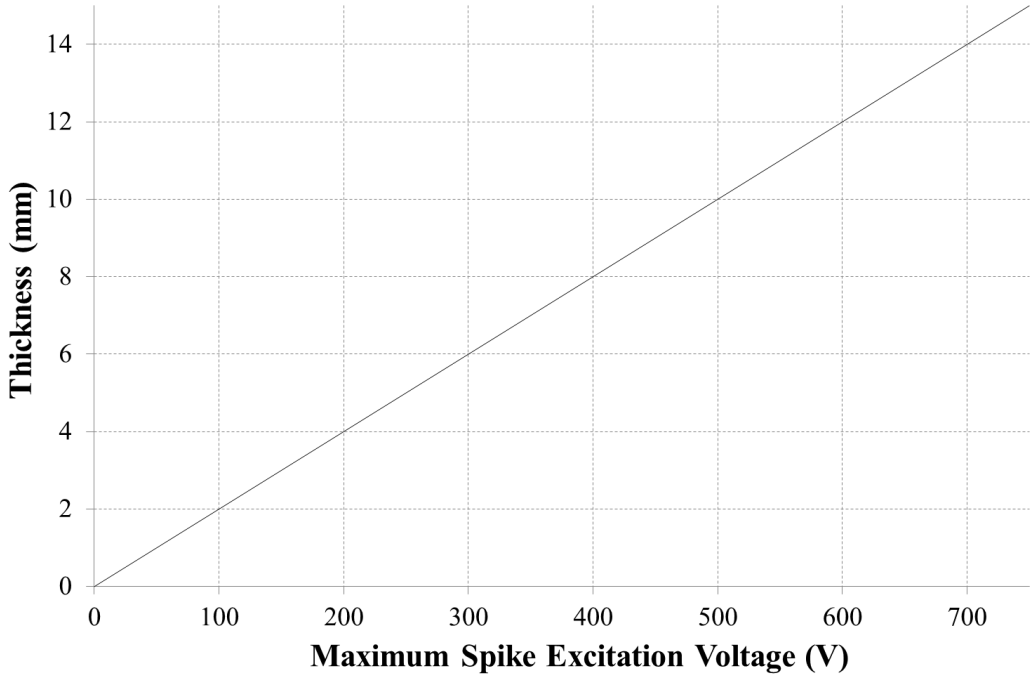

Figure 3-3. A plot showing the maximum spike excitation voltage of the piezoelectric element in terms of thickness.

When using ultrasonic elements bonded directly to the material, the required voltage is reduced due to the high level of coupling that can be achieved. The voltage and pulse width determine the amount of energy transmitted to the transducer and should be tuned so that the transducer vibrates at its natural frequency. Care must be taken to ensure the transducer does not overheat by subjecting the transducer to too much power, so attention must be paid to the applied voltage and duty cycle. The most common excitation pulse shape is a spike as it is relatively easy to create in hardware and is suitable for driving high frequency transducers for use in NDT where a

broadband response is required. The negative square wave or inverted ‘top-hat’ pulse is also popular as the user has control over the pulse width. The rise time is the time taken for the excitation pulse to reach maximum amplitude. A fast rise time (< 5 ns) is required for high frequency transducers.

3.1.2 Pulse Repetition Frequency

The pulse repetition frequency or PRF (pulses/sec) is the frequency of measurement and can be limited by a number of things. Modern ultrasonic hardware is capable of pulsing and receiving at a rate of 10’s of thousands of pulses per second with some capable of pulsing up to 100,000 pulses per second. The pulse rate is often limited by the thickness of the host medium. If the pulse repetition rate is too high, the second pulse will interfere with the subsequent reflections of the first. A method to check would be to calculate the time for the subsequent reflections to attenuate until no longer visible and this will be the minimum delay between pulses.

3.1.3 Signal Amplification

The low voltage (in the order of 1 mV) output from the transducer must be amplified before digitisation. This is usually performed in two steps; an initial low noise amplifier raises the voltage to the order of 1 V and then a variable gain amplifier is employed to increase the voltage to a level specified by the user, [Harper 2008]. This should be done to ensure the maximum range of the digitiser’s vertical resolution is being utilised. In pulse-echo mode, the same cable is used to send and receive the signal so the UPR must have switching circuitry to direct the received signal through the low noise amplifier after the generation of the excitation pulse. In pitch-catch mode the circuitry is less complicated and an external preamplifier may be employed.

3.1.4 Band Pass Filters

The returned signal can be subjected to band pass filtering that can decrease the band width of the RF signal. Low pass filters can be used to improve the signal to noise ratio for applications that do not require the full receiver bandwidth. High pass filters can be used to eliminate unwanted low frequency energy from the signal and can be used as a way of increasing receiver recovery time from strong signals such as the excitation pulse, [Imaginant, 2011]. Filtering can occur before or after amplification.

3.2 Digitisers

A digitiser is a device that converts an analogue voltage into a digital number in terms of magnitude, known as an analogue-to-digital converter (ADC). Once the signal has been digitised, it is no longer subject to the common forms of radio frequency (RF) attenuation or noise that is common in ultrasonic hardware and is therefore relatively well maintained for processing in real-time or at a later date if stored. Digital signals are still subject to noise depending on the transfer bus, but this is usually insignificant compared to analogue signals. An example of a modern digital storage oscilloscope can be seen in Figure 3-4 (a). These devices store and analyse the signal digitally and enable the user to view the signals on screen in real-time, similar to the traditional cathode ray oscilloscopes. Stand-alone digitisers are often PCI cards used in conjunction with a PC and make use of the latest high performance processors allowing the configuration and real-time processing in software. An example of a PCI digitiser can be seen in Figure 3-4 (b).

The main factors to consider when selecting an ADC are sampling rate, number of channels. amplitude resolution, bandwidth, on-board memory, noise, over sampling, data transfer rate and communications bus.

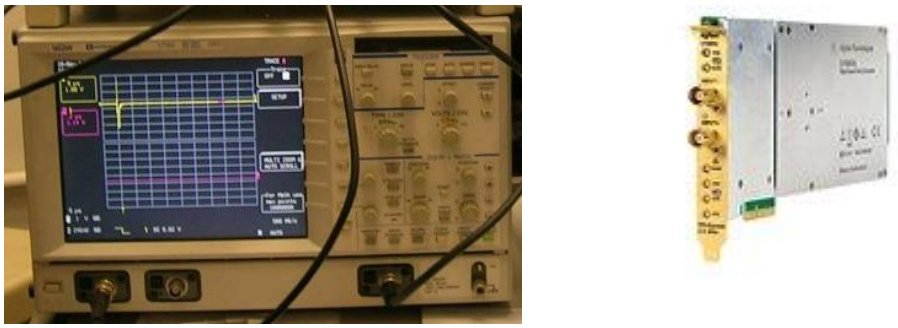

(a) (b)

Figure 3-4. (a) shows a LeCroy Waverunner digital storage oscilloscope and (b) shows an Ultraview PCI card digitiser.

3.2.1 Sample Rate

The sample rate is the number of samples per second that the analogue signal is digitised to. This is often referred to as the 'clock speed' and is measured in Hz. Most applications require the shape of the waveform to be maintained for processing and as a rule of thumb this requires a sample rate 10 times higher than the resonant frequency of the transducer to prevent aliasing. For example, if using a 10 MHz transducer, a 100 MS/s digitiser should be used to accurately retain the information in the signal (assuming a constant clock speed).

3.2.2 Amplitude (Vertical) Resolution

The amplitude resolution determines the number of voltage steps in which the signal can be divided, for example a 14 bit digitiser will split the signal into 2^{14} (=16384) vertical steps. This higher resolution is particularly important when looking at small magnitude changes in the waveforms. For the majority of applications, a 12-bit digitiser is sufficient resulting in 4096 vertical steps. Many digitisers have multiple input voltage options. The output from the digitiser will be in bits so it is important to understand the input voltage range to convert bits to volts.

3.2.3 Bandwidth

The bandwidth characteristics of a digitiser determine the range of frequencies the hardware is built to accommodate. The manufacturer will describe a frequency range of the input signal that can pass through the input with minimal amplitude loss. As a rule of thumb, it is recommended to use a digitiser with bandwidth at least twice as high as the highest frequency content of your signal to preserve the true shape of the signal.

3.2.4 On Board Memory

When operating a high speed digitiser, the data transfer rate can be in the order of GS/s. Due to this high volume of data, it is not always possible to stream the data directly to a PC as the amount of data transfer is limited by the bandwidth of the connecting bus. Data is therefore often collected in blocks and stored in a buffer on the on-board memory on the digitiser. This can then be read by the PC. Consideration must be given to ensure the net read rate is higher that the net write rate to ensure no data is lost. Some systems have the capability to perform on-board, real-time signal processing, allowing the processed signal to be transferred over the communication bus.

3.2.5 Number of channels

This is the number of different signals that can be recorded concurrently. High channel count digitisers can be useful to synchronise multiple signals such as those from encoders. Care must be taken as the number of channels can affect the individual channel sample rate. This apparatus has been miniaturised and presented in numerous forms from multi-channel PC based systems to handheld devices, but the principles of operation have stayed the same.

3.3 Ultrasonic Transducers

A transducer is a term describing any device that converts one form of energy into another, [Gallego-Juarez, 1989]. In terms of ultrasonic transducers, it is the transformation of electrical energy into mechanical energy in the form of sound and vice-versa. There are numerous different types and configurations of transducer but they all rely on the same principle. Most commonly in ultrasonic transducers, a piezoelectric (but sometimes ferroelectric) 'active' material is sandwiched between two electrodes and when electrically excited, the element vibrates in such a way that a sound wave is created which propagates through any adjacent material. The active element is polarised with electrodes attached to opposite faces. When an electric field is applied across the electrodes, the molecules align resulting in a deflection of the material. Often with ultrasonic transducers the same element is used to both transmit and receive the signal. Any reflected waves will in turn deflect the active material creating a low voltage signal.

3.3.1 Piezoelectric Materials

The piezoelectric effect is displayed by a large number of materials but only a few are of practical use for ultrasonic reflectometry. Vigoureaux & Booth [1950a] have come up with the following criteria to determine if the piezoelectric material is suitable to become a transducer:

- The material should display satisfactory piezoelectric characteristics for the modes of vibration required
- It should be homogenous throughout
- It must be capable of being worked to the desired shape and size
- The material should only display small variations of its properties with temperature
- Internal friction should be minimal
- It should be physically and chemically stable

Materials that fall within the above criteria include quartz, barium titanate, lead meta-niobate and lead zirconate-titanate (PZT), [Blitz 1963]. PZT in its pure form and PZT with various additives have been the most common material for use in ultrasonic transducers because of its strong and stable piezoelectric characteristics and its wide range of operating parameters, [Gallego-Juarez, 1989].

New advances in piezoelectric polymers and composites are being used more commonly. An important factor to consider when choosing a material is the sensitivity which dictates the resultant voltage from an applied electrical field (m/V) and vice-versa (V/m). Attention must also be paid to the curie temperature of the material. This is the temperature at which piezoceramic begins to lose its polarity and the sensitivity will be permanently reduced.

3.3.2 Element size

The thickness of the piezoelectric element determines its resonant frequency. The active elements are often disk shaped and the thickness is the dominant vibratory mode. These elements vibrate with a wavelength that is twice its thickness, [NDT-Resource Centre, 2012]. The relationship between thickness, *t*, and centre frequency, f_c, is as follows:

$$f_c = \frac{c}{t} \qquad 3\text{-}1$$

where *c* is the sound velocity in the material. For a common piezoceramic material PZT5A1, the sound velocity is approximately 2000 m/s. Therefore to have a 10 MHz sensor, the element must be 0.2 mm thick. Figure 3-5 is a logarithmic chart relating element thickness to centre frequency.

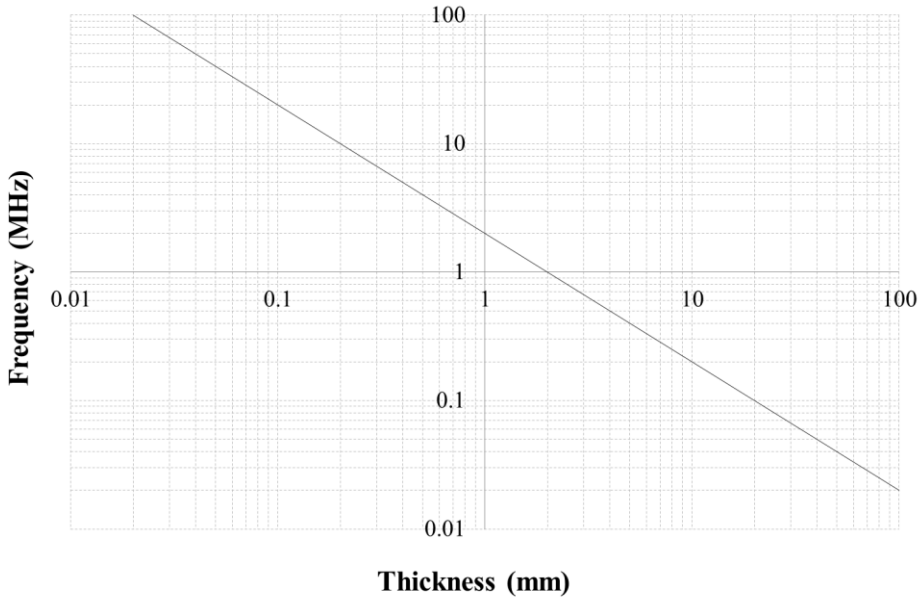

Figure 3-5. A logarithmic graph showing various elemental thicknesses and the associated centre frequency.

The element size, often referred to as element diameter if a disk shape, affects the amount of energy created by the transducer and also affects the near-field range explained in Section 2.1.6. A larger receiving element will also be more sensitive. Element size is limited because if the element is made too small, the resonant vibrational behaviour of the element will be changed by edge effects of the crystal. As a rule of thumb, the width of a material should be at least 3 times the thickness to prevent the transducer oscillating the perpendicular plane resulting in a secondary frequency mode in the transducer response.

3.3.3 Transducer Waveforms and Frequency Response

The shape of reflected waveforms can be affected by a number of external factors such as the material composition and the interface. Generally speaking the waveform shape is determined by the frequency of the element and the damping applied. The damping of the transducer determines the frequency response of the element by affecting the duration of vibration after excitation, known as transducer 'ringing'. Damping is controlled by bonding various backing materials to the rear face of the active element. By attenuating the energy behind the active element, it is possible to control the duration of the sound-wave in the time domain.

Transducers are often characterised in terms of bandwidth (%) which can be calculated as follows:

$$Bandwidth(\%) = \frac{Bandwidth}{CentreFrequency} \qquad 3\text{-}2$$

A highly damped transducer will result in a very short pulse and a broadband signal as shown in Figure 3-6 which has a bandwidth of 92 %. The bandwidth of a transducer is characterised as the bandwidth value at 50 % (or -6 dB) of the signal in the frequency domain. Figure 3-7 shows a lightly damped or un-damped transducer which results in a wide pulse with a narrowband signal of bandwidth 14 %.

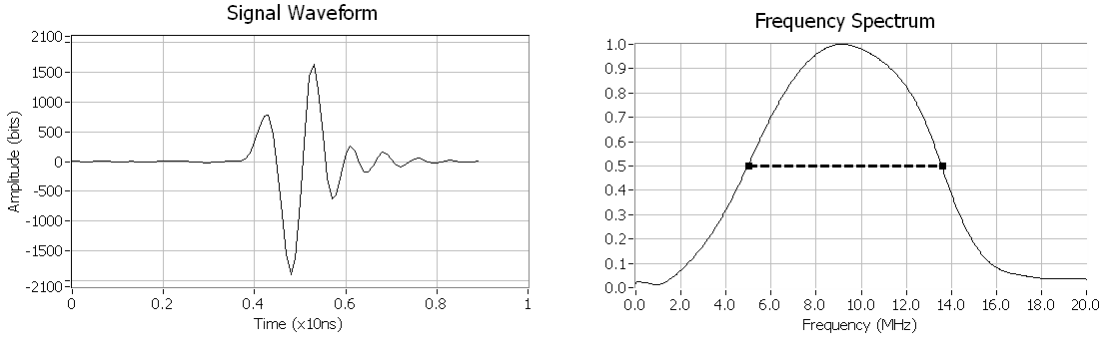

Figure 3-6. A heavily damped time-domain signal with a resultant broadband frequency spectrum.

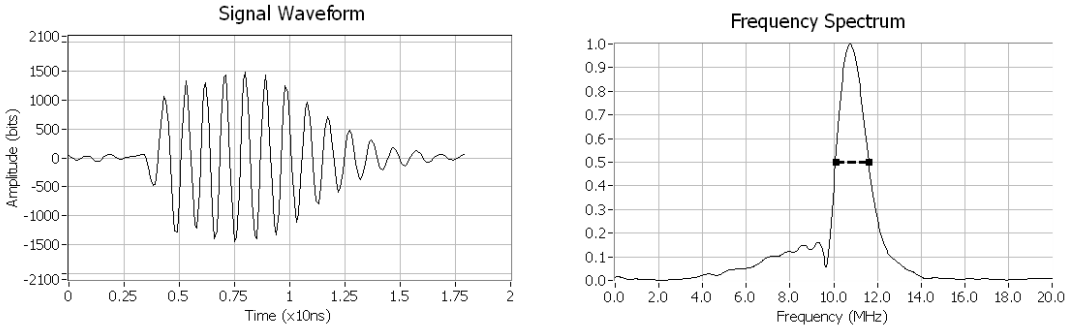

Figure 3-7. A lightly damped time-domain signal with a resultant narrowband frequency spectrum.

Bonding the transducers directly to the surface limits the amount of ringing that can occur as the vibration of the element is easily transferred to the adjacent material. This results in a relatively well damped signal without the need for bonding backing material to the rear of the active element.

3.3.4 Commercial NDT Contact Transducers

Numerous types of commercial contact transducers are available to cater for different types of measurement and have intensively been developed for non-destructive crack detection and medical diagnostics. Traditional commercial probes have an acoustically matched backing layer to control signal damping. On the underside of the element, it is common for the transducer to be finished with a wear plate which protects the active element when moving it across a surface. It is important to match the acoustic impedance of the wear plate to the material to maximise the amount of energy transferred at the interface as shown in Figure 3-8 (not drawn to scale).

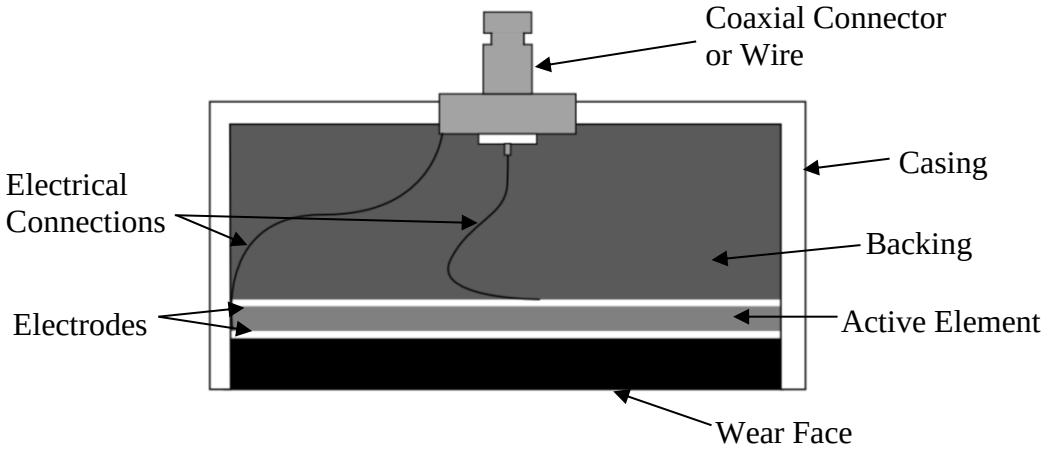

Figure 3-8. A cross sectional diagram of a commercial ultrasonic transducer.

3.3.5 Commercial NDT Immersion Transducers

Immersion transducers are those designed to be coupled with a liquid. They can be unfocused but by using a concave lens, it is possible to focus the sound wave on to a point in space, the size of which is determined by element diameter *D*, the acoustic velocity of the host material(s) and the focal length F_l. These transducers are used with a liquid medium so that is it possible to move the element closer or further away to achieve a focus at the area of interest, but also to scan in multiple dimensions. Figure 3-9 is a diagram showing two focussed immersion ultrasonic transducers. The focussed wave paths have been included. The transducer of the left is focussed onto the upper interface. The transducer of the right is focussed onto the middle interface between the two solid materials. It can be seen that the wave path is refracted due to the different acoustic impedances of the liquid and the solid. This phenomenon is explained by Snell's law, see Section 2.1.8. Consideration therefore must be given when calculating the gap between the transducer and the solid material.

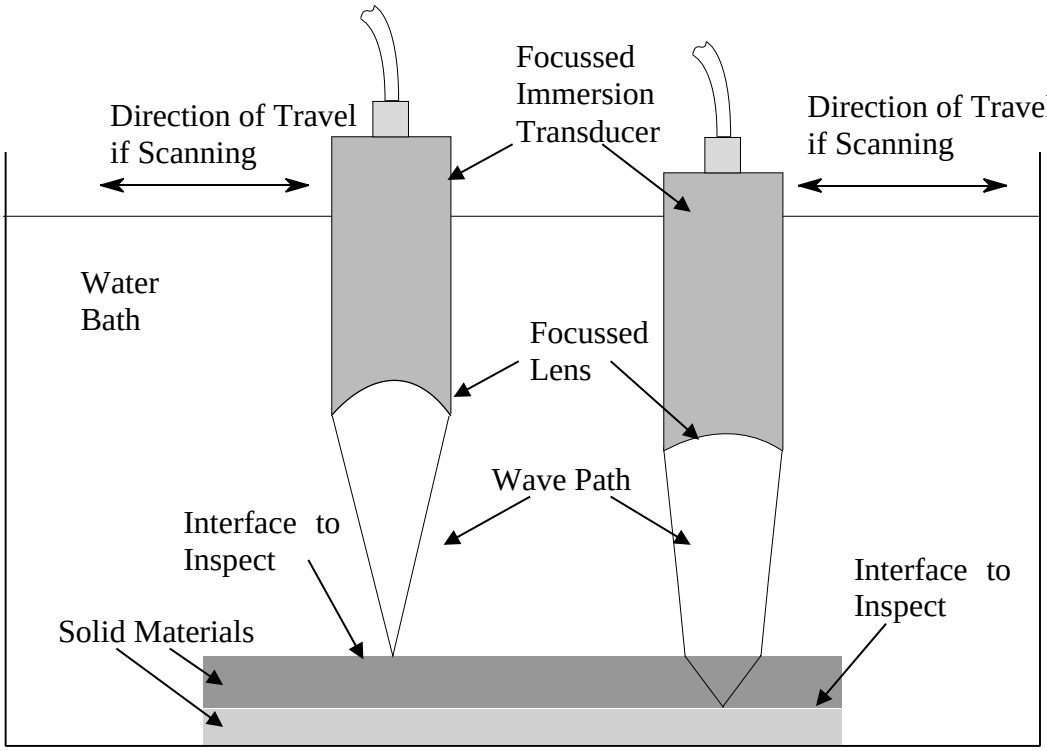

Figure 3-9. A diagram showing two focussed immersion ultrasonic transducers. The focussed wave paths have been included.

Immersion transducers can either be a linear focus or a point focus. The focal spot size, F_s, (diameter) can be calculated from Equation 3-3 from the Panametrics/Olympus technical notes [2006].

$$F_S(-6dB) = \frac{1.02F_l c}{fD} \qquad 3\text{-}3$$

where c is the sound velocity in the host material and f is the centre frequency.

3.3.6 Shear Sensor

Shear waves are a result of refracted wave mode conversion produced by angled wedges discussed in Section 2.1.8 Snell's Law, but they can be created using a transducer polarised in the direction parallel to the mating face. Shear transducers are commonly used to measure shear stiffness and Young's modulus of elasticity. It is important to note that liquid cannot support a shear wave therefore shear sensors only exist as contact transducers and a special highly viscous couplant must be used.

3.3.7 Piezo-Coatings

It is possible to deposit a piezoelectric film directly onto the component. It is an expensive process and is only suitable for high volume applications such as ultrasonic bolt monitoring. These films are thin (10's of μm) and thus are only available in high frequency. Progress is being made in the field of piezoelectric paint such as the sol-gel spray technique that will reduce the cost of application making it viable for non-destructive testing, [Kobayashi *et al.* 2007].

3.4 Coupling

Ultrasonic coupling is the term given to the medium that facilitates the transmission of a sound wave between two media, most commonly from the transducer to the host material of interest. This is achieved by the minimisation or removal of air gaps, thus creating the constant path of elastic particles required for the pressure wave to propagate sufficiently. The coupling of a transducer can radically affect the shape of the waveform and particularly affects the damping of the signal. Water based viscous liquid couplants are most commonly used in NDT contact probe applications as they are safe, low cost and simple to administer. As sound waves propagate well through water, it is possible to have the transducer at a remote location and scan the work-piece in multiple dimensions, all the time relying on the liquid to support the pressure wave.

With shear sensor applications, ultra-high viscous couplants are required; alternatively honey can be used successfully to achieve a similar result. The liquid couplant acts as a thin film and when conducting tests over a long period of time. This thin lubricant film can change and affect the magnitude of the signal over time. This is particularly apparent when the materials are under load. Solid rubber couplants can be used instead as they are less affected by this but they are highly attenuative. By bonding the transducer to the surface of the material, the adhesive becomes the couplant and allows for excellent sound wave transmission and an unparalleled degree of repeatability. This is covered in detail in Section 3.9 titled Permanently Embedded Sensors and the Measurement Process. This repeatability has facilitated many of the measurements described in this thesis.

3.5 Ultrasonic Array Systems

An ultrasonic array transducer is a device with a number of separate elements mounted together in a single housing. They typically have between 16 and 256 elements and are traditionally in a linear arrangement, although they can be built to any specification and are sometimes mounted in an annular arrangement or in a matrix grid. Figure 3-10 is a photograph of a 5 MHz 64 element ultrasonic array transducer.

Figure 3-10. A 5 MHz 64 element ultrasonic array transducer.

Phased array systems are named as such because they have the ability to pulse and received from each element separately in a programmable pattern allowing a great amount of control in the form of beam angle, focal distance and spot size. By pulsing a group of elements simultaneously with a slight delay, starting with the central element and diverging out, it is possible to create a focused beam in that plane. This can be done at high speed resulting in a two dimensional image where each pixel has had the beam focused on to it. Phased array systems and controllers are used extensively in medical diagnostics as they have the ability to rapidly scan in two dimensions through tissue and organs. Phased array systems require individual pulsing circuitry for each element and therefore are very expensive.

3.5.1 Manual Array Switching System

A novel, low cost solution has been created to enable an 8 channel ultrasonic system to take measurements using all 64 channels on a linear ultrasonic array transducer. To achieve this, it was necessary to develop an intermediate switching system to allow independent control of any of the 64 individual elements in the array transducer. A photograph of the switching box can be seen below in Figure 3-11 that was manufactured in conjunction with Tribosonics ltd.

Figure 3-11. The ultrasonic array switching box.

This apparatus is only suitable for static or highly repeatable dynamic contacts. The switching system is based on eight individual single-pole-octal-throw (SPOT) rotary switch configurations to relay the signals from the 8 channels on the pulser/receiver to the 64 elements on the array transducer. This low speed manual switching system can be set to any preconfigured pattern limited by the hard-wired SPOT configuration. These limits are described in Table 3-1 where the top row signifies the pulse/receive channel on the system and the numbers below detail the elements which the signal can be relayed to. It is possible to have any configuration of elements, one from each column, but not more than one from each column at the same time.

	Channel 1	Channel 2	Channel 3	Channel 4	Channel 5	Channel 6	Channel 7	Channel 8
Set 1	1	2	3	4	5	6	7	8
Set 2	9	10	11	12	13	14	15	16
Set 3	17	18	19	20	21	22	23	24
Set 4	25	26	27	28	29	30	31	32
Set 5	33	34	35	36	37	38	39	40
Set 6	41	42	43	44	45	46	47	48
Set 7	49	50	51	52	53	54	55	56
Set 8	57	58	59	60	61	62	63	64

Table 3-1. Possible sensor configurations of the array switching system.

3.5.2 Automatic Array Switching System

To enable a dynamic measurement, it was necessary to speed up the array switching and acquisition system. A Pickering PCI based multiplexer was used in an eight individual SPOT configuration to automatically relay the signals from the 8 channels on the pulser/receiver to the 64 elements on the array transducer. This enabled high speed automatic switching in any preconfigured pattern limited by the hard-wired SPOT configuration. The switches were configured in the same way as the manual switching systems described in Section 3.5.1. The multiplexer is capable of measuring on each of the 64 channels at a rate of 750 Hz. If the number of active channels decreases, the measurement rate of each individual transducer increases. For example, it is possible to measure on 24 channels at 2000 Hz. The maximum possible pulse repetition frequency that can be achieved with a set amount of channels can be seen in Figure 3-12. A photograph of the multiplexer connector and array transducer adaptor can be seen in Figure 3-13 manufactured in conjunction with Tribosonics ltd.

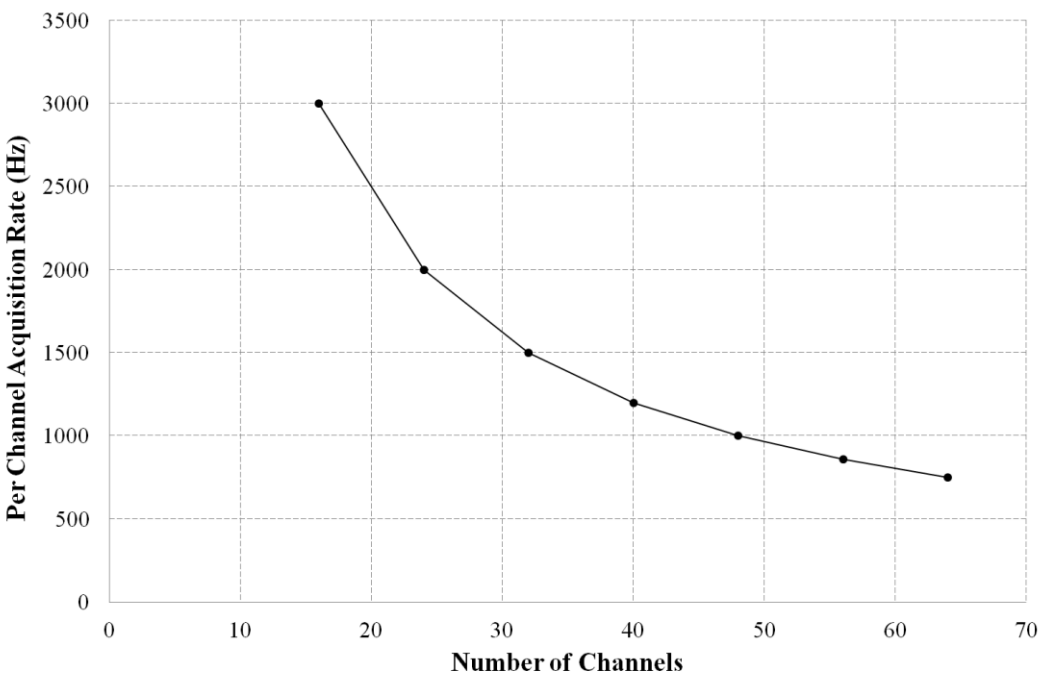

Figure 3-12. The maximum possible pulse repetition frequency achievable as a function of the number of active channels.

Figure 3-13. Pickering multiplexer connector and the adaptor to fit the array transducer.

3.5.3 Permanently Embedded Array Transducers

Section 3.4 highlighted the influential effect that the coupling has on the measurement conditions. This is particularly important when measurements are required over a long period of time or when relating to any reference measurements previously taken. Attempts were made to use a traditional array system to take a series of measurements over a period of days, but it proved impossible to recreate the same coupling condition once the transducer had been moved. These results have not been presented. Traditional systems are also at risk of being moved whilst taking measurements resulting in the entire measurement process failing due to the reliance on a reference measurement.

To overcome these issues, an array transducer that can be permanently installed was created, allowing the bonding of the transducer to the component resulting in unparalleled repeatability and a robust measurement. The piezoelectric elements were cut to size and positioned equidistantly in a linear array. Ultra-thin coaxial cables were soldered on to each element, all having a common ground. An aluminium housing was manufactured and positioned around the transducers and then filled with epoxy backing. The transducers are manufactured in such a way that the elements stand proud of the assembly ensuring optimum transmission when bonded onto the component. A schematic diagram and photograph of a 12 channel permanently installed array transducer can be seen in Figure 3-14 (a) and (b) respectively.

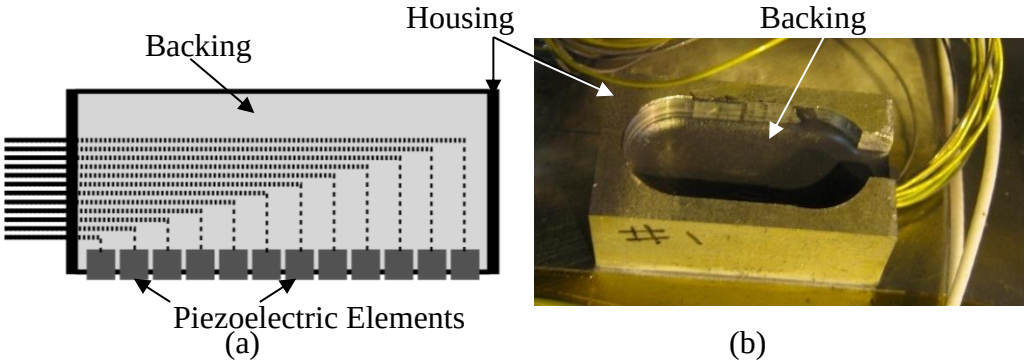

Figure 3-14. (a) a schematic cross section of a 12 channel permenantly embeddable ultrasonic array and (b) an example of one installed.

3.6 Multi-dimensional Scanning System

Scanning systems are used to move an immersion transducer to build up a multi-dimensional profile of the component under inspection. The position information of the scanning system is logged alongside ultrasonic data and then processed into an intensity plot. In the field of ultrasonics, this is commonly referred to as a C-Scan. Scanning systems are often used in NDT to automatically cover large areas. It is particularly useful for characterising static components but cannot be used for dynamic measurements due to the slow acquisition time.

3.7 Cabling

The transmission of high frequency signals requires careful consideration to ensure signal integrity is maintained. This is often achieved by using coaxial cables. Coaxial cables are termed as such because the different layers share the same geometric axis. The voltage is applied to the centre core and the metallic shield is the ground. This design minimises noise and attenuation. All connectors used in an ultrasonic system should also be coaxial. Most commonly used types include BNC, SMB, SMA, LIMO, MICRODOT and MMCX, a selection of which can be seen in Figure 3-15.

Figure 3-15. Various coaxial cables and terminations.

3.8 Measurement Set-up

The following factors must be considered when configuring an ultrasonic measurement.

3.8.1 Voltage

This is the amplitude of the excitation pulse. For commercial transducers, a pulse voltage as high as 30 V to 400 V is not uncommon. Lower frequency transducers often require a higher excitation pulse. Manufacturers usually recommend a pulse voltage value for each transducer. When bonding transducers directly to the material, much lower pulse voltages can be used, i.e., 2 V to 30 V.

3.8.2 Pulse Width

If using a square wave excitation pulse, the pulse width is the duration of the square wave in nanoseconds (see Section 3.1.4 for more information).

3.8.3 Pulse Repetition Rate/Frequency

This is the rate at which the transducer is excited per second, (see Section 3.1.2 for details).

3.8.4 Pulse Train Length

Some hardware allows the use of a pulse train which is a series of repeated excitation pulses that will affect the magnitude of the response of the transducer. The spacing between pulses is important and has to be in the same phase as the resonant frequency of the transducer to result in maximum amplitude response of the transducer.

3.8.5 Range

The range is the length of the measurement window for visualisation and data storage purposes. With ultrasonic reflectometry, it is common to only save the reflection of interest to save disk space and maximise writing speed.

3.8.6 Delay/Window Start

This is the initial start point of the measurement window.

3.8.7 Band Pass Filters

Filters must be adjusted according to sensor type and materials (see Section 3.1.4 for more information).

3.8.8 Gain

The gain is the amplification of the signal (dB) from the variable gain amplifier. Increasing the gain will amplify the noise as well as the signal of interest.

3.9 Permanently Embedded Sensors and the Measurement Process

The tribological applications of ultrasound discussed in this thesis have pushed the limits of standard ultrasonic apparatus and methods. Through a process of trial and error, the investigations have resulted in the development of new methods, the most influential of which is the use of permanently embedded ultrasonic sensors. Traditionally, NDT based ultrasonic probes have been used to generate the required signals. These devices, as discussed, require very careful development to control the damping and are therefore expensive. Another issue is the mounting of the sensors. Great care must be taken to ensure the sensors are secure and that the coupling medium stays constant throughout the duration of the measurement. Material characterisation, attenuation, contact pressure and lubricant film thickness measurements are based on a change in the magnitude of the signal. These measurements require taking a reference and then calculating a reflection coefficient,

R, as outlined in Section 2.3.2. This relationship is fed into the equations to calculate contact pressure.

In any situation when a comparison needs to be made between a reference and a measurement, consideration must be given to all external factors that may affect the measured signal. It is the experimentation and investigation into the use of permanently embedded sensors that has facilitated all of the work presented in this thesis. By bonding a sensor onto a surface, both the position of the sensor (the measurement window) and the coupling (the adhesive bond line) stay constant throughout the test. This means it is possible to take a reference measurement on one day and return at a later date to take the necessary real-time measurements. The stability of the sensor conditions allows for much smaller changes in the signal to be measured and processed, thus facilitating these new technologies and approaches. It is therefore important to fully understand what factors influence the ultrasonic signal so that they can be accounted for.

If a single reference measurement is to be used over a long period of time, these external factors can change the ultrasonic response of the measured signal thus making the reference invalid. The author devised a calibration method to account for this. It requires the instrumentation of a section of similar material referred to as a calibration sample. This sample is placed with the measured component, but it is not experiencing the changes that are trying to be measured, i.e. contact pressure or wear. By monitoring the response of the calibration sample it is possible to monitor the changes in the reflected wave (magnitude or time) and use this to adjust the reflection coefficient accordingly. It is also possible and preferential to perform this calibration by bonding a sensor onto a part of the measured component itself in a position that does not undergo change from the parameter being measured

3.9.1 How Temperature Can Affect the Measurement

Temperature can affect the measurement in numerous ways. Some adhesives change properties at certain temperatures and care must be taken to observe the glass transition temperature of the adhesive which is when the normally brittle material begins to turn into a molten rubber-like state which will result in higher signal attenuation. Figure 3-16 shows the measured changes in peak-to-peak magnitude calculated as the maximum value of the reflected waveform plus the modulus of the minimum value during a heat ramp for two different adhesives. It can be seen that the signal drops off dramatically at certain temperatures.

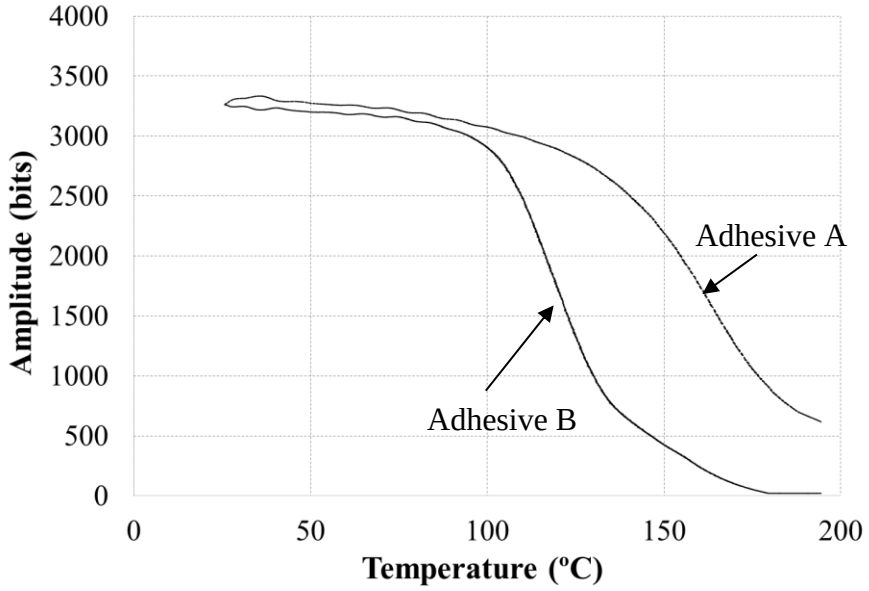

Figure 3-16. A graph showing the peak-to-peak measurements of two different adhesive combinations during an temperature ramp.

As previously discussed in Section 3.4, the coupling between the sensor and the material is of great importance. Any slight changes in this layer will massively affect the signal due to different damping modes and changes in signal attenuation. The temperature effect of different adhesives is relatively well understood in terms of glass transition temperature etc. and the manufacturers are often willing to provide this information. A test must be carried out to characterise the signal integrity is over the complete temperature operating range. Temperature will also affect the attenuation due to absorption of a sound wave as discussed in Section 2.1.5. This is

particularly evident in plastics but the affect is so small that it can generally be ignored with metal components. Both effects from temperature can be accounted for by heating the component and monitoring change in signal amplitude and time. If the change is significant, it can be recorded and accounted for in the post processing stage.

3.9.2 Electronic Hardware Influencing the Measurement

All electronic systems display individual characteristics that have an affect on ultrasonic signals due to slight variations in components such as position, resistance, the amount of solder used etc. The electrical components themselves will exhibit variation in their characteristics. These variations can be quite considerable when they are compounded, and it is important to use the same equipment at each measurement stage if comparisons are to be drawn. Another important point to consider is that the temperature of the equipment can influence the signal. This should be monitored to prevent erroneous results. The measurements that rely on time are not affected greatly but the measurements relying on changes of signal amplitude must have a dedicated channel with a reference measurement so any differences can be measured and accounted for in the post processing.

3.9.3 The Effect Electrical Noise Can Have on the Measurement

Electrical noise can have a devastating effect on ultrasonic measurements as it can often influence the A-Scan response. Care can be taken to minimise this by ensuring the equipment is electrically shielded and that the wires used are coaxial. Problems can arise when sensors are bonded onto electrically noisy components such as motors as they will then share a common ground. The noise can often be filtered out or overcome using averaging techniques.

3.9.4 Stress and Material Deformation Effecting the Measurement

The acoustoelastic effect, discussed in Section 2.1.9 can influence the measurement in a number of ways. This is particularly important to consider with time based measurements because the stress affects the speed that sound propagates through a material and this must be accounted for. It has been noticed that stresses in a material can also affect the magnitude of the signal by means of deflecting the sound wave. It stands to reason that if the speed of sound changes in different parts of the material, the sound wave path will change as dictated by Snell's law.

4 WEAR MEASUREMENT USING TIME-OF-FLIGHT

4.1 Introduction

Understanding wear behaviour of components is paramount to material selection and machine element design. Nearly all engineering components will experience some level of wear and material transfer when they are subjected to dry sliding contact conditions. It is also important in order to optimise component life, reduce maintenance cycles and maximise operating efficiency whilst minimising cost. The different methods of measuring wear that are currently available have been discussed in Section 1.7.1. It is evident that there is a lack of options available for many industrial real-time applications so an ultrasonic method has been hypothesised, tested and the findings presented in this chapter.

Section 2.2.1 describes how ultrasound can be used to measure thickness of a material by sending a sound wave travelling at a known speed through a component and measuring the time the sound wave takes to travel through the material. From this the author hypothesised that wear in the form of material removal can be measured in real-time using ultrasonic reflectometry. As the material experiences wear, the thickness will reduce and this will be seen in a change in the ultrasonic time-of-flight. This is achieved by conducting a wear test whilst measuring the change in material thickness using ultrasonic reflectometry, along with concurrent wear measurement techniques.

4.2 Pin-on-Disk Wear Experiment

It was necessary to create controlled conditions in which a component is subjected to wear so that the ultrasonic measurements can be compared to other wear measurement methods. In doing so, it should be possible to validate the method and develop an understanding of the strengths and weaknesses of the proposed technique.

4.2.1 Test Apparatus

A sliding configuration was selected as it is one of the most common causes of wear found in industrial applications. The pin-on-disk testing arrangement was chosen as it is often used as standard to measure kinetic friction and sliding wear. It is one of the most common tribometers due to the simple geometry and the large amount of control the user has over the testing parameters. An Eyre/BICERI universal wear testing machine, now known as the Cameron Plint TE99, was employed for this series of tests. A photograph of the equipment can be seen in Figure 4-1.

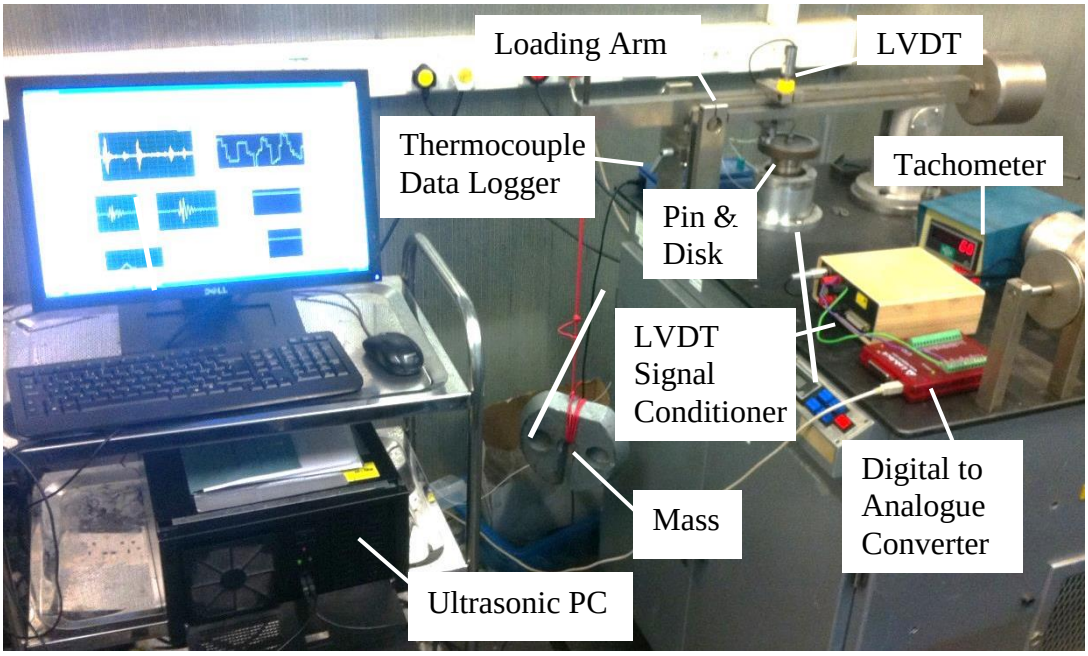

Figure 4-1. The BICERI/Plint testing rig in the pin-on-disk configuration.

The pin specimen is mounted on to a counter-balanced pivot arm that is loaded onto a horizontally rotating disk using dead weights. The resultant lateral frictional force can be measured using either a load cell or an LVDT linear potentiometer with a sprung bar.

The rugged and open design of the machine can accommodate a large range of specimen sizes and allows easy access to the contact, making the necessary additional instrumentation of the rig and specimen possible. This is often not the case with the more compact tribometers. The user has the ability to control the following parameters;

- Sliding speed
- Load
- Temperature
- Material of both fixed and moving specimens
- Surface topography of both fixed and moving specimens
- Lubricant condition
- Contact pressure (resultant)
- Environmental conditions

4.2.2 Test Specimen

The pin specimen was made from 10.8 mm diameter 1050A aluminium. This material was chosen as it is particularly effective in transmitting sound waves without creating internal reflections from grain boundaries and voids. This is important as it makes it easier to define a zero crossing point which aids when post processing. A flat bottomed slot was machined in the top of the pins to mount the ultrasonic transducer and allow the load to be transferred directly through the pin into the loading arm. A 2 mm x 7 mm 10 MHz ultrasonic sensor was bonded to the surface using thin bond line high temperature adhesive. A thermocouple was also bonded to the surface next to the transducer to monitor temperature. The slot was then back filled with a high temperature epoxy to damp the transducer and protect the sensors. A diagram of the testing specimen can be seen in Figure 4-2 on which the path of the ultrasonic wave has been drawn for illustrative purposes.

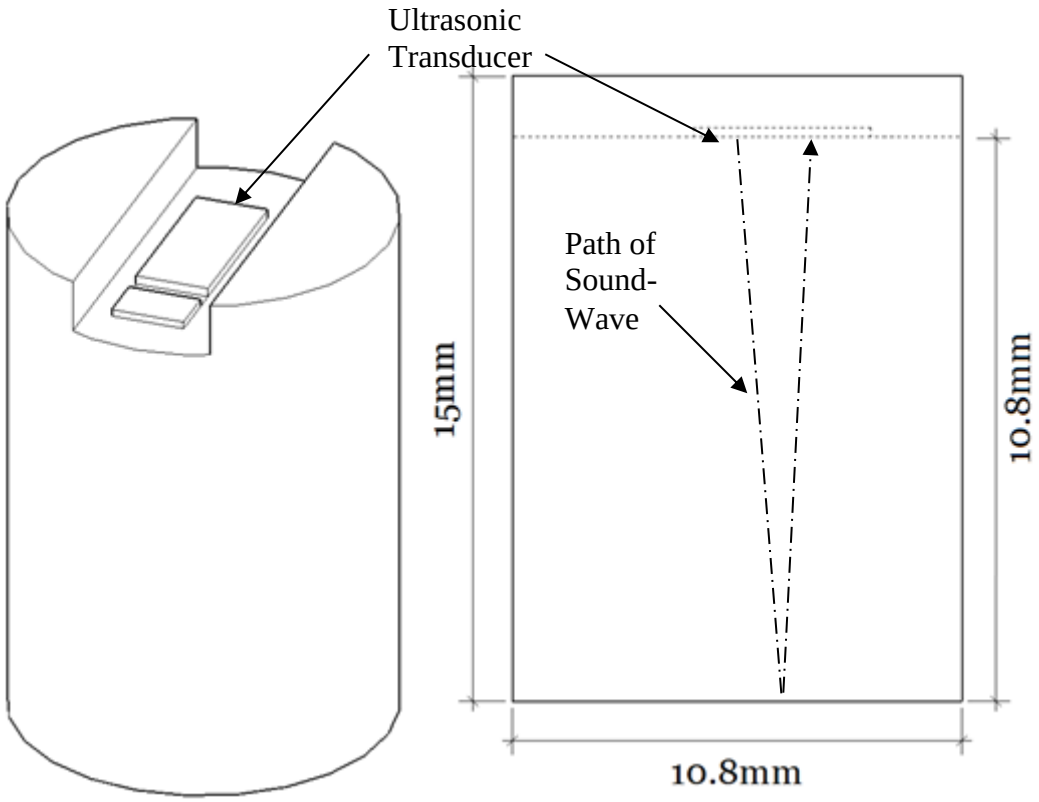

Figure 4-2. A diagram of the instrumented pin specimen.

The 80 mm diameter disk was made from AISI 01 tool steel with a ground surface of 0.4 *Ra*. The combination of aluminium on hard steel should result in a substantial amount of wear.

4.2.3 Test Condition

The tests were carried out using recommendations from ASTM G 99-95a entitled "Standard Test Method for Wear Testing with a Pin-on-Disk Apparatus". The disk was rotated at a speed of 60 rpm with the pin in contact at a radius of 40 mm, resulting in a sliding speed of 0.25 m/s. A fixed load of 5 kg was applied at the end of the loading arm with a resultant contact pressure of 1.15 MPa at the pin and disk interface. A photograph of the test arrangement can be seen in Figure 4-3.

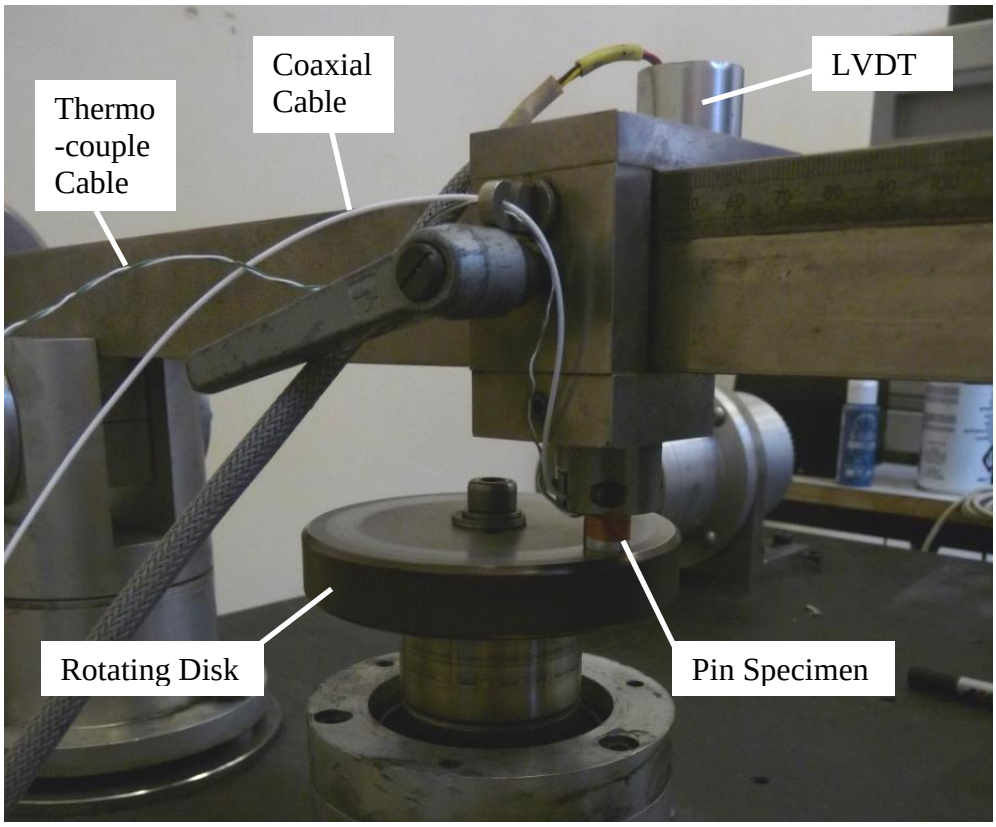

Figure 4-3. The instrumented pin-on-disk test set-up.

4.2.4 Instrumentation

Numerous wear measurement methods were employed to draw comparisons with the time-of-flight based ultrasonic wear measurement. Displacement measurements were logged throughout the tests using an LDVT fixed to the frame of the rig with the needle resting on the loading arm. This gave a live reading of the displacement of the loading arm, which is an indication of the combined wear of the pin and the disk. The displacement reading is also affected by any misalignment of the disk, the deflections in the beam and the thermal expansion effects of the assembly. The temperature from the thermocouple in the head of the pin was logged, along with test time and ultrasonic data. Mass and pin length measurements were taken at 30 minute intervals using Sartorius BP 210 D precision scales and a pair of CD-15CPX Mitutoyo digital vernier calipers respectively. The pin, cables and the specimen holder were all measured to ensure the pin was returned to the same position after being removed from the rig.

The ultrasonic measurements were taken using a Tribosonics Ltd FMS100 high performance PC based ultrasonic pulser/receiver/digitising system. The sensor was driven with a -100 V square wave pulse with a width of 120 nS. The pulse repetition rate was 2 kHz. The reflected signal was amplified by 6 db. A digitised A-Scan measurement at a single point in time can be seen in Figure 4-4.

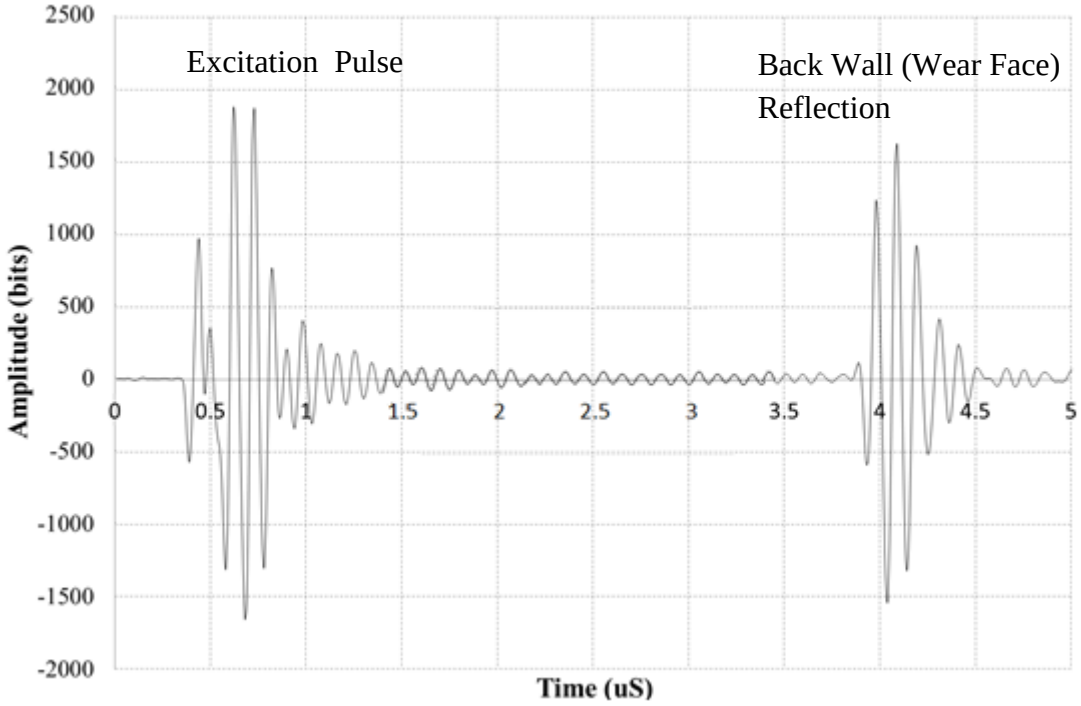

Figure 4-4. The time-domain A-Scan from the instrumented aluminium pin.

Full A-Scans were recorded at 2 kHz, along with temperature, displacement and time data. The time-of-flight (ToF) measurement points were calculated in real-time and were taken from the first downward zero crossing interval after the initial rising edge over a pre-defined threshold. More details of the zero crossing measurement method can be found in Section 2.2.1. The sound velocity, *c*, in the aluminium is 6404 m/s. The time gap, *t*, between the excitation pulse and the reference reflection is 3.37 µs therefore the distance, *d*, that the sound wave travelled can be calculated to be 0.0216 m from Equation 2-7. As the sound wave travelled both up and down the pin, the distance should be halved to relate to length of the pin, resulting in a distance of 10.8 mm.

4.2.5 Results

Figure 4-5 shows the results from a 30 minute test. The temperature measurement from the thermocouple is shown in a dashed line with the units on the left axis. The change in time-of-flight of the back wall echo is represented with a solid line with the units shown on the right axis. The recording continued after the wear test had ended and was stopped when the pin reached the starting temperature according to the thermocouple mounted on the top of the pin.

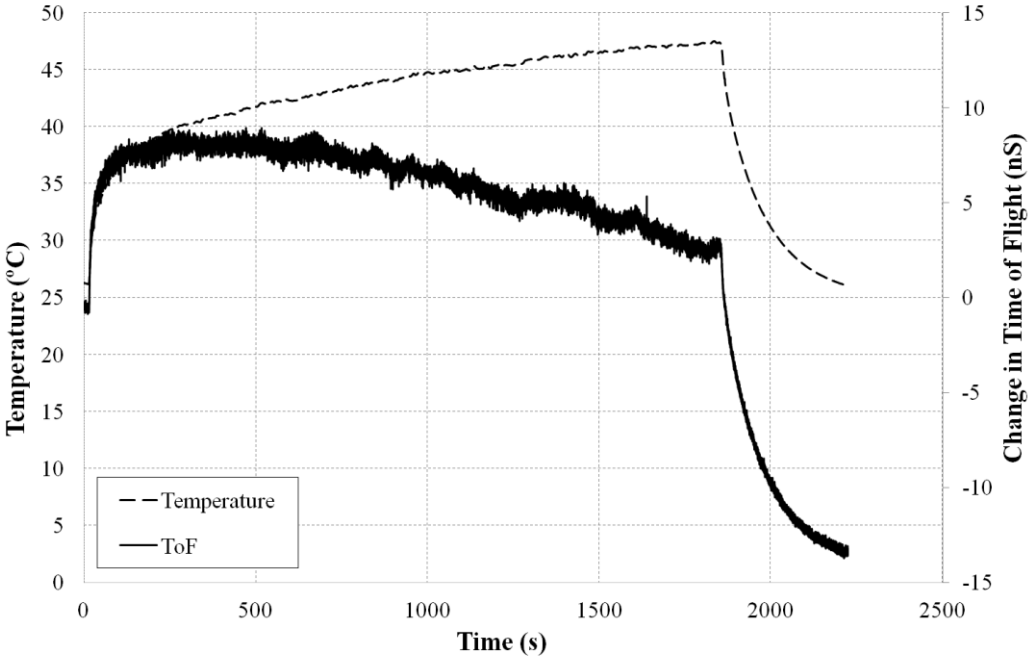

Figure 4-5. The temperature and ultrasonic time-of-flight data.

After cooling, a change in time-of-flight of 13 ns was observed, relating to a change in pin length, Δl, of 42 µm from Equation 2-7. It was then possible to calculate volumetric wear, V_w, by the geometrical relationship between the length of a cylinder, l, and the cylinder radius, r, using Equation 4-1.

$$V_w = \Delta l \pi r^2 \qquad 4\text{-}1$$

Figure 4-6 shows the volumetric wear data from the different measurement methods. The wear from the LVDT and micrometer were converted to volumetric wear using Equation 4-1 and have been plotted alongside the ultrasonic data. The measured mass lost was 0.0094 g and the wear volume was calculated using a density of 2.71 g/cm^2. The final volumetric wear measurements can be seen in Table 4-1.

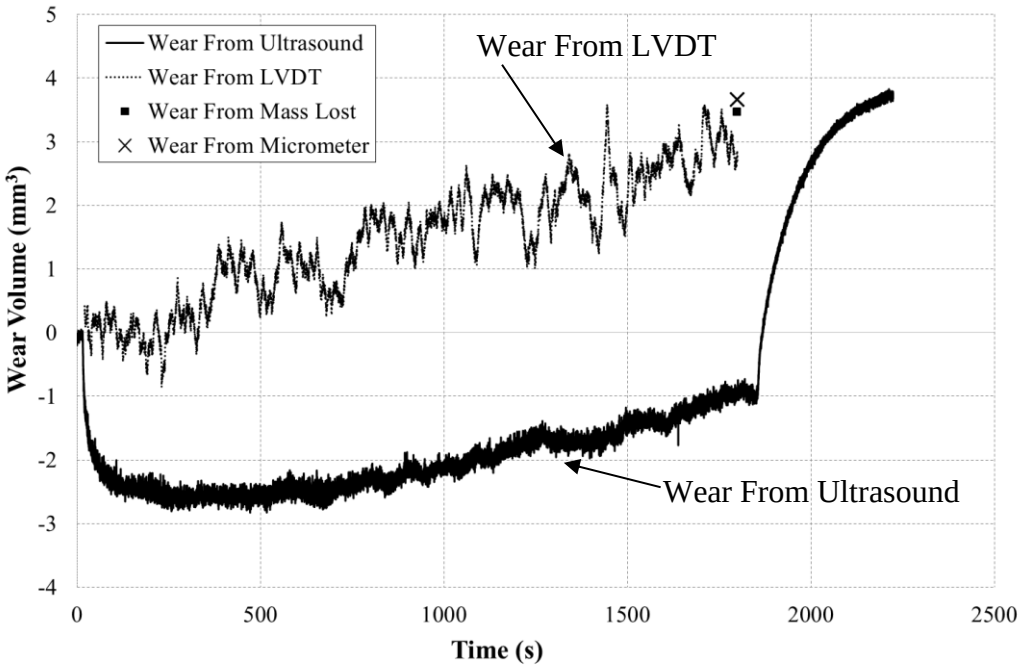

Figure 4-6. Wear test data from the pin-on-disk test.

Measurement Type	Ultrasound	LVDT	Mass Lost	Micrometer
Wear Volume at end of test (mm^3)	3.68	3. 34	3.47	3.67

Table 4-1. The wear volumes from each measurement method at the end of the wear test.

4.2.6 Discussion of Pin-on-Disk Wear Measurement

Figure 4-5 clearly shows the extent to which temperature affects the ultrasonic measurement. After 2 minutes, the measured temperature at the top of the pin had increased by 11 ºC and the measured time-of-flight had increased by 7 nS, relating to an apparent increase in material thickness of 22 µm. It would be expected that the material would reduce in thickness when subjected to a sliding wear test assuming no material transfer has occurred from the steel disk onto the aluminium pin. This measured change from the ultrasonic sensor is due to the thermal effects of the material in terms of thermal expansion and the decrease in the speed of sound in the material. Once the temperature gradient reduces, it can be seen that the thickness of the material decreases with time as expected.

It is clear that for this test set-up that the thermal expansion effects of the material are substantial relative to the wear. The ultrasonic method is very sensitive to the change in length due to thermal expansion and is therefore more suited to measurements during steady state conditions.

The results in Table 4-1 show a maximum variation in final volumetric wear measurements of 0.33 mm^3 between different measurement methods. Although each measurement method is valid in its own respect, they are all a measurement of different things.

The digital calipers provide a measurement for the change in length of the pin, but are subjected to an error from thermal expansion and there is an aspect of user variability and human error. The measurement made was of the longest point of the pin. Substantial differences from the other measurement methods will therefore arise if the wear face is not parallel to the top of the pin as the measurement would be an underestimation.

The LVDT measures the change in position of the loading arm during the test, thus indicating the real-time wear rate. As the pin and disk both wear, the arm will lower but the measurement will not be able to distinguish between the two. If material is transferred from one component to the other, this will have an effect on the results.

The LVDT is also sensitive to vibrations and irregular disk shapes, so care must be taken when processing the results and enough data points must be captured in order to average the measurement. The LVDT mounting was affected by vibration which could have led to errors being introduced.

The weighing of test specimen before and after a test is a traditional method to measure wear, but it is only an indication of total mass lost and does not consider displaced material that is not detached. It is often the case that material is displaced out of the contact zone due to plastic deformation. The density value used to calculate wear volume was given by the material supplier but variations in this value could introduce errors

Profilometry is not possible due to the geometry of the pin specimen, but is often a very powerful tool in the measurement of wear and could be applied to measure the wear on the disk.

As it is a time based measurement and the material is under load, the time-of-flight will be affected by the acoustoelastic effect and will be subjected to the errors discussed in Section 2.1.9. A loading ramp was carried out and the effects in this case were negligible.

Care must be taken when setting the measurement window to make sure it is large enough to capture the reflection throughout the entirety of the test as it moves in time when the pin experiences wear. Also the threshold of the zero crossing algorithm is important as if the waveform might change shape as discussed in Section 2.2.1.

4.3 Temperature Compensated Pin-on-Disk Wear Experiment

It can be seen from the results of Section 4.2 that the thermal effects are too significant to ignore. One method of compensating for the thermal effects would be to create a heat dependency curve. This could be achieved by conducting a heat ramp whilst logging the temperature and resultant change of time-of-flight. By monitoring the temperature of the pin during the wear test, the effect of temperature could be

looked up from the heat dependency curve and accounted for accordingly. This method would not account for the thermal gradient of the pin and further compensation would be required as this pin wore down. A more robust method was necessary.

The preferred solution would be a method that automatically compensates for the change in temperature without having to rely on a temperature measurement. An artefact was created part way down the pin specimen that resulted in a second reflection in the time-domain plot. The time-of-flight of this reflection changes due to temperature, but is not affected by wear. It is possible to use this as a reference to measure the extent that the temperature effect has on the time-of-flight of the wear face echo.

4.3.1 Test Specimen

A reference reflection was created by cutting a notch in the side of the pin specimen as shown in Figure 4-7. The path of the sound wave has been sketched and it can be seen that part of the sound wave is reflected from the solid air interface at the notch, thus creating a reference reflection. Figure 4-8 shows the A-Scan with both the reference reflection and the back wall echo. The time gap, t, between the excitation pulse and the reference reflection is 1.87 μs therefore the distance, d, that the sound wave travelled can be calculated at 0.012 m from Equation2-7.

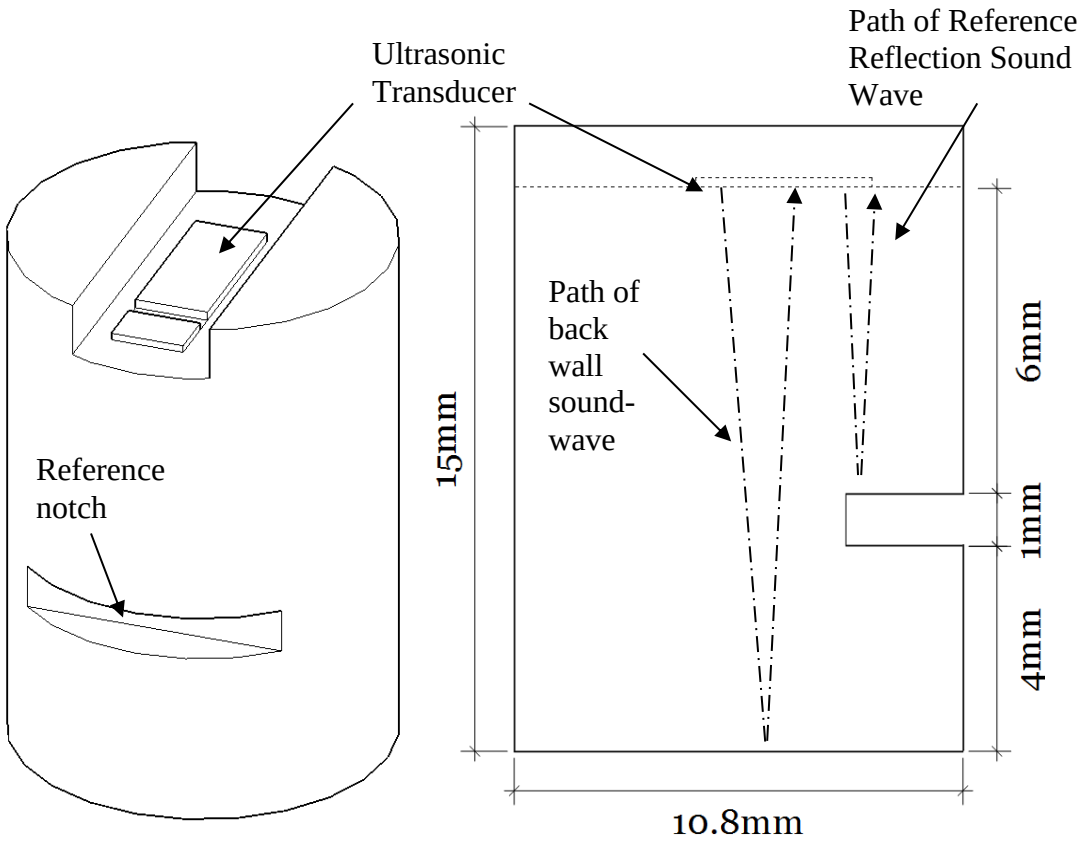

Figure 4-7. A diagram of the modified instrumented pin specimen.

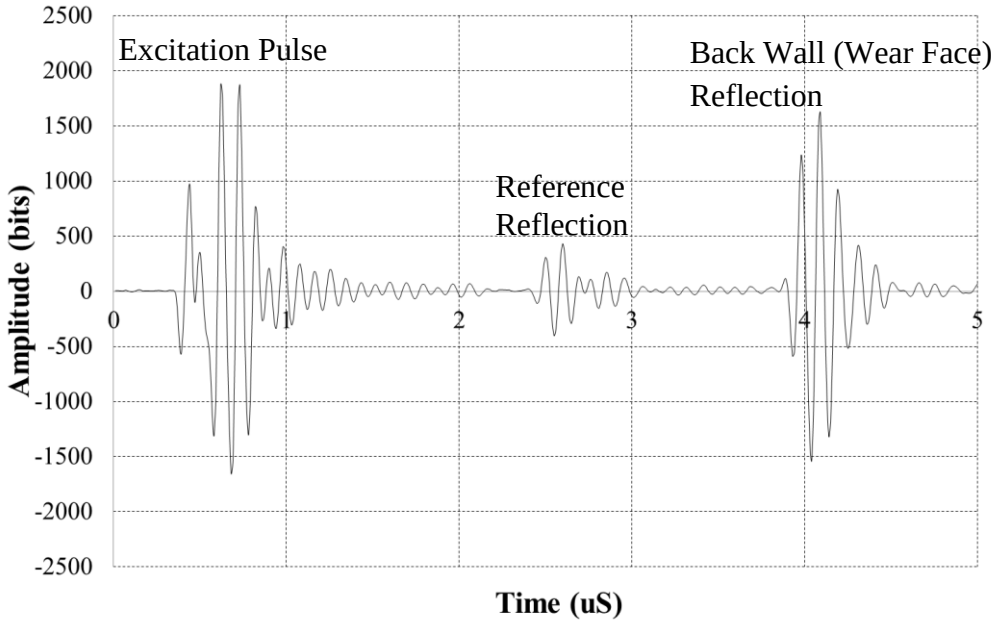

Figure 4-8. The time-domain A-Scan reponse from pulsing a sound wave through a pin with a reference notch.

4.3.2 Test Set-up

The same pin-on-disk testing equipment and testing parameters were employed as those used in Section 4.2 with the addition of the modifications to the pin specimen. Please refer to Section 4.2 for details.

4.3.3 Temperature Calibration

During the tests, the time-of-flight data was recorded for both the reference reflection, *RL*, and the full length from the back wall echo, *FL*. In assuming a linear thermal gradient, the thermal expansion measured from the reference reflection can be used to estimate the change in length of the entire pin due to thermal expansion using the Equation 4-2.

$$TL = FL_n - \left(\frac{\left(RL_n - RL_1\right)}{RL_n} \times FL_n \right) \qquad 4\text{-}2$$

where *TL* is the temperature compensated length and *n* is the measurement count. To test the method, the sample was placed in the oven and heated to 130 ºC. The results can be seen in Figure 4-9.

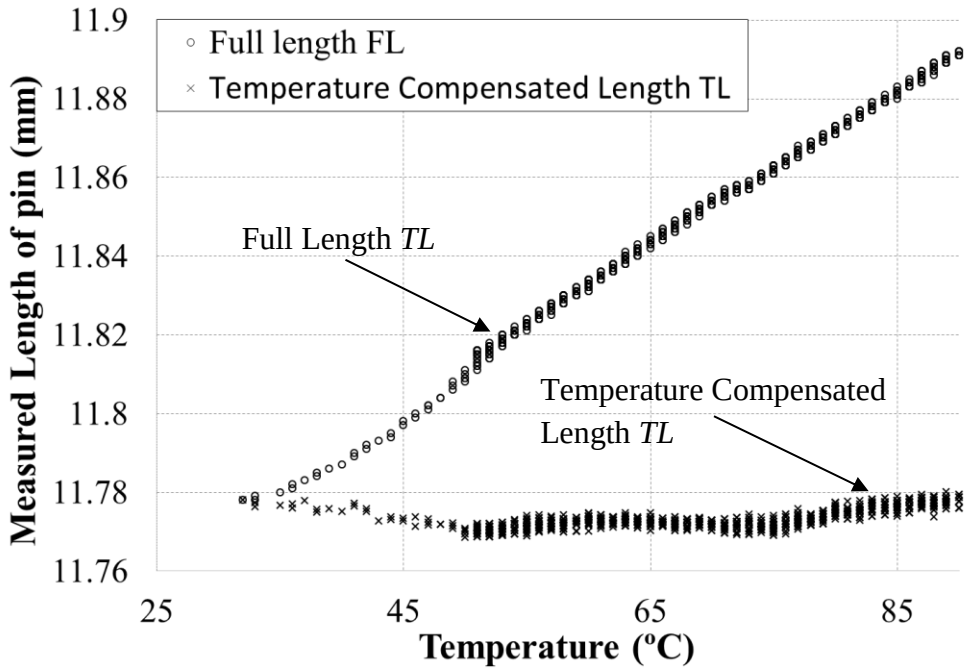

Figure 4-9. Results from the heat ramp temperature test showing the measured length and the temperature compensated length.

Figure 4-9 shows both full length from the backwall echo and the temperature compensated length from the method described. The fact that the temperature compensated length is approximately linear indicates that Equation 4-2 can be successfully used to automatically compensate for the thermal effects on the pin. Temperature affects the measurement in two ways, firstly the pin itself will expand with an increase in temperature and secondly the acoustic velocity in the material is altered. By working out the expected extension of the pin due to thermal expansion, it is possible to determine to what extent there is a change in acoustic velocity. The thermal expansion relationship can be seen in Equation 4-3.

$$\Delta L = \alpha \times L_1 (T_2 - T_1) \qquad 4\text{-}3$$

where ΔL is the change in length due to thermal expansion, L_1 is the initial length, α is the thermal expansion coefficient and T_1 and T_2 are the initial and final temperatures respectively. The thermal expansion coefficient of aluminium is

$22.2x10^{-6}$ m/mK. The ultrasonically measured change in length of the pin from an increase in temperature of 58 ºC was 0.113 mm. The expected change in length calculated from the linear thermal expansion relationship, Equation 4-3, was 0.015 mm. Comparing this with the results from the oven test, it can be seen that the dominating factor affecting the ultrasonic measurements is not the thermal expansion of the pin, but rather the change in the acoustic velocity in the material with temperature to the ratio of approximately 7.5:1. The empirical relationship Equation 4-2 accounts for both the thermal expansion of the material and the change in acoustic velocity. If the temperature across the pin was accurately know, it could be possible to estimate TL from Equation 2-1 and 4-3.

4.3.4 Results

The results from the first test can be seen in Figure 4-10. The test was halted every 30 minutes to take the static wear measurements. The plot shows the temperature compensated wear from the ultrasonic (UT) method, wear from the mass measurements, the wear from the digital calipers and the wear from the LVDT.

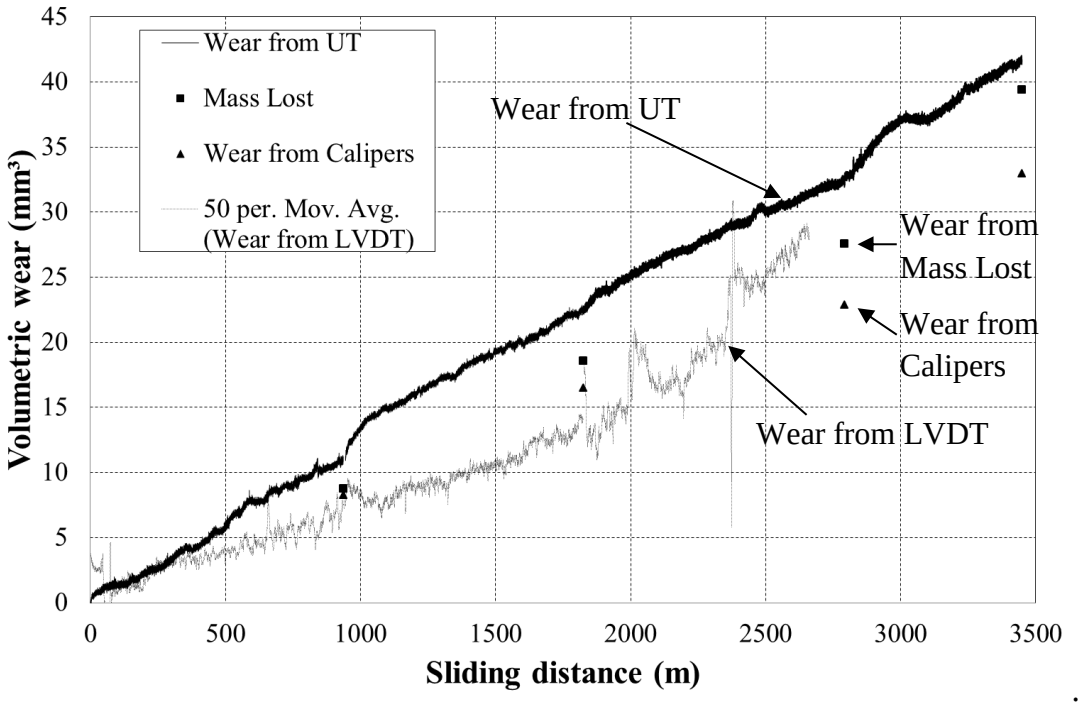

Figure 4-10. The results from a wear test showing measured wear from ultrasound (UT), mass lost, digital calipers and an LVDT.

4.3.5 Discussion of Temperature Compensated Wear Measurement

The temperature compensation appears to have worked successfully as the measurement seems relatively unaffected by temperature. The measurement of full length varied 0.95 % over a 60 ºC increase in temperature and the temperature compensated measurement varied by a maximum of 0.08 %. There is considerable variation in the different measurement methods shown in Figure 4-10. The reasons for these differences have been discussed in Section 3.9.1. The temperature compensation model assumes a linear temperature profile across the length of the pin. This is quite a large simplification as the temperature profile would be exponential.

The digital calipers have reported the smallest wear volumes as they are taking a reading at the maximum point on the pin. The mass loss method has reported smaller wear volumes than the UT measurements. A contributing reason for this is that the method does not consider displaced material as wear. An example of displaced material during a wear test can be seen in Figure 4-11. It would be possible to manually remove the displaced material, but this would disturb the natural behaviour of the specimen and introduce some human interaction effects which could vary between repeated tests.

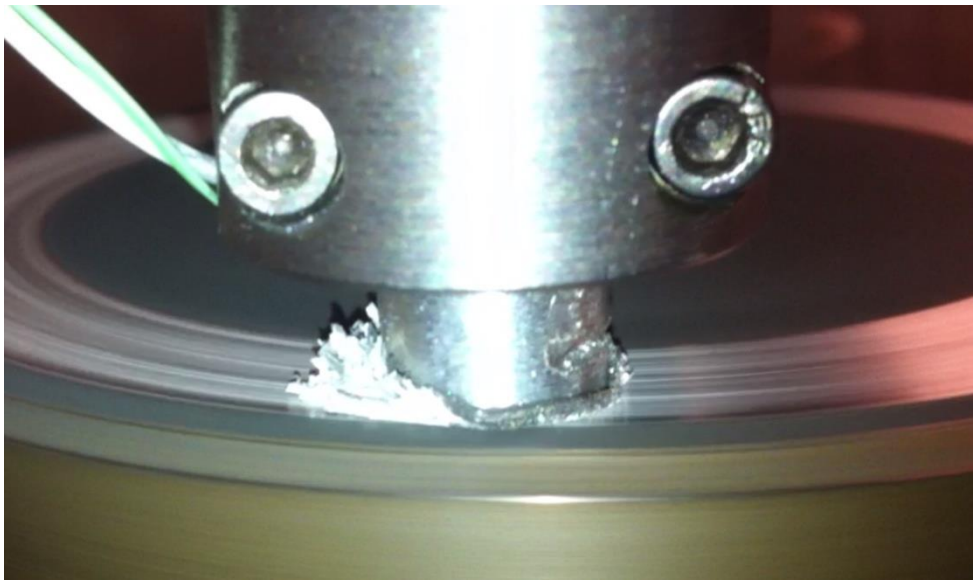

Figure 4-11. The pin and disk mid-test with the pin experiencing a large amount of material displacement.

The LVDT measurements were not very reliable due to the experimental set-up. The disk was not perfectly flat, necessitating the use of a moving average. Furthermore, the LVDT went out of range after 2700 m sliding distance resulting in an incomplete data set. Testing using a tribometer with a better displacement measurement system would provide a more thorough validation.

4.4 Further Work and Industrial Applications

The fact that the method is non-invasive means that it is suitable for the measurement of wear in industrial applications without affecting the tribosystem. The low cost sensors are small in form and can easily be retrofitted to existing machines. Care must be taken to position the sensor so that the wave strikes the interface at the correct position and some modification of the component might be required. This would then mean that the measurement system was no longer non-invasive. Measurements in components with more complicated geometries can be achieved using the pitch-catch configuration.

The ultrasonic time-of-flight wear measurement technique is a measurement of change in the length of the pin alone. It is potentially possible to also measure the wear of the disk using the same sensor. Depending on the wearing interface, a

proportion of the sound wave might be transferred to the disk and would reflect off the back-wall. Some of this wave will then be transferred back into the pin and this will be sensed by the transducer. The time-of-flight will be visible in the time domain plot, and from this the thickness of the disk could be calculated.

Temperature compensation through referencing can be achieved by carrying out a time-of-flight measurement on any part of the component that does not experience wear, but undergoes similar thermal changes as the point of desired wear measurement. Component geometries like these are often easy to find in industrial applications thus making temperature compensated wear measurement using ultrasound a viable method.

4.5 Conclusions

This work has proven that ultrasonic reflectometry can be used to measure wear in a sliding contact. Errors are introduced with temperature in terms of thermal expansion and the change in acoustic velocity of the material. A method has been presented to account for these changes but further work could still be carried out by calculating the thermal gradient of the pin and working out the resultant change in time-of-flight from this. There are more robust methods of measuring time-of-flight discussed in Section 2.2.1. These methods could be explored further to create a more robust measurement system. If the component was at steady state temperature, the wear rate would be independent of temperature.

5 WEAR MEASUREMENT FROM FREQUENCY FEATURE

5.1 Introduction

The wear from time-of-flight method explored in Chapter 4 was limited in measurement accuracy due to the large effects that temperature has on the measurement. It can be difficult to achieve the required measurement accuracy when applying the technique to a working industrial environment. A method is presented in this chapter that aims to reduce these temperature induced discrepancies to an absolute minimum by creating a temperature reference point very near the running surface. The issue with this approach is that when the two reflected waveforms get so close to each other, they begin to overlap and the zero crossing method cannot be used. The phenomenon known as the resonant dip method described in Section 2.2.2 has been used successfully to measure thin lubricant layers by looking at the reflected waveforms in the frequency domain, [Dwyer-Joyce *et al.* 2002]. The author hypothesises that this technique could be used to measure wear from Equation 2-9, whilst minimising the temperature effect.

If a reference artefact such as a small hole is created very close to the running surface, it will partially reflect the sound wave, shown as the arrow t_1 in Figure 5-1 (a). The rest of the wave will continue to travel through the material and reflect off the solid-air interface, shown as arrow t_2 in Figure 5-1 (a). If the hole is close enough to the solid-air interface, i.e. if t_1 tends towards t_2, the two wave fronts will begin to interfere with one another and each individual reflection becomes difficult to distinguish in the time domain, shown in Figure 5-1 (b). By performing an FFT, the frequency domain plot reveals destructive interferences that are a function of the distance between the two waveforms, related by Equation 2-9. See Section 2.2.2 for further details about the method.

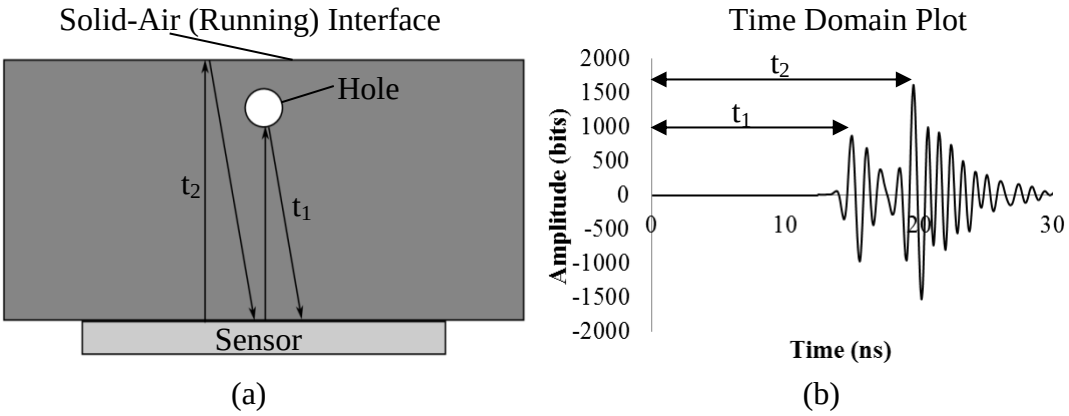

Figure 5-1. A diagram showing an instrumented block of material with a hole near the running surface.

If it is possible to accurately measure the distance between the reference artefact and the running face using ultrasound, it stands to reason that it therefore possible to measure the wear. As material is removed, the distance between the reference artefact and the wear face will decrease. This is the concept of the wear measurement technique using the frequency feature method.

5.2 Reference Geometry Investigation

The first task was to establish the optimum method of creating this subsurface reference reflection. A series of different designs were cut into a material and then a controlled wear test was carried out to assess the functionality of each design.

5.2.1 Test Specimen

It was decided that subsurface circular holes would be the preferential option to create a reference reflection as they are simple to manufacture using standard or spark drilling and they can be positioned in such a way that does not alter or interfere with the running surface. Small slots or square holes might yield a better result as the wave would strike a perpendicular interface, rather than a curved one, but the holes themselves would be difficult to manufacture.

An AISI 01 tool steel test block was designed with 8 different configurations made up of 0.6 mm holes in different spacings. Figure 5-2 shows the diagram of the block with 0.6 mm holes and Figure 5-3 is a photograph of the test block. The ultrasonic sensors used were 7 mm diameter 10 MHz piezoceramic sensors bonded onto the surface using m-bond 610 cured at 140°C. This frequency sensor is ideal for this size hole as higher frequency waves will attenuate too much as they passes through the steel and if the frequency was lower, they not be as effected by the frequency features. The sensors were mounted on the far side of the block.

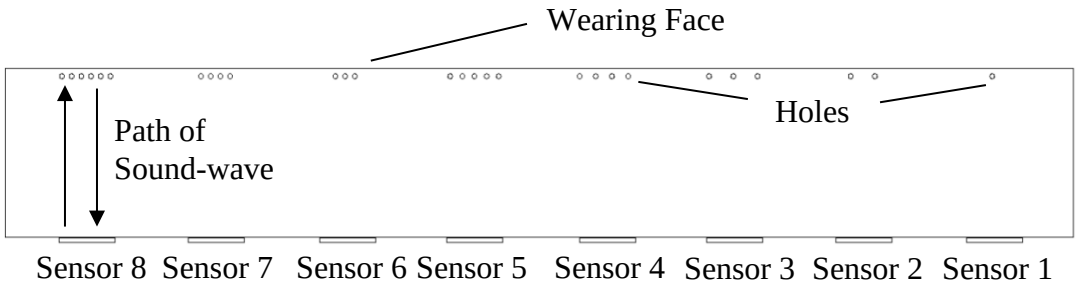

Figure 5-2. A diagram showing the different 0.6 mm hole spacing configurations.

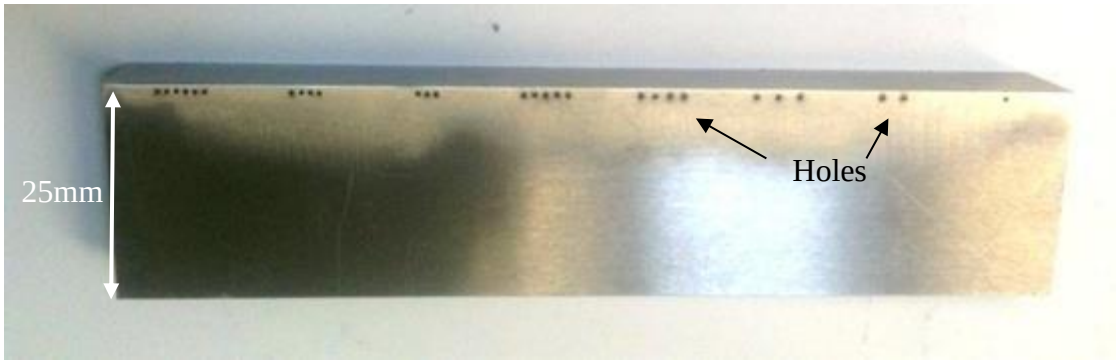

Figure 5-3. The test block with the 0.6 mm holes in various spacing configurations.

5.2.2 Experimental Set-up

The test block was mounted in a vice on the two axis magnetic bed of a surface grinder, the schematic arrangement shown in Figure 5-4. The grinding wheel was used to remove the material and simulate wear by a controlled amount in each step. A small known step, validated with dial gauge with an error of 0.02 mm, was systematically removed from the upper face of the instrumented block. A photograph of the test set-up can be seen in Figure 5-5 with a close up image of the contact shown in Figure 5-6. The ultrasonic sensors were pulsed at 30 V with a pulse width of $7x10^{-6}$ s. The reflected waveforms were recorded with the depth information and temperature after each pass. The material removed was calculated using the resonant dip technique from Equation 2-9 after the test during post processing, see Section 2.2.2 for details. The optimum configuration will result in clearly defined dips in the frequency domain in order to easily track their movements to measure the change in thickness from Equation 2-9. Two example hole configurations and the resultant affect they have on the ultrasonic signals have been described in this Section.

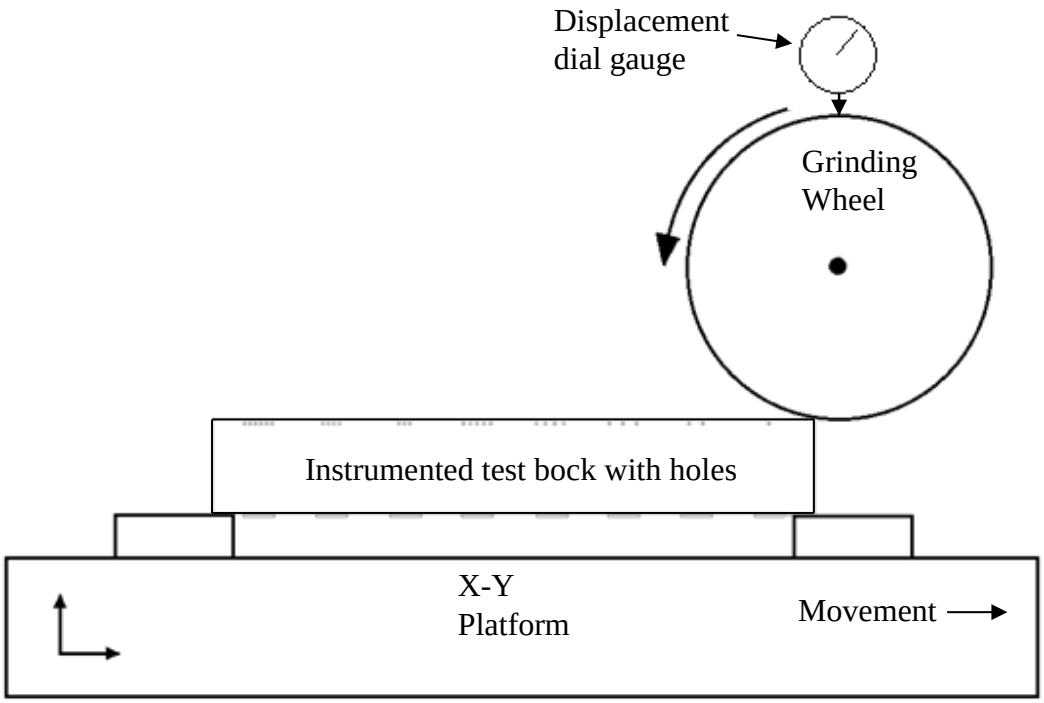

Figure 5-4. A schematic diagram of the testing arrangement.

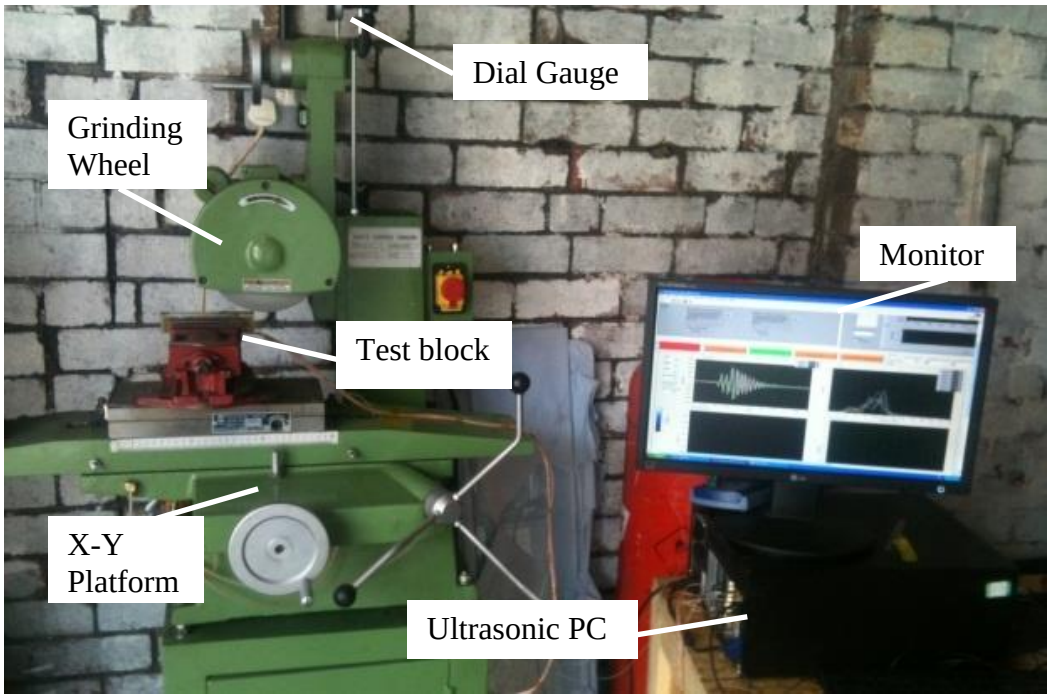

Figure 5-5. The testing arrangement.

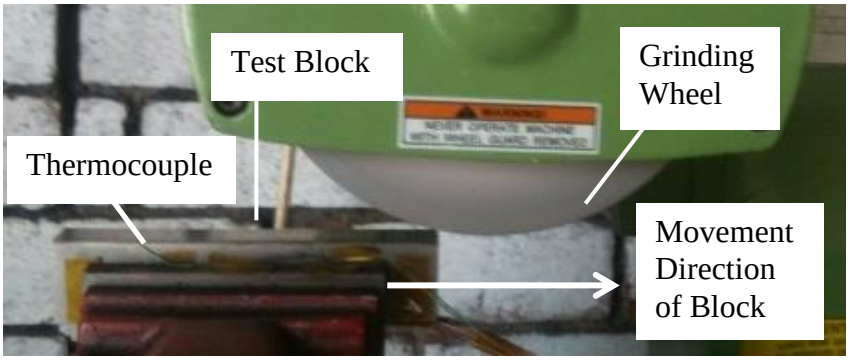

Figure 5-6. The grinding disk and the test block.

5.2.3 Results from a Good Feature Configuration

The configuration of the holes determines the shape of the reflected waveform for reasons described in Section 2.2.2. Figure 5-7 (a) shows the position of the holes relative to the running face of the block that resulted in an ideal response. Figure 5-7 (b) shows the reflected signal in the time domain and Figure 5-7 (c) shows the FFT of the signal with the dip numbers (M) highlighted. The resultant dips from this

configuration are clearly defined meaning they will be easily tracked as they move position as the material is removed.

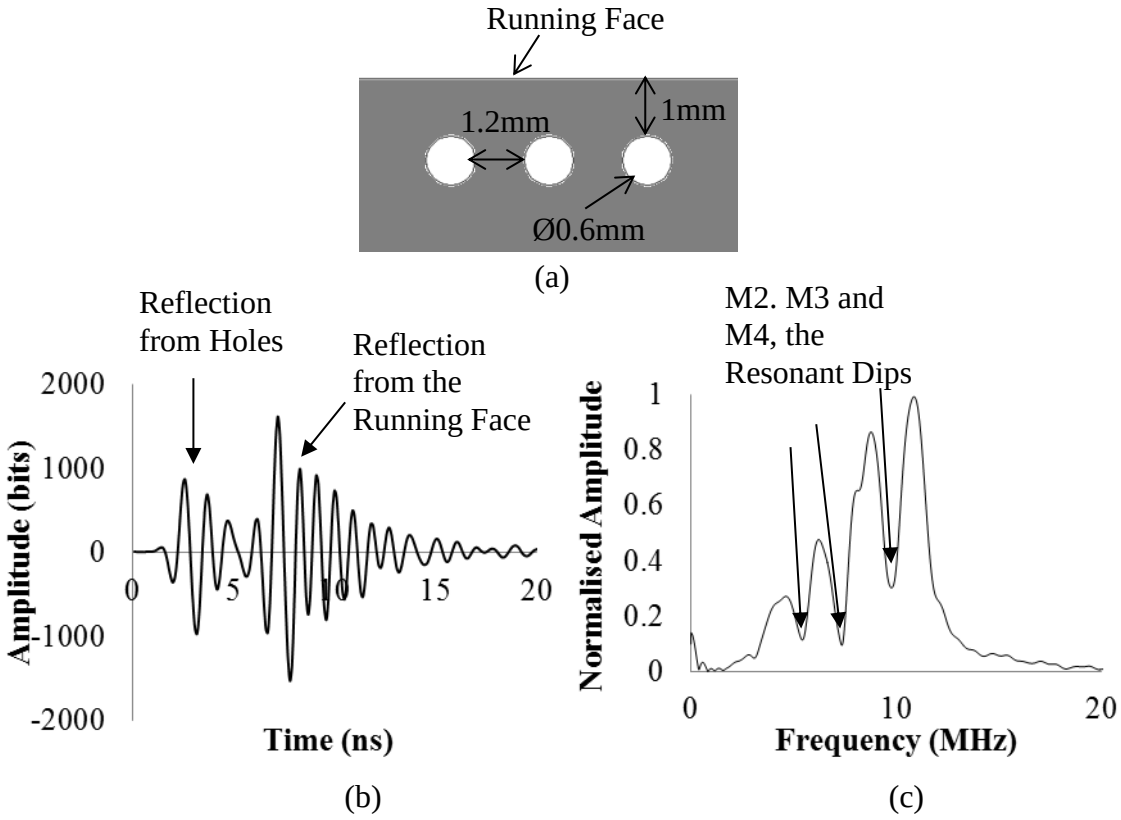

Figure 5-7. (a) shows the position and size of the holes relative to the running face of the block, (b) shows the reflected signal in the time domain and (c) shows the FFT with the dip numbers (M) highlighted.

Figure 5-8 shows all of the dip (or valley) indices from the FFT throughout the test. The points where taken at the lowest value of each dip. This data was obtained by using a valley detect algorithm with a threshold limit of 3, meaning that at least three consecutive data points must have decreased in magnitude for the algorithm to consider the waveform feature to be a valley or a dip.

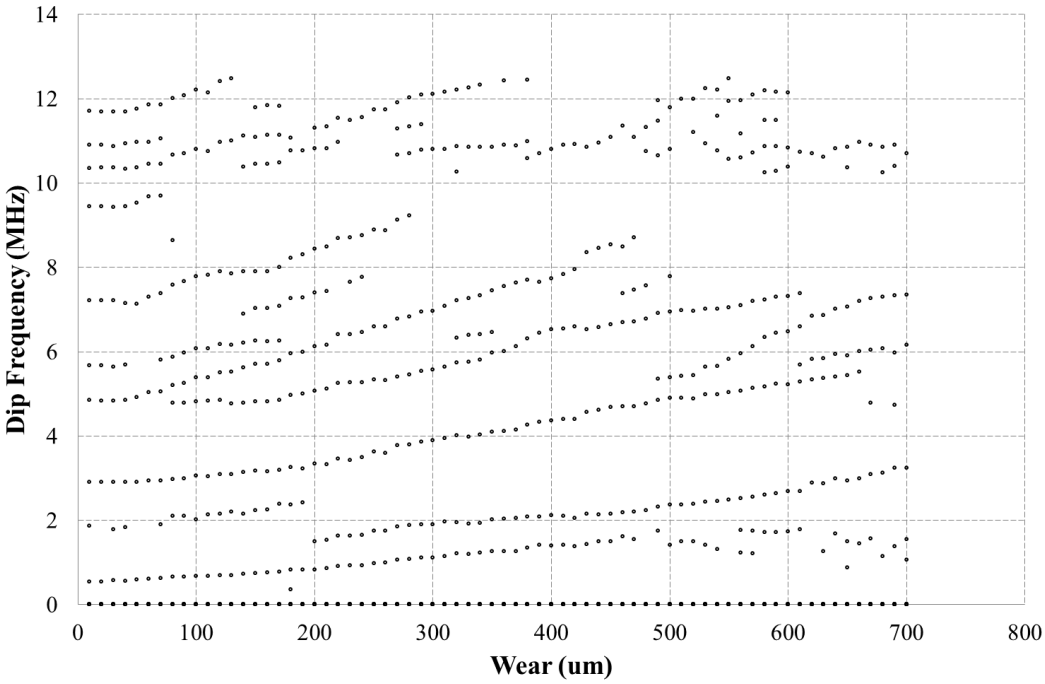

Figure 5-8. The frequency index of all of the dips as material is removed from the block.

It can be seen that using this threshold for the valley detection algorithm has recognised numerous dips in the FFT. There is no differentiation between the very prominent dips seen in Figure 5-7 (c) and the minute dips that occur from noise and other influencing factors. It is possible to reduce this effect by increasing the threshold, but this is not ideal as it can prevent valuable information from being presented. Using a more intelligent detection method, it is possible to detect only the very prominent dips of interest in a more robust manor. In order to extract the index of the frequency dip features, a signal processing algorithm was developed. This consisted of creating an idealised or reference frequency spectrum that was of similar shape to the measured waveform. By dividing the measured signal by the reference signal, the result is a flat line with the dips now represented as peaks..

After performing this operation, it is easier to create a threshold for the LabVIEW peak detection algorithm. By squaring the result, the peaks become even more clearly defined.

The results using this method can be seen in Figure 5-9. It can be seen in this chart that only the very prominent dips are indexed (M2, M3 and M4) and all of the others are ignored. It can be seen that as material is removed simulating wear, the frequency index of the dips clearly changes.

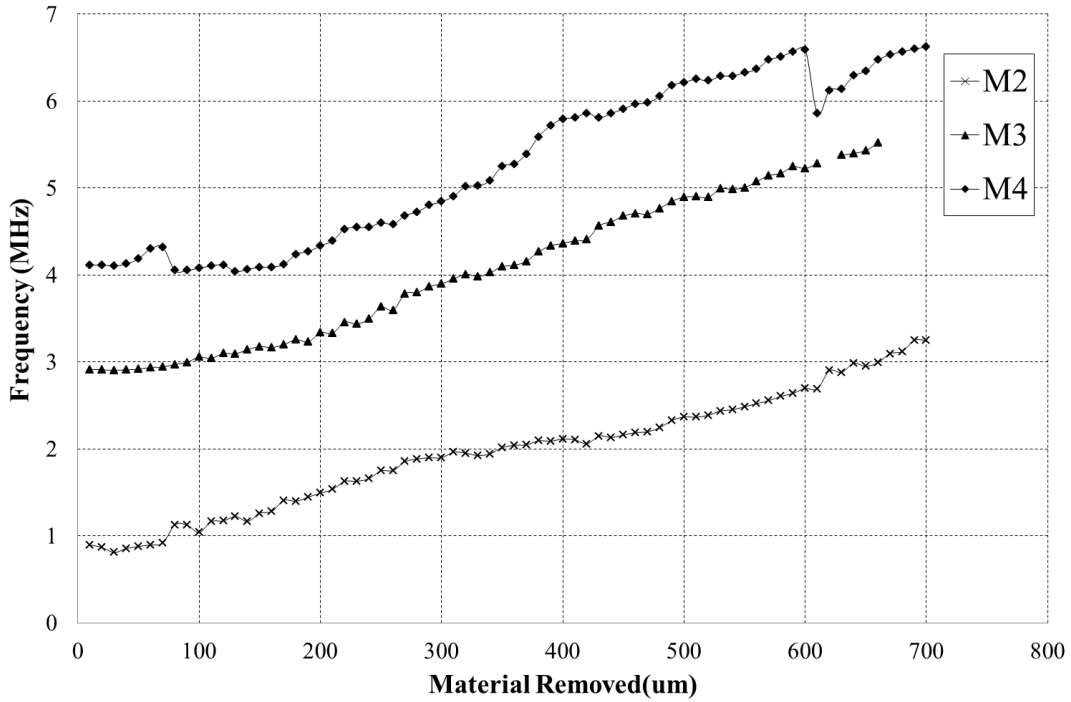

Figure 5-9. The frequency index of the dips from the wear test using the intelligent detection algorithm.

The values for dip count *M* and *f* where inserted into Equation 2-8 along with the acoustic velocity in steel to calculate *h*, the distance between the two wave fronts or the distance between the bottom of the holes and the running surface. The results can be seen in Figure 5-10, along with the actual change in thickness from the dial gauge. The actual thickness was calculated from starting thickness of 1.6 mm minus the displacement of the dial gauge as the grinding wheel was lowered onto the block with each pass.

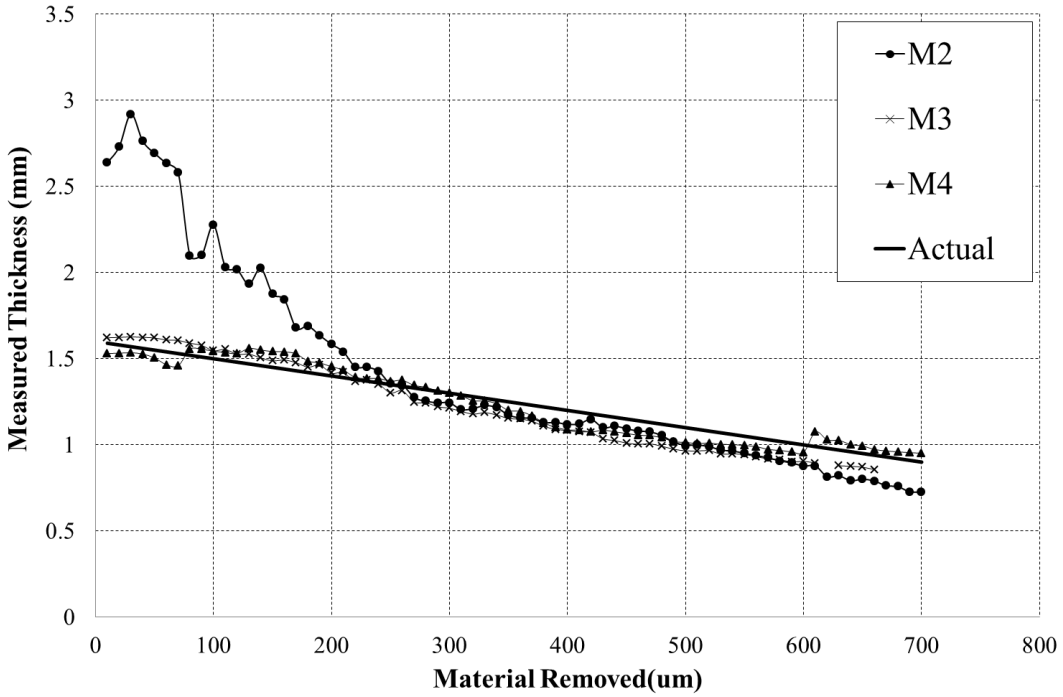

Figure 5-10. A plot showing the measured thickness between the bottom of the hole and the running surface of the test block.

From Figure 5-10, the cases of M3 and M4 show that the calculated thicknesses are in good agreement with the actual thickness. With the case of M2, the results are not accurate in the low frequency region (shown in Figure 5-9) until the dip moved into the region of approximately 1.5 MHz at 200 μm when it converged with the others.

5.2.4 Results – An Unclear Feature Configuration

In this section, the results from a different hole configuration are presented. Figure 5-11 (a) shows the position and size of the holes relative to the running face of the block. In this example six 0.6 mm holes where made 1 mm below the surfaces spaced 1.2 mm apart. Figure 5-11 (b) shows the reflected signal in the time domain and Figure 5-11 (c) shows the FFT of the signal. It can be seen from the frequency domain plot that the dips are not clearly defined like those seen Figure 5-7 (c). This is evident in the dip index plot Figure 5-12, obtained using the valley detect algorithm with a threshold of 3. It can be seen that numerous dips have been detected using this method.

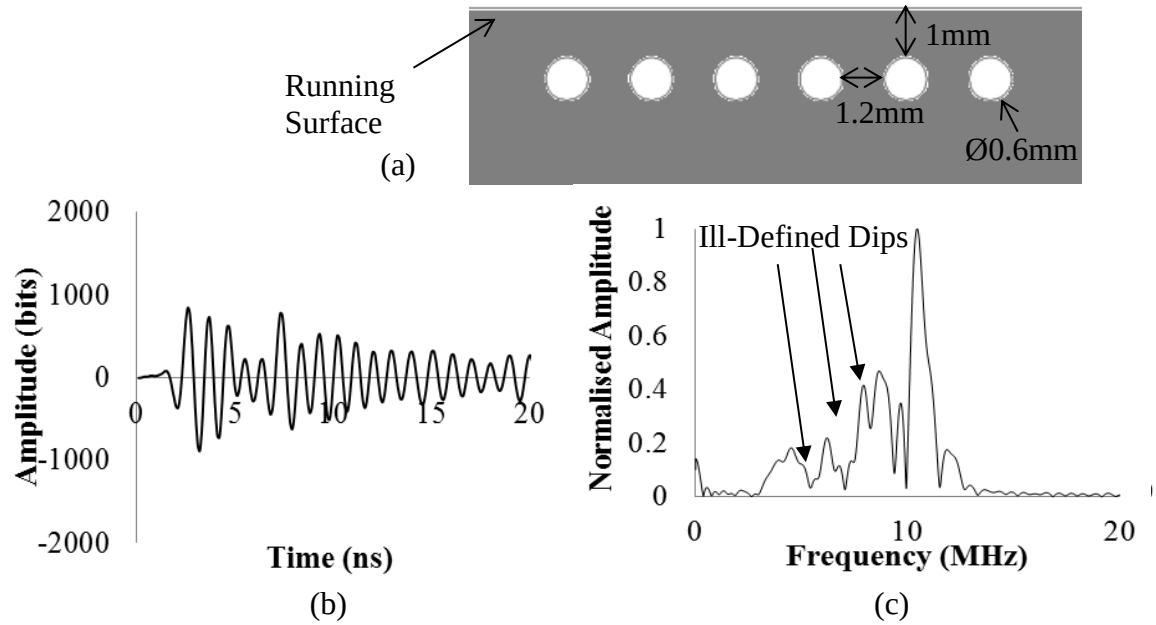

Figure 5-11. (a) shows the position and size of the hole relative to the running face of the block, (b) shows the reflected signal in the time domain and (c) shows the FFT with the dips poorly defined.

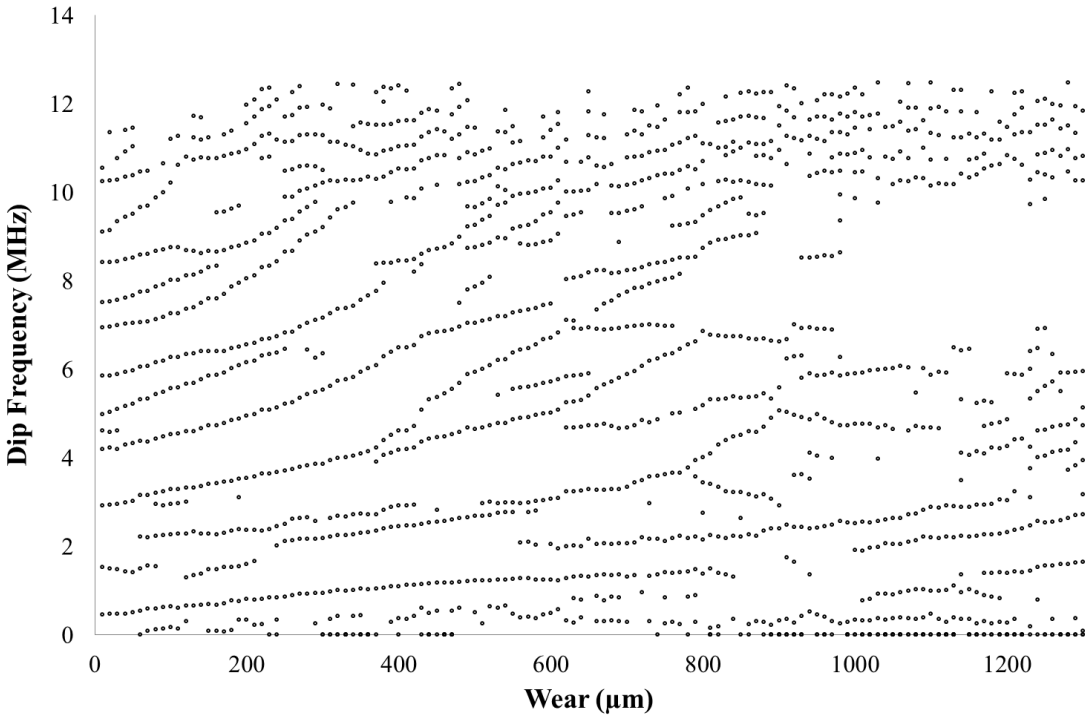

Figure 5-12. The dip positions at the different distances between the running face and the reference reflection using the simple valley detect alogrythm.

The advanced dip detection algorithm, it was applied to the time domain response (the starting waveform shown in Figure 5-11 (b). The resultant dip frequency indexes have been plotted in Figure 5-13.

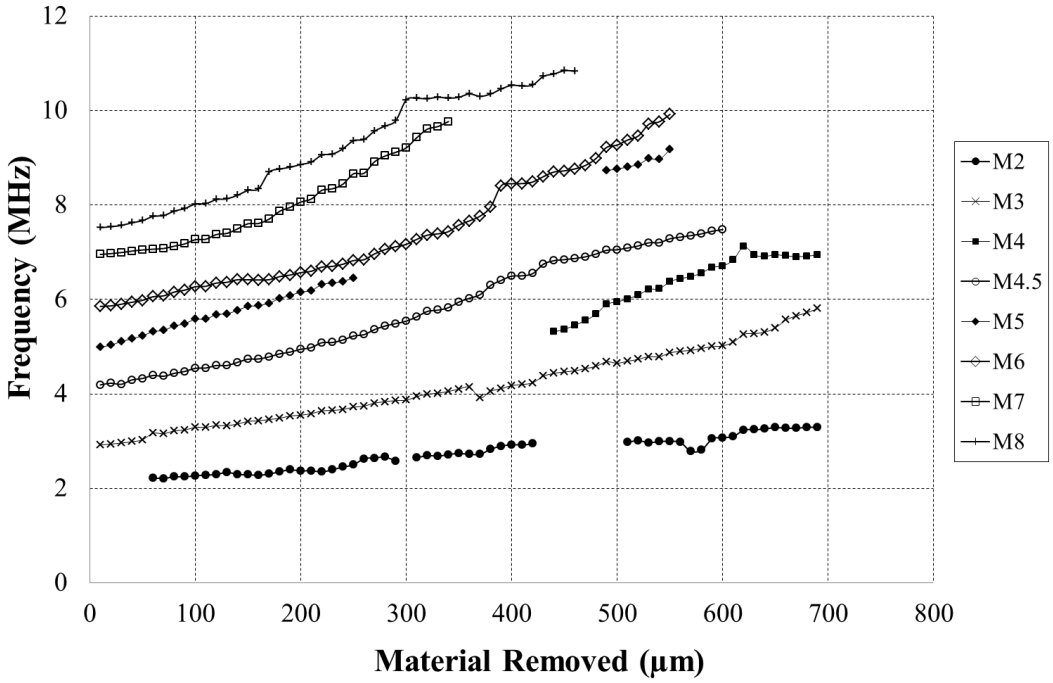

Figure 5-13. The dip index positions calculated using the intelligent dip detection algorithm.

It can be seen that fewer dips have been detected using this method. Using Equation 2-9, the distance between the two overlapping reflections has been calculated for each dip. This can be seen in Figure 5-14. The values are in agreement with the calculated values from the grinding wheel displacement validated with the dial gauge.

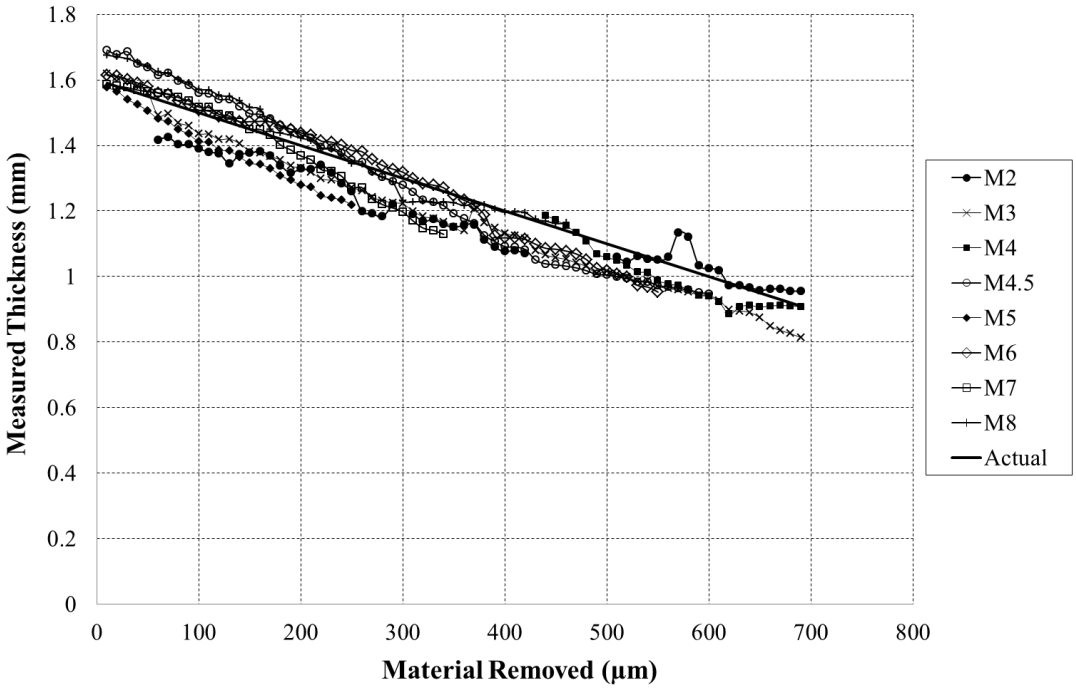

Figure 5-14. A plot showing the measured thickness between the bottom of the hole and the running surface of the test block.

5.2.5 Discussion of Wear Measurement from frequency Feature: Reference Geometry Investigation

This work has proven that the resonant dip technique can be applied to measure the thickness of a very small part of a wearing component. By placing a reflector feature near the running face, the method can measure the distance between the feature and the wear face. As this distance changes due to the wear, the thickness changes and this can be measured and monitored to provide a real-time measurement. As the part of the component that is measured is so small (>2 mm), the effect that temperature has over the entire component is negligible.

Figure 5-7 and Figure 5-11 show the extent that the positions of the holes have on the frequency content of the reflected wave. Using a valley detection algorithm with a threshold of 3 yields a large number of dip index points. It is clear that this makes it difficult to detect the individual dip number making the use of Equation 2-8 difficult as this relies on this knowledge. Furthermore, this work has shown how hard it is to

determine at what point the dips begin, i.e., which dip is M1, and therefore it is not possible to use Equation 2-8 without some trial and error. Equation 2-9 however does not require the knowledge of individual dip counts as it purely relies on the difference between consecutive dips, and is therefore a more robust technique. The more advanced dip detection method has proven successful in detecting only the substantial dips of interest. Using this method, it is possible to apply the algorithm in real-time to detect wear during the test, rather than relying on post processing to calculate the results.

Figure 5-10 and Figure 5-14 have shown that it is possible to trend wear using the resonant dip technique. Theoretically all of the calculated thicknesses should have yielded the same results. It can be seen that although the results show similarity, there is some evident variation. These differences could have occurred due to errors introduced in the peak detection algorithm. It has become evident that in areas of low frequency magnitude, i.e. at low frequency, the results are highly erroneous as seen in Figure 5-10 with the calculated thickness from M2. Figure 5-14 also displays a frequency index of M=4.5, this indicates that there are some other mechanisms happening in the waveform that require further investigation, indicating that this method is not robust enough to use in real-time and must rely on careful post processing to determine the correct frequency index.

5.3 Applying the Measurement Technique in a Standard Wear Test

An industrial partner was interested in using the technique to measure wear on a specific material pair using a bespoke pin-on-disk tribometer. As previously discussed in Section 1.7.1, the accurate measurement of real-time wear in tribometers is a difficult task. This is particularly true when dealing with applications that see only small amounts of wear like those experienced with cast iron on steel in combustion engines. As this is sensitive data, some of the test parameters have not been presented.

5.3.1 Test Set-up

A bespoke pin-on-disk test rig was used to assess the wear behaviour of sliding cast iron on polished steel. The rig has an eddy current displacement sensor that measures the displacement of the pin thus indicating wear in real-time. This was used to validate the wear measurement from the ultrasonic resonant dip method. A photograph of the test equipment can be seen in Figure 5-15. The pin was held in place using a collet arrangement. The rig has the capability to heat the specimen and a has a heated lubrication delivery system. A rotational velocity of 120 rpm was used throughout the tests and all tests were conducted with a drip mineral oil lubrication feed at 80 ºC to replicate a more commonly seen tribosystem. Dry metal on metal sliding is an unrealistic arrangement and rarely seen in machine element components.

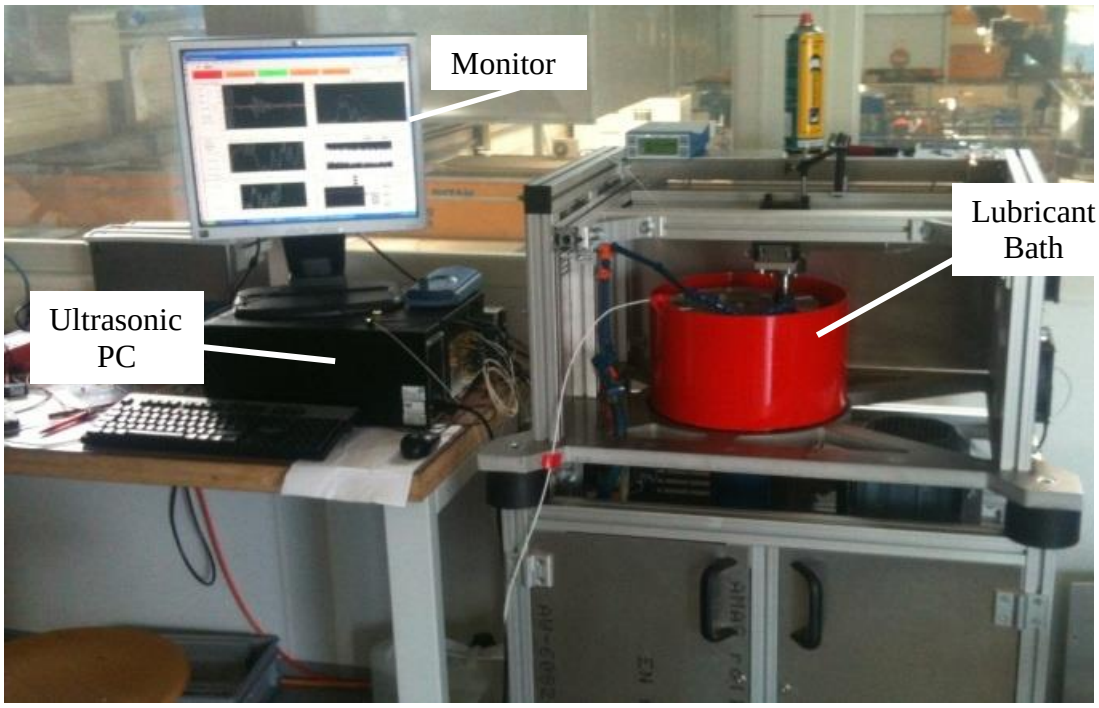

Figure 5-15. The bespoke pin-on-disk testing equipment and ultrasonic PC.

5.3.2 Test Specimen

The pin specimens were manufactured from cast iron with three holes spark eroded near the running surface to create a reference reflection. Due to the porous and acoustically poor nature of the cast iron, it was necessary to use a low frequency

ultrasonic transducer. A 10 mm 2 MHz PZ46 high temperature piezoelectric element was bonded to the rear face of the pin using MBond-610 cured at 300 ºC. A high temperature coaxial cable was used and the sensor was potted using Robnor high temperature epoxy in a cast. A photograph of the un-instrumented specimen can be seen in Figure 5-16 (a), (b) shows the pins with sensors bonded onto the back face showing the two electrodes and (c) is the instrumented pins in their final form partially worn. Figure 5-17 is a schematic diagram of the pin configuration.

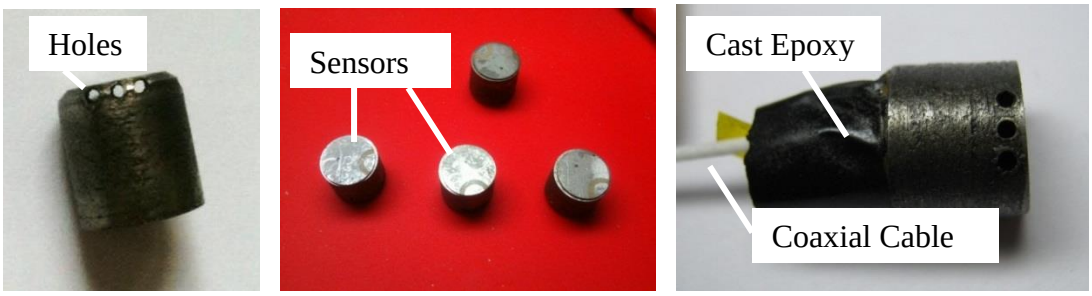

(a) (b) (c)

Figure 5-16. (a) an unistrumented pin specimen. (b) shows the specimens with the piezoelectric element bonded to the upper surface and (c) shows a partially worn instrumented pin.

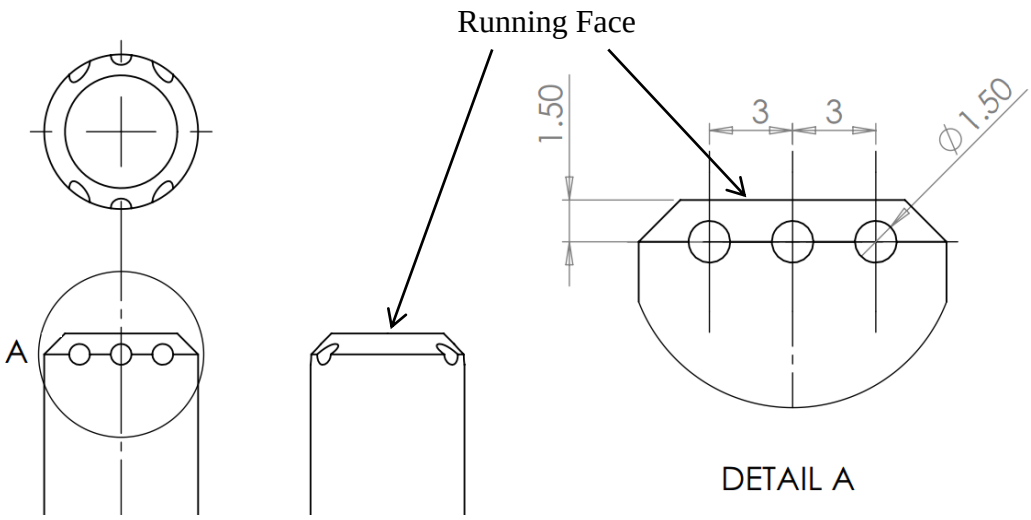

Figure 5-17. The pin specimen showing the configuration of the holes.

The disk specimen was made of AISI 01 steel. The centre of the disk was manufactured from stone to achieve an initial high wear rate in the cast iron pin at the start of the test. This was to achieve conformity between the two interfaces and ensure flat on flat sliding. The pin was initially placed on the stone part of the disc and once conformity had been achieved, it was moved onto the steel and the actual representative test was initiated. Figure 5-18 is a photograph of the test showing the pin sliding on the stone section of the disk.

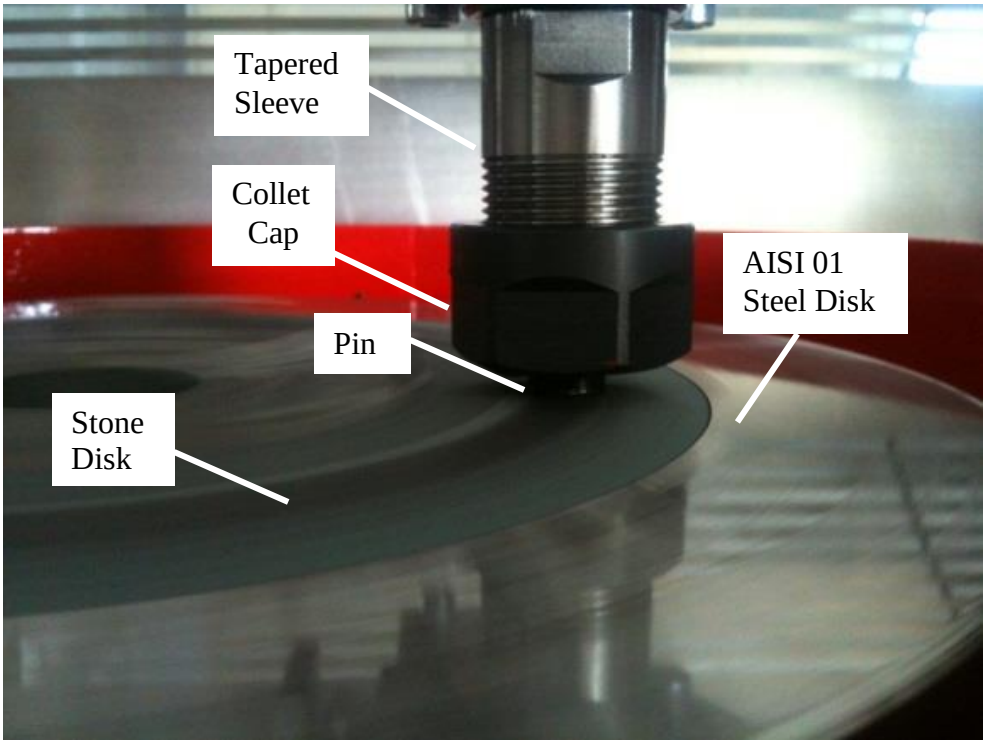

Figure 5-18. The sliding contact with the pin in position on the stone section of the disk.

5.3.3 Results

Figure 5-19 (a) shows the A-Scan time domain response from the reflected wave in an instrumented pin and (b) shows the frequency domain plot of the time domain signal.

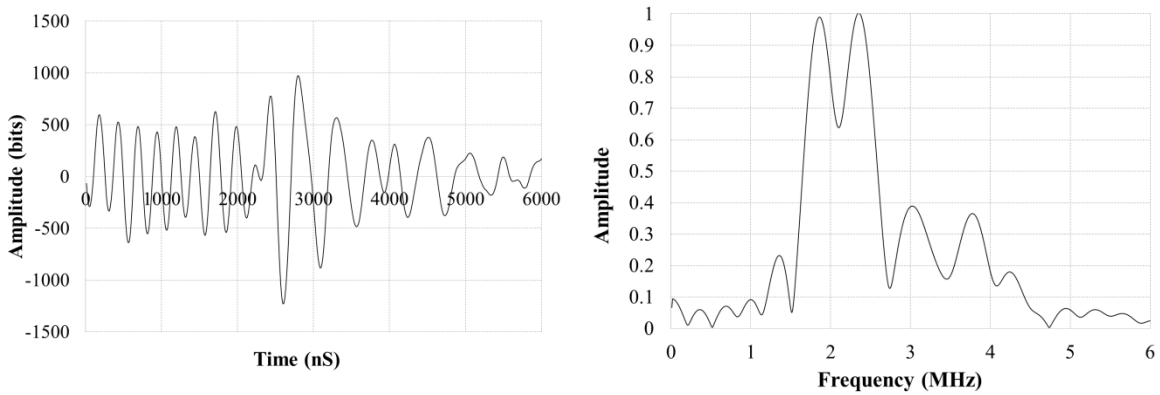

(a) (a)

Figure 5-19. (a) shows the A-Scan response and (b) shows the FFT of the reflected signal.

Figure 5-20 shows the results from the pin-on-disk wear test. The eddy current displacement measurement was zeroed, inverted to read wear and a 25 point moving average was applied to smooth the results. The ultrasonic wear results have been calculated from Equation 2-9 for 3 different dip positions Ma, Mb and Mc.

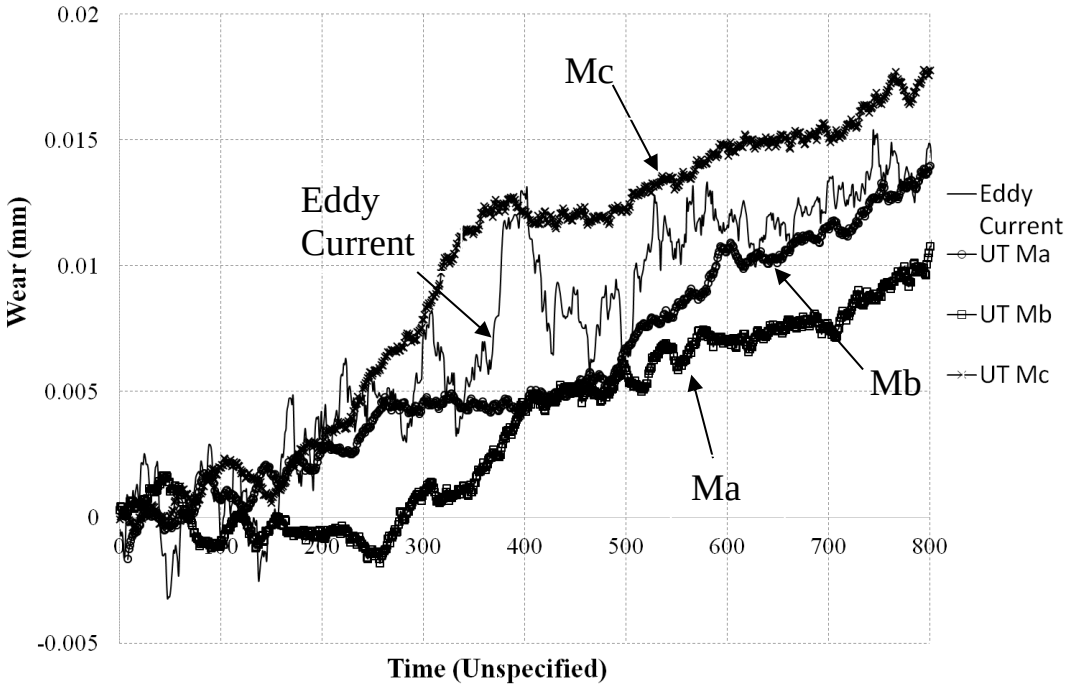

Figure 5-20. The wear measurements of the pin-on-disk test with an eddy current displacement transducer and an ultrasonic sensor using the resonant dip technique.

5.3.4 Discussion of Wear Measurement from Frequency Feature Pin-on-Disk Test

The time domain signal from the instrumented pin, shown in Figure 5-19 (a), shows the reflections from the reference holes and from the back face. The two reflections are not as clearly defined as in the initial study shown in Figure 5-7 and Figure 5-11. This is due to the use of lower frequency transducers resulting in a longer wavelength and the wave is not as well reflected by smaller features. The dips are therefore not as clearly defined in the frequency domain. A solution to this would be to use larger reference holes, but this is not suitable due to the size of the pin specimens.

The wear results shown in Figure 5-20 show some variation in the wear measured ultrasonically between the different dips. Theoretically these measurements should all be the same. These differences are likely to have been introduced from the dip detection method as the dips are poorly defined as a result of using lower frequency transducers. Another source of error could have been introduced from the lubricant filling the reference holes. Although this would not have affected the reflected waveform in the time domain, it would have affected the magnitude of the reflected wave. This is due to a higher proportion of the sound wave being transmitted into the lubricant as from Equation 2-4 the ideal reflection coefficient of cast iron and air is 0.97 and cast iron and oil is 0.91. This would in turn have resulted in a smaller reflection from the reference features thus introducing a variation in the dip definition.

5.4 Conclusions

The work in this chapter has shown that the ultrasonic frequency feature wear measurement technique has the potential to be a usable method that is virtually unaffected by the temperature of the material. The results are erroneous as some of the resonant features provide more accurate results than others, depending on where they are in the frequency domain and how much energy is at each particular dip. The size of the frequency feature must be large enough to provide a detectable reflection, but must not affect the natural attributes and behaviour of the component. The lower

frequency ultrasonic transducer yielded less clear reference reflections with smaller artefacts and is therefore not suitable from small specimens.

By using Equation 2-9, it is not necessary to know the number of the dip. Assuming it is possible to detect at least two consecutive dips at any one time, it would be possible to perform the necessary calculations in real-time, making the method a viable option for the monitoring of wear in industrial applications. Figure 5-13 shows a frequency index of M=4.5. This means Equations 2-8 and 2-9 must be used with care as other mechanisms are occurring in the waveforms that are not fully understood. Waveform modelling software such as COMSOL Multiphysics® could be used to investigate the affect the voids have on the waveform and obtain an optimum configuration.

Inserting frequency features on test specimen such as the ones used in this chapter is a relatively simple task. For industrial applications, through holes near the running surface may not be possible due to geometrical restrictions and are likely to be undesirable. There are other ways to create a frequency feature, such as creating a small pattern directly onto the running surface. This would, however, affect the interaction between the contacting surfaces.

6 METAL-TO-METAL SEAL CONTACT CHARACTERISATION

6.1 Introduction

In any pressurised system, seals are of critical importance and are often the point at which failure occurs. The seal is achieved by ensuring the contact pressure is sufficiently high and it is understood that if an area of contact is of sufficiently higher contact pressure than an adjacent fluid, it will prevent leakage and thus act as a pressure seal, [Electric Power Research Institute, 1995].

Metal-to-metal seals are often created by deforming or swaging one or more of the contacting surfaces like those seen in ferrules or olive joints in compression seals. These deformations ensure conformity of the two surfaces to ensure no passage of fluid across the seal. The forces holding the two surfaces together must be of sufficient magnitude to prevent the fluid forcing the surfaces apart as the hydrostatic pressure increases. By carefully designing the geometry of the seal system, it is possible for the internal pressure to actually increase the contact pressure of the sealing interface; this is known as pressure energising.

Compression seals are commonly used to seal piping in plumbing applications, but are also employed in larger high pressure piping networks in the oil and gas industry. In this application, metal-to-metal seals are responsible for preventing crude oil at pressures in the range of 200 MPa from being leaked into the ocean at pipe connections. End fittings are attached to the end of the flexible pipes and facilitate the joining of components together whilst preventing leakage. Attaching an end fitting assembly onto the end of a flexible pipe made up of multiple layers of steel and polymers is a difficult task. It is the metal-to-metal seal within the end body fitting that is to be investigated in this section.

Understanding the behaviour of the components during swaging is of fundamental importance to ensure the interface pressure is sufficiently high to prevent seal failure. Finite element analysis has traditionally been used to predict the contact pressure at

the interface but empirical data is required to validate the model. The author conducted all of the ultrasonic measurements presented for GE Wellstream International Ltd and co-wrote a conference paper, see Fernando *et al.* [2012]. with the aims of providing some validation for their finite element contact analysis. The possibility of using this method as a quality assessment tool during manufacture is also explored

6.2 End Fitting Seal Design

Figure 6-1 is a schematic diagram of an end fitting on a pipe. As the bolts are tightened, the taper of the work hardened metal seal ring is forced against the tapered section of the end fitting body. As the two surfaces come into contact, the seal ring plastically deforms thus creating a seal. The design of this seal is critical to ensure no leakage occurs during operation which comprises of high temperature crude oil being piped through at high pressure. As the internal section is pressurised, the contact pressure at the seal ring interface should increase. This is known as pressure energisation. Figure 6-2 is a diagram showing the cross section of the assembly with details of the metal-to-metal seal interface, from Fernando *et al.* [2012].

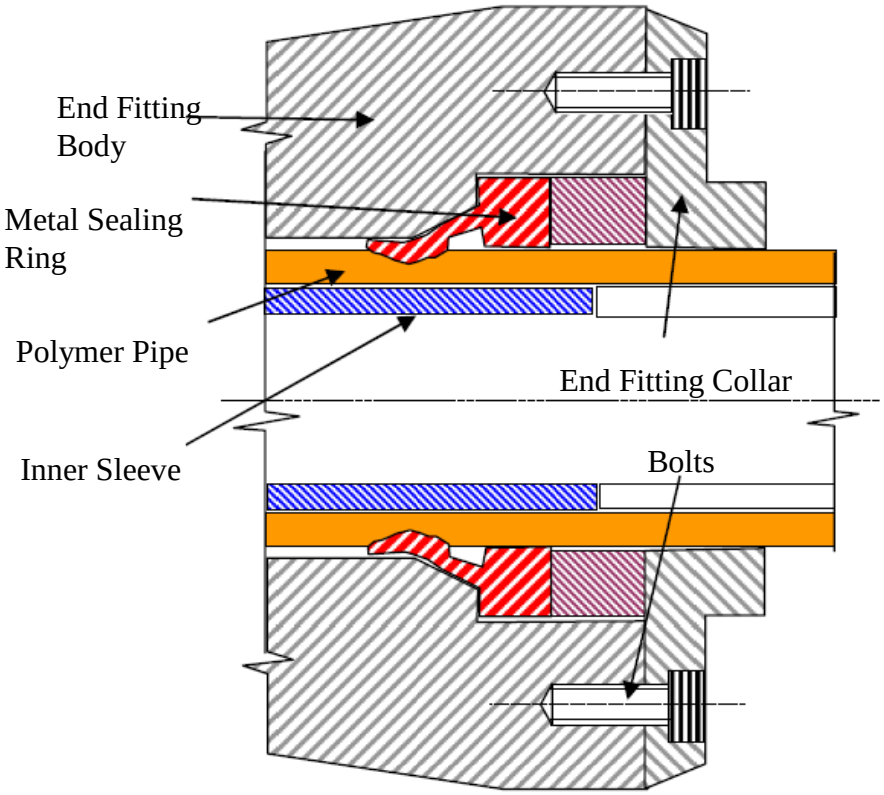

Figure 6-1. The end fitting seal assembly, from Fernando et al. [2012].

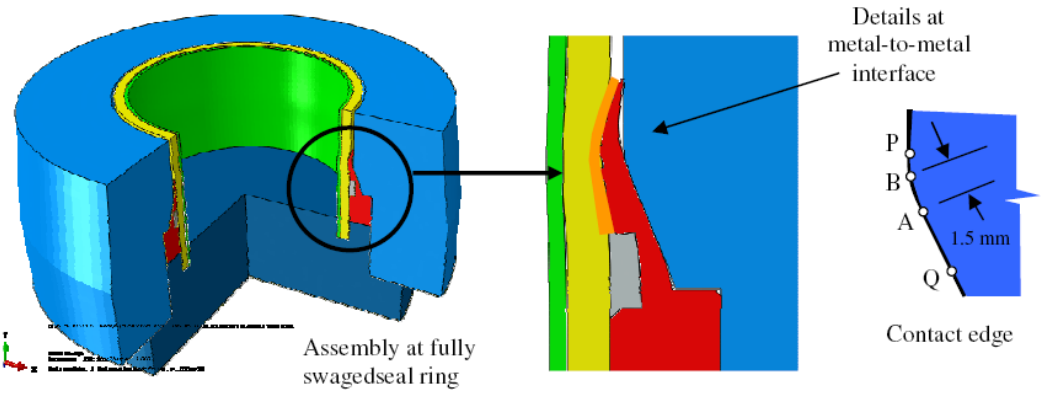

Figure 6-2. The details of the metal-to-metal interface, from Fernando et al. [2012].

6.3 End Fitting Compression Test

An initial test was conducted to develop understanding of the seal interface and to test the ultrasonic method. GE Wellstream International Ltd. provided a modified end fitting assembly that was mounted in a loading rig to simulate the swaging that occurs as the bolts in the end fitting are being tightened. As the load is applied, the seal ring plastically deforms and conforms to the taper of the end fitting body. A number of ultrasonic sensors were mounted on the outside of the end fitting body in such a position to measure the contact during swaging.

6.3.1 Test Specimen

The end fitting body and seal ring interface was simplified in order to have a greater amount of control over the experimental parameters and to allow the design to fit in a loading rig. An end block was manufactured to house the polymer pipe and the inner metal sleeve and to support the seal ring. The inner section of the assembly can be seen in Figure 6-3. The end fitting body was lowered on top of the inner section and placed in the loading rig. Flat edges were machined into the outside surface of the end fitting body to ensure that the surface to which the transducer was mounted was parallel to the sealing interface. This will ensure that the sound wave will reflect off the interface back to the same position it started, which is a requirement of the ultrasonic method in pulse-echo mode. Two tests were carried out with slight variation in the thickness of the polymer tube.

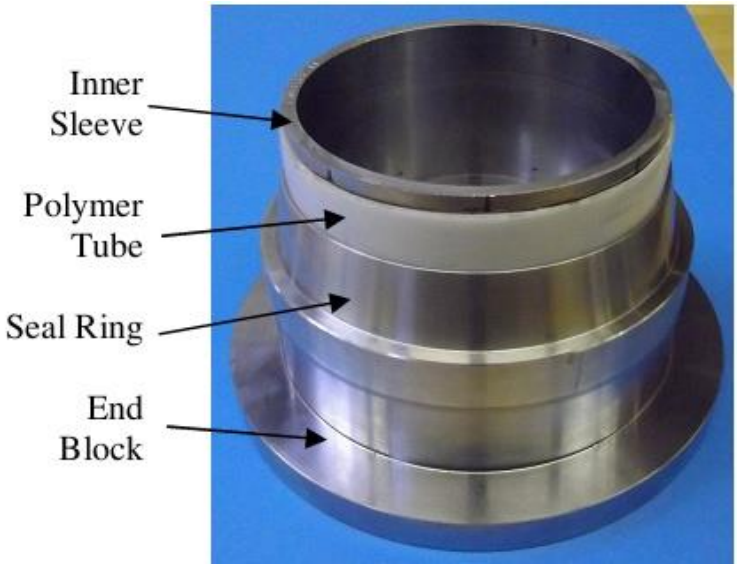

Figure 6-3. The inner section of the end fitting assembly.

6.3.2 Test Set-up

A 500 kN Mayes servo-hydraulic controlled universal testing machine was used to apply a load to swage the metal-to-metal seal. The inner section was mounted on the loading frame bed and the end fitting body was forced against the seal ring by applying a series of displacement steps. The temperature, displacement and normal load was fed into the ultrasonic acquisition PC and logged alongside the ultrasonic A-Scans. Reference A-Scans were taken before the test in order to calculate reflection coefficient and the stiffness of the contact was calculated from Equation 2-11. The contact pressure was obtained using a calibration procedure in which two materials of the same surface roughness with a known contact area where loaded together resulting in a relationship between stiffness and contact pressure, see Section 2.3 for further details.

6.3.3 Instrumentation

As the seal rings are consumable parts, it was only feasible to carry out two tests. In order to obtain the maximum amount of data and minimise risk, numerous ultrasonic measurement techniques were employed simultaneously. A 10 MHz focusing transducer was used as a single point measurement positioned to measure the contact pressure at a single point. A picture of the instrumented end fitting can be seen in Figure 6-4.

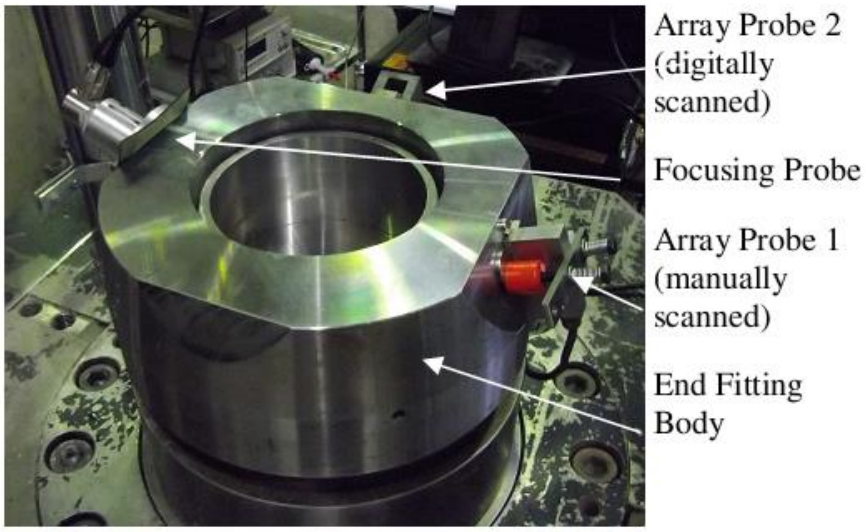

Figure 6-4. The complete end fitting assembly with three ultrasonic transducers.

A flexible mounted water bath was manufactured to ensure the sensor could be moved during set-up to optimise signal response. The axisymetrical shape of the assembly meant that the sensors had to be positioned perpendicular to the tangent of the contact to maximise the reflected energy. The transducer was moved in the vertical plane to focus the beam and ensure the correct focal depth of field. Both of these positioning challenges are achieved through trial and error by moving the transducer whilst monitoring the response until the reflected energy reaches a maximum. The transducer was positioned so that the sound wave was focused at the point of interest. For the first test, the probe was focussed on the edge of the seal ring fillet; location B in Figure 6-2. For the second test, the probe was moved 1.5 mm away from the edge of the fillet, location A, in Figure 6-2.

Two 10 MHz 64 element ultrasonic array transducers, described in Section 3.5, were used to obtain a 2D linear measurement across the sealing interface.

(a) (b)

Figure 6-5 is a schematic diagram showing the position of an array transducer on the end fitting body. The paths of the sound waves have been included.

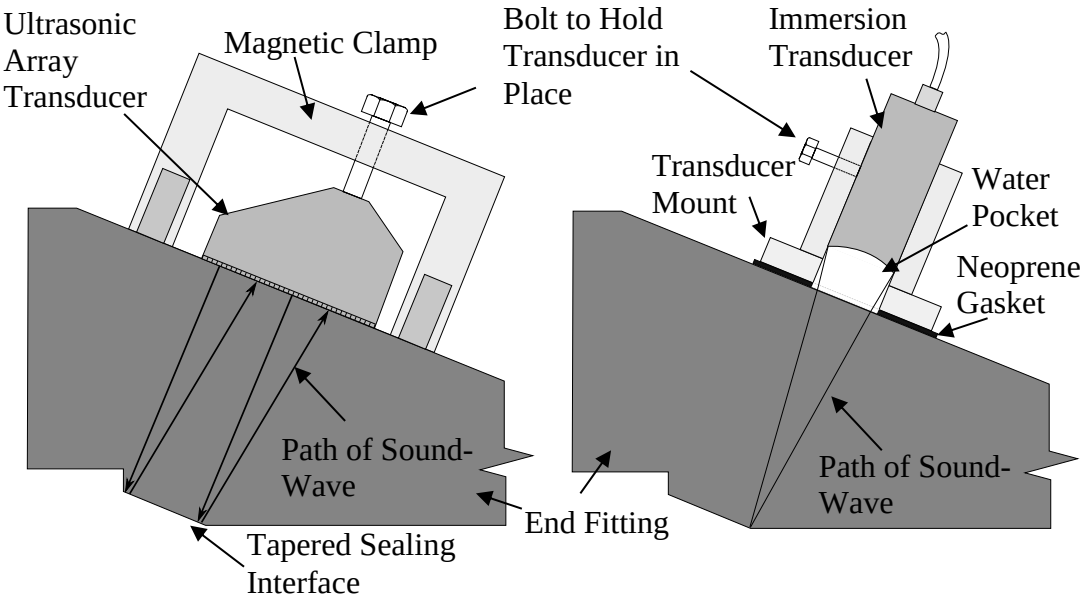

Figure 6-5. A schematic diagram showing the position of the array transducer (a) and the immersion transducer (b) mounted on the end fitting body with the paths of the sound wave included.

6.3.4 Results

Figure 6-6 shows the resultant swaging force from the load cell for each displacement step for two repeated tests with the transducer placed at different positions. The predicted results from the finite element analysis have also been plotted. Due to the sensitive nature of the results, the two methods were normalised by making a maximum contact pressure and displacement equal to unity.

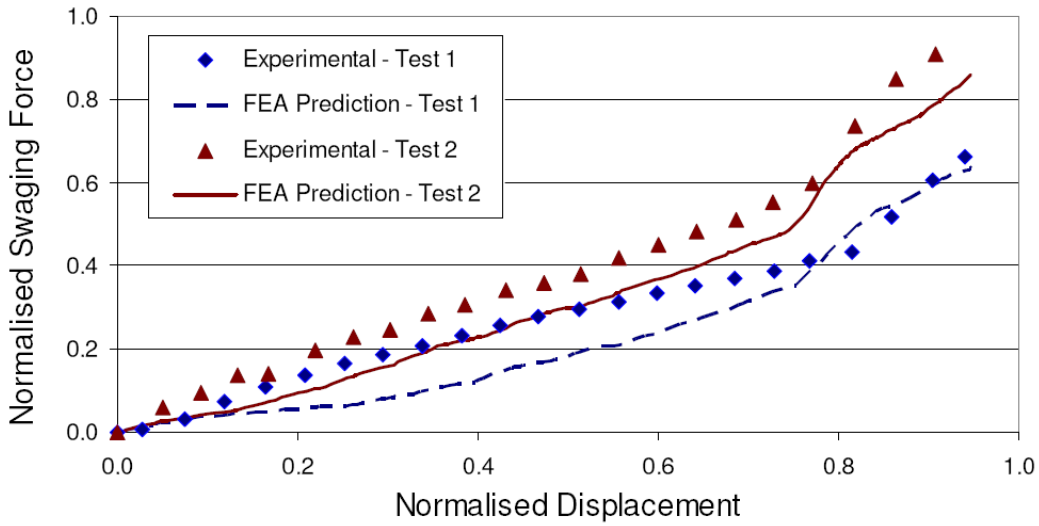

Figure 6-6. A graph showing the resultant swaging force from the applied displacement, from Fernando et al. [2012].

Figure 6-7 shows the results from the focussed immersion transducer. The results have been presented in normalised format. In both cases, the predicted values from the FE are in agreement with the experimental results.

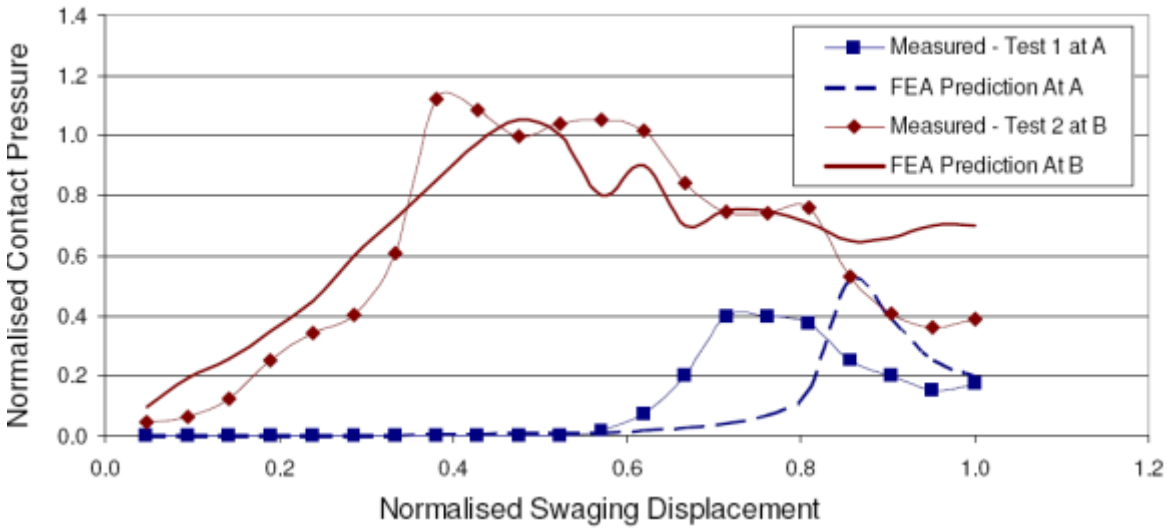

Figure 6-7. The normalised contact pressure at point A in Test 1 and point B in Test 2 from the FE and the ulrasonic contact pressure measurements for the increasing displacement steps, from Fernando et al. [2012].

The measured contact pressure profile obtained from the digitally switched ultrasonic array transducer can be seen in Figure 6-8. The graph compares three displacement (δ) values, of 5 mm, 8 mm and 10 mm. The case where δ=10 mm represents the fully swaged seal. The results have been presented in normalised format achieved by dividing all results by the peak value.

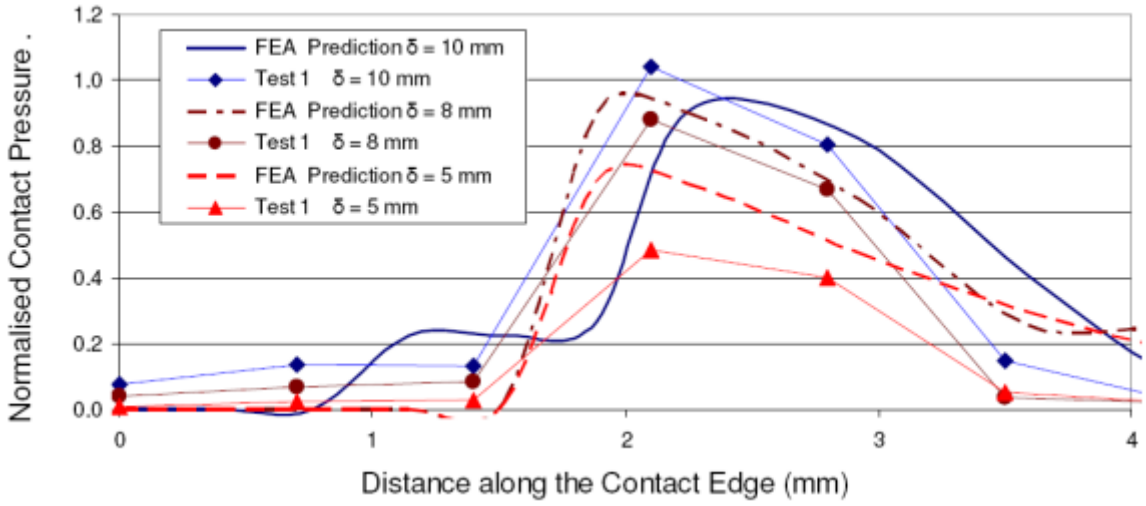

Figure 6-8. The normalised contact pressure profile from ultrasonic measurements and FE across the length of the metal-to-metal seal, from Fernando et al. [2012].

6.3.5 Discussion of Contact Pressure Measurement of the End Fitting Compression Test

The initial FE models predicting the required swaging force are in agreement with the experimental output as shown in Figure 6-6. This builds confidence in the FE model and shows that the modified specimen is representative of the pipe assembly. In both tests, the experimental results have shown a slightly higher swaging force than the finite element predictions. The results show an increase in swaging force for the final 20 % of the test which was accurately predicted in the FE analysis.

The single point measurements at the interface, shown in Figure 6-7, again show good agreement to the finite element analysis with the majority of experimental results within ±15 % of the simulated contact pressures. The onset of contact

pressure at location A was found to be earlier than predicted. At location B, the final contact pressure value after swaging was found to be lower than predicted.

The contact pressure profile obtained from the ultrasonic array system is also in agreement to the results predicted with the FE analysis. It can be seen that the pressure profile at the interface increases in magnitude as the displacement increases. Each element of the ultrasonic array transducer is 0.7 mm wide so the discrete measurement points are an average over that area, meaning that the ultrasonic output is of lower resolution than the FE model. The FE predicted slightly higher pressures at lower deflections. The results from the manually switched array system are very similar to the automatically switched system so were not fully processed or presented as they were only put in place in case of redundancy.

6.4 Measurement of Pressurised Seal

To develop a greater understanding of the metal-to-metal seal interface as it experiences stress during operation, a pressurised test was performed on a real pipe and end fitting to measure any change in seal contact pressure during internal pipe pressurisation.

6.4.1 Test Specimen

This test aimed to reproduce the conditions that a pipe end fitting would experience during operations. A standard multi-layered pipe was cut to a short section and sealed at one end using a bespoke epoxy sealing bung. The seal ring was placed on the pipe and then the end fitting was bolted in place using the standard assembly procedure. This swaged the seal ring onto the end fitting. The end fitting was pressure sealed at the end using a bespoke sealing bung that was fitted with an inlet in which to pump water to build up the internal pressure. This simulated the high pressure oil that would be pumped through the pipe section. The test was conducted at ambient temperature, in the real application; the process fluid would be at higher temperature. A schematic diagram of the pressure sealed end fitting can be seen in Figure 6-9.

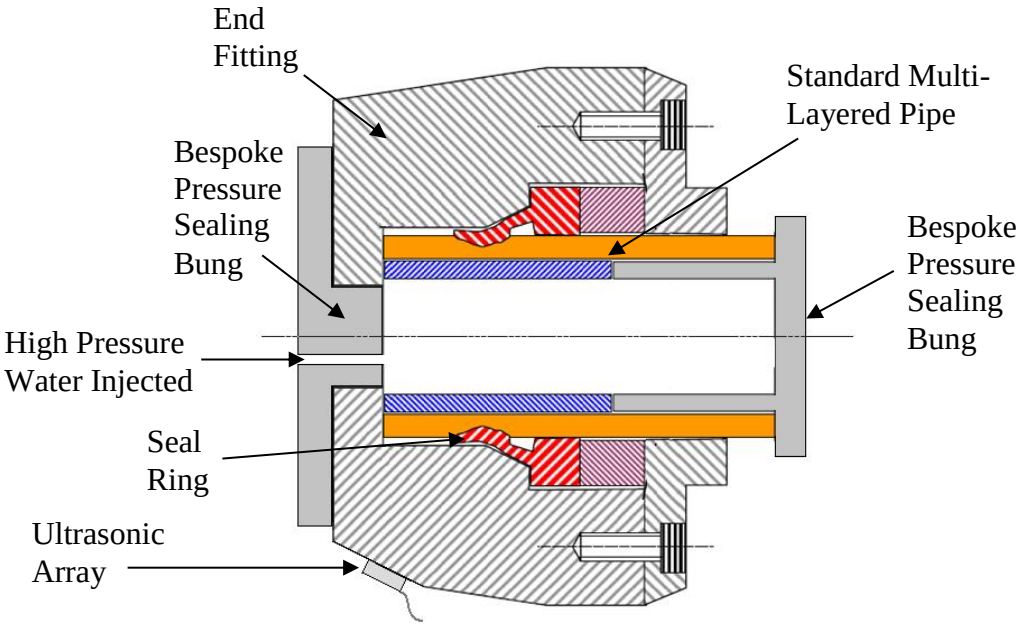

Figure 6-9. A diagram of the end fitting assemlby swaged onto a pipe showing the modifications to allow pressure retention, modified from Fernando et al. [2012].

6.4.2 Test Details

The test was split into two sections. The first section involved swaging the seal by tightening a series of bolts around the end fitting body. Reference measurements were taken prior to swaging and then each of the bolts was tightened in steps. Ultrasonic measurements were taken at each step to measure the contact pressure profile evolution throughout the swaging process. After the end fitting was in place, the system was sealed to hold the pressurised water. Once sealed, water was pumped into the assembly creating an internal pressure of similar magnitude to which the pipes would experience during operation. Ultrasonic measurements were taken during pressurisation to measure any changes in the metal-to-metal seal contact pressure and area.

6.4.3 Instrumentation

The interfacial coupling between the array transducer and the surface in which it is mounted on is of crucial importance as discussed in Section 3.4. The sensitivity of the interfacial coupling means extreme care has to be taken when performing measurements so as not to disturb the sensors. These factors mean that the ultrasonic transmission is subject to change if used over a long period of time. It is critical that the position of the transducer must not move between reference measurement and test measurement. In order to overcome these problems, a permanently embeddable ultrasonic array transducer was developed for this work and was bonded into position to ensure this crucial interface did not change over time, thus ensuring the measurement position was kept the same.

A 10 MHz 12 element ultrasonic array transducer was developed for the purpose of this test described in Section 3.5.3. The transducer was bonded on a flat section of the end fitting body using Tribobond cyanacrolyte based room temperature cure adhesive. The element spacing of the array transducer is 0.7 mm per sensor. Only 7 sensors could be used at any one time. The ultrasonic pulsing-receiving-digitising hardware had 8 channels and one channel was reserved for the external calibration sample. The array was positioned so that the sound waves reflected at the interface in which the seal contact was at highest contact pressure, shown in Figure 6-10.

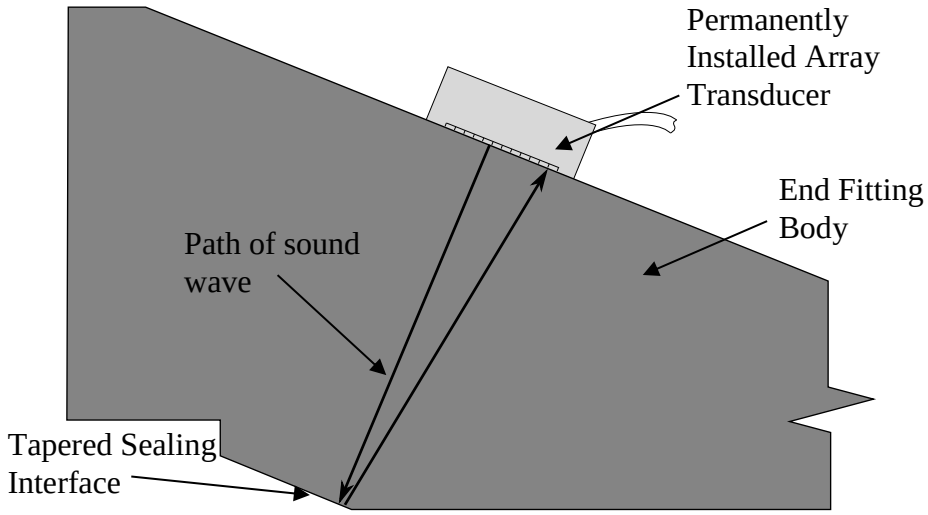

Figure 6-10. A schematic diagram showing the bonded array transducer in position on the end fitting body.

A linear scan was performed by exciting each element individually with negative 100 V square wave signal with a pulse width of 70 ns. The reflected response was captured from the same element, the signal amplified and digitised. A delay of 1700 µs was employed with a capture range of 400 µs with a gain of 35 dB and a pulse repetition frequency of 2000 Hz. A photo of the array transducer can be seen in Figure 6-11.

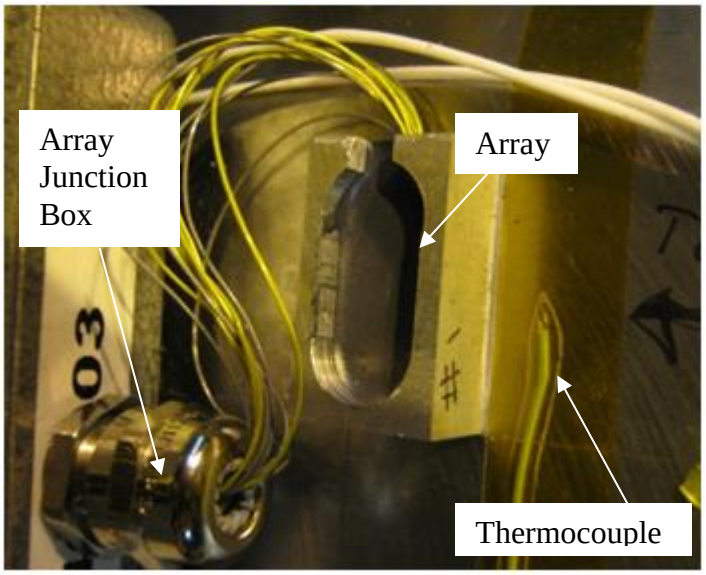

Figure 6-11. The 12 element permanently bonded array transducer.

This investigation introduced new measurement challenges because the complex pipe end fitting assembly had to be built up in stages over the space of weeks. The swaging process took place a number of days before the pressure test could commence. The contact pressure measurements rely on a reference measurement which is an ultrasonic reflection measurement of the interface with no contact, i.e., 100 % reflection. This reference is then used to calculate the reflection coefficient, R, by dividing this number by the measured reflection when contact occurs. The time gap (weeks) between the different measurements makes referencing extremely difficult as the reference measurement is traditionally obtained seconds before contact occurs, which was not possible in the pressurised test. There are numerous things that affect the ultrasonic measurement so a reference reflection obtained on one day will be different to one obtained on another as discussed in 3.9.

A way of overcoming this issue is to conduct a concurrent external calibration measurement as discussed in Section 3.9. This was achieved by instrumenting a metal sample that is subjected to the same environmental factors as the measured component, but does not experience change from contact pressure. External factors affecting the ultrasonic measurement over time can then be accounted for by adjusting the magnitude of the reference measurement accordingly.

6.4.4 Results

An initial ultrasonic reference measurement was taken with a steel-air interface. The seal ring was then put in position and swaged by tightening the flange bolt set. Ultrasonic measurements were taken throughout the swaging process. A series of reflection coefficients have been plotted in Figure 6-12 that show the evolution of the pressure profiles over time. The distance across the contact area has been normalised and the timing has not been shown as the information is commercially sensitive.

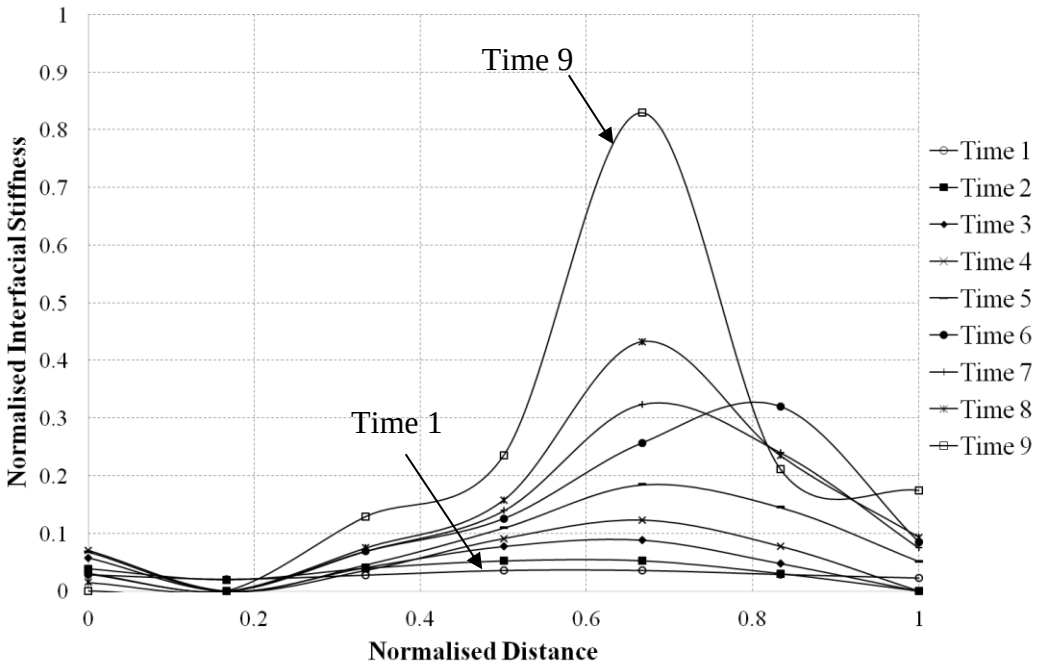

Figure 6-12. Interfacial stiffness during seal swaging.

The seal ring and end body was greased prior to swaging resulting in an interface that is a mixture of two stiffness regimes: solid/solid contact and solid/liquid/solid contact. This means that the reflected wave is determined by the interfacial stiffness of both the solid-solid contact and the thin lubricant layer.

The end body was internally pressurised until the system failed by bursting and the array transducer was pulsed using the same configuration as during swaging. The resultant change in interfacial stiffness can be seen in Figure 6-13 below. P0, P1, P2 etc. represent increasing internal pressures in the vessel.

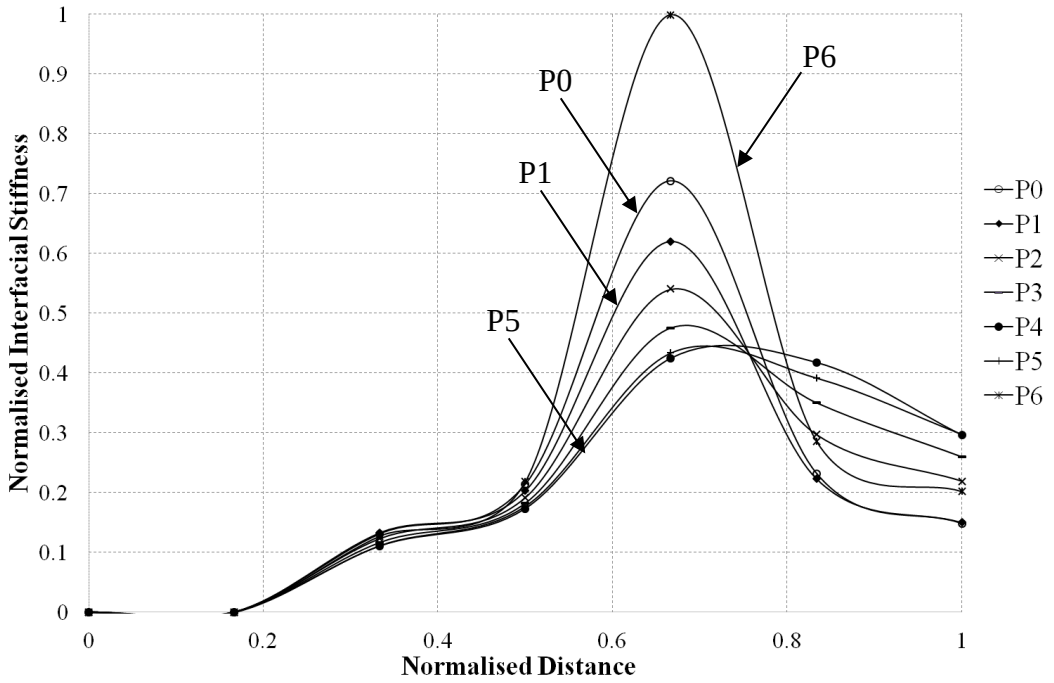

Figure 6-13. Interfacial stiffness during internal pressurisation.

6.4.5 Discussion of Contact Pressure Measurement of a Pressurised Seal

Figure 6-13 shows that the contact patch magnitude and interfacial stiffness changes over time as the seal ring is swaged. The sensor position has meant that the edge of the contact profile was not measured. As the pressure was increased, a change in contact pressure was observed. The interfacial stiffness decreases as the vessel is pressurised thus indicating that the contact pressure decreases. This indicates that the seal is not pressure energised; this was as expected. Failure occurred between P5 and

P6, a sharp increase in interfacial stiffness can be seen after failure to the extent that it was higher than before pressurisation. At one measurement point, the reflection coefficient was greater than one. To calculate the interfacial stiffness, any results above one had to be made to be one as a negative stiffness is not possible. This occurred as the sensor was at the edge of the contact area and indicated that the contact was only partially over the measurement window; see Section 2.1.7 for more information.

It was not known prior to testing that the contact was going to be lubricated. The contact was therefore operating in the boundary lubrication regime. The total stiffness of the interface is the sum of the stiffness of the solid-solid contact and the lubricant layer. This meant that an accurate value for contact pressure could not be determined from Equation 2-11 as it does not consider the stiffness of the lubricant. Investigations have been carried out to calculate the total interfacial stiffness, see Dwyer-Joyce *et al.* [2011], but this falls beyond the scope of this work which is concerned with dry contacts. This is a potential area for future work.

6.5 Conclusions

In the laboratory based compression test, the ultrasonic results were in agreement with predictions from the finite element analysis. This has given confidence in the FE model, allowing it to be used to design the next generation seal geometries with smaller margins of safety thus resulting in a cheaper construction whilst maintaining functionality. The results of the pressurised test were of great interest to GE Wellstream International Ltd., allowing them to further their understanding of the contact pressure distribution for the seal when it is subjected to similar conditions to those seen in service. The investigation was successful in detecting whether or not the contact was pressure energised with fluid pressure. Subsequent tests were carried out with new designs in which the contact pressure increased with internal pressure resulting in a more reliable sealing system.

The purpose built bespoke permanent array transducer worked successfully in the industrial application allowing measurements to be taken with substantial time gaps between referencing and the actual measurement. This is of particular interest as it

implies that sensors could be permanently installed into the end fittings during manufacture to ensure a proper seal has been made. This could then be used as a condition monitoring tool in service to monitor the contact pressures over time and detect the onset of failure preventing potentially catastrophic damage and substantial fines. Future work will investigate the feasibility of this application in terms of costs and return on investment.

7 ROLLING WHEEL/RAIL CONTACT PATCH CHARACTERISATION

7.1 Introduction

The rail vehicle wheel and rail contact interface is a critical component of any rail based system that must be carefully controlled in order to provide safe and efficient operations for passenger and freight services alike. There is a wide range of influential factors that affect wheel/rail contact conditions including vertical and lateral forces, distribution of mass, attack angle of wheel-set, speed, friction, debris on the track and curve radius to name a few [Makoto *et al.* 2001]. These factors all effect wear of both the wheel and the rail which can lead to failure and derailment.

Wear is an unavoidable consequence of wheel/rail interaction and rolling contact fatigue (RCF) is one of the primary outcomes of improper contact conditions that result from worn wheels and rail. It is the management and maintenance of this process that is of critical importance. There are numerous methods to minimise wear including the addition of friction modifiers to the interface, grinding the rail head and re-profiling the wheel-sets to ensure ideal contact conditions in terms of contact pressure, area and position on the wheel and rail. Improper contact conditions are the root cause of all wheel and rail damage mechanisms such as RCF, corrugation and wear. Logistical and political complications occur as the rail vehicles in the UK are owned by different private organisations and often travel across numerous different track networks, meaning that it can often be difficult to determine which body is responsible for the maintenance and the associated costs.

The majority of the current designs and maintenance cycle predictions heavily rely on analytical and numerical techniques to model the contact conditions and wear at the wheel/rail interface, [Marshall *et al.* 2005]. A common approach to model the contact pressure under normal loading conditions is to calculate the area of interpenetration of measured profiles. By fitting an ellipse to this, the Hertzian model can be applied to calculate the contact pressure, [Rovira *et al.* 2012]. There is a wide variety of complex numerical solvers such as FASTSIM, CONTACT or STRIPES

that use the real profiles to create accurate dynamic contact area and pressure predictions considering the tangential load, [Kalker, 1982].

To accurately predict the contact pressure, area and wear, most of these methods require the accurate measurement of the wheel and track profiles to input into the calculations. This is possible for research based applications but impractical to apply this to nationwide track maintenance predictions. Obtaining the required profile information would be a costly procedure considering there is over 15,777 km of track in the UK alone, [Railway-Technical, 2013]. The computational time would also be extensive.

Very few experimental methods exist to measure the wheel/rail contact. Pressure sensitive films have been used but these introduce a thickness that will inherently change the contact conditions. Also the dynamic nature of the system limits the application, [Pau *et al.* 2001]. Dynamic measurements have been obtained using a modified rail section with a grid of small holes passing low pressure air through the surface of the railhead. As the wheel moves over the rail, some of the holes will stop the flow of air. This results in low resolution contact evolution data, [Poole, 1987].

The aim of this work was to develop a dynamic measurement system based on the fundamental static work carried out by Marshall, *et al*. [2005], [2006] in the investigation the contact of a rolling wheel on a rail using ultrasonic techniques. In this investigation, a constant series of ultrasonic pulses reflecting off the interface will measure the contact evolution as a wheel is rolled over the railhead in order to obtain the contact pressure distribution. This should result in high resolution data that can be obtained in-situ in real-time for monitoring applications. This information could be used to validate numerical models or used directly to determine maintenance schedules and optimise wheel/rail profiles. The possibility of using this method as a real-time safety system for train driver feedback is also discussed.

7.2 Static Contact Measurement using Scanning Immersion Transducer

Marshall *et al.* [2006] have successfully used a 2D scanning system with a section of wheel and rail to measure the contact pressure distribution at the wheel rail interface using ultrasonic reflectometry. The correlation achieved between ultrasonic results and numerical models was excellent and thus provided validation for the method. This work was repeated with a new set of wheel and rail profiles to validate a FASTSIM model developed by Rovira *et al*. For further detail of this work, see Rovira *et al.* [2012].

7.2.1 Experimental Set-up

The wheel and rail specimen were cut from full size sections and can be seen in Figure 7-1.

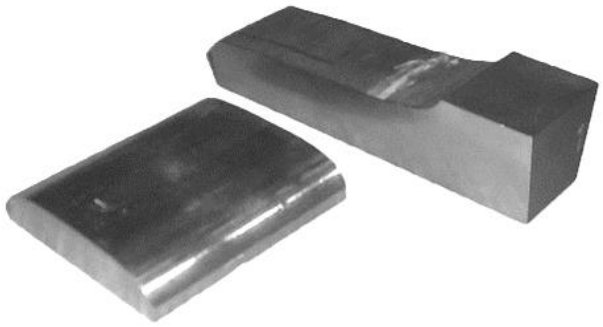

Figure 7-1. The wheel and rail sections.

Two tests were carried out, the first with specimen set cut from a worn wheel and rail and the other test, the specimens were cut from a new wheel and rail. The specimens were mounted in a steel loading frame with the wheel section set at a 1:20 incline to replicate the real application. The wheel and rail sections were hydraulically loaded together with a force of 50 kN to simulate the resultant forces from the mass of the railroad vehicle. A water bath was mounted on top of the rail section to support the ultrasonic wave. The loading frame was mounted on a 2D scanning table to traverse the loaded specimen arrangement under the focussed ultrasonic transducer in order to achieve the 2D contact patch measurement. See Sections 3.3.5 and 3.6 for further detail on the immersion scanning method. A schematic of the testing arrangement can be seen in Figure 7-2, [Rovira *et al.* 2012].

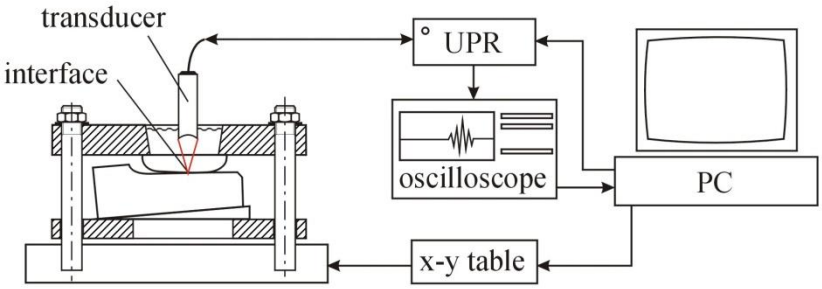

Figure 7-2. A schematic diagram of the static wheel/rail ultrasonic measurement testing arrangement, from Rovira et al. [2012].

7.2.2 Calibration Details

According to the calibration test done by Marshall *et al.* [2005], the empirical equation to best fit the calibration data is contact pressure Cp=263 K MPa. Figure 7-3 shows the calibration curve for the same specimens, see Section 2.3.5.

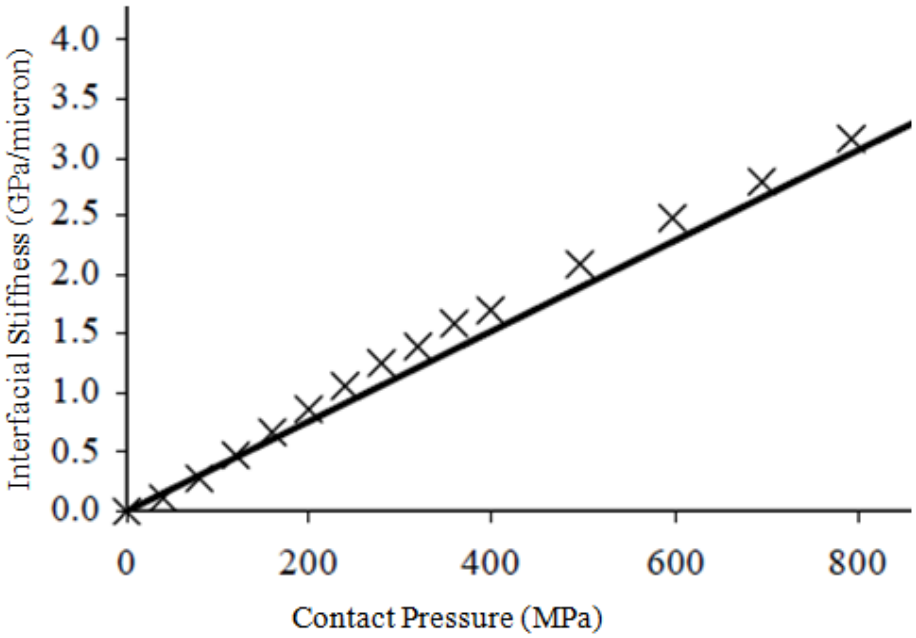

Figure 7-3. The calibration curve relating interfacial stiffness to contact pressure, from Marshall et al. [2005].

7.2.3 Results

The two-dimensional scan results from the new and worn specimens can be seen in Figure 7-4 showing the contact pressure at the wheel/rail interface. The contact pressures were calculated from the reflection coefficient using Equation 2-11, see Section 2.3 for details.

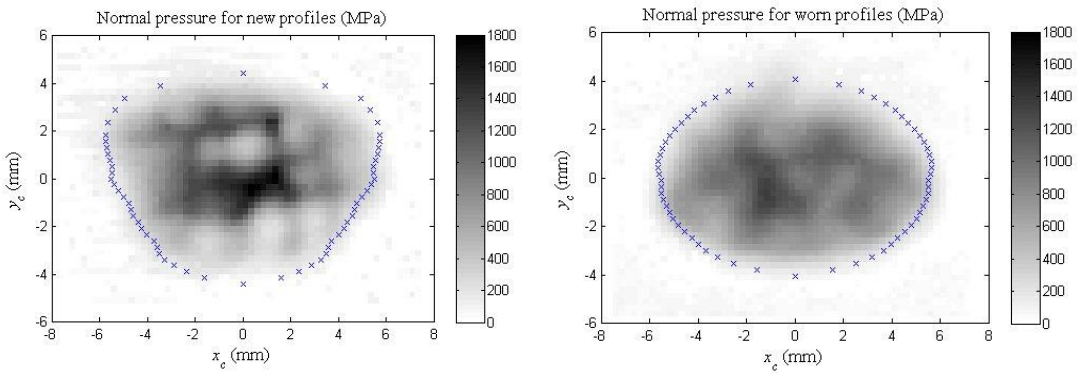

(a) (b)

Figure 7-4. Two dimensional reflection coefficient surface plots of the wheel/rail interface. (a) is with 40 kN applied load and (b) is with 60 kN applied load, from Rovira et al. [2012].

The contact area obtained by the interpenetration method has been overlaid on the contact pressure measurements. More information about this method and the Hertzian contact pressure modelling can be seen in Rovira *et al.* [2012] and Kik [1996].

7.2.4 Discussion of Static Contact Pressure Measurement using Scanning Immersion Transducer

The results obtained using the two dimensional scanning system have resulted in high resolutions contact patch measurements that show good agreement with the Hertzian model. This has been proven a successful method by a number of previous authors as discussed in Section 1.3. This method is confined to the laboratory environment with component sections under static conditions. A dynamic method has been developed by the author to use the technique in real life dynamic applications

7.3 Static Contact Pressure Measurement with an Ultrasonic Array Transducer

An ultrasonic array transducer can provide a high speed 1-dimensional line scan; see Section 3.5 for more details. By mounting an ultrasonic array transducer in the rail, it is possible to have a real-time measurement of the wheel/rail contact as the wheel passes over the sensor. In this investigation, the array transducer was mounted in the rail and the wheel is manually traversed across the rail head to simulate the rolling wheel.

7.3.1 Experimental Set-up

The wheel and rail specimen were cut from full sections and can be seen in Figure 7-5. Transducer placement is important to obtain the optimum signal reflection condition from the interface. It was necessary to remove a section from the wheel or the rail to position the array transducer in such a way that the waveforms reflected off the contact interface. A hole was wire eroded in the rail to house the array transducer. A spring was used to load the array transducer against the top of the rail and a solid rubber couplant was used to prevent the fluid film couplant effects discussed in Section 3.4. The through hole allows the array transducer to be positioned at any point in the rail head to ensure the contact patch is fully captured. The manually switched ultrasonic array system was used for the test, see Section 3.5.1 for more details.

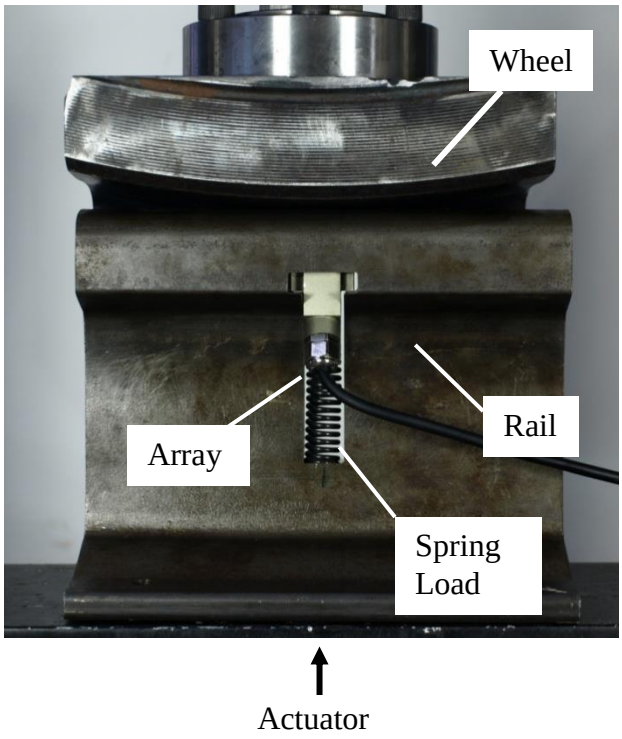

Figure 7-5. The static wheel/rail loading rig with a 5 MHz 64 element ultrasonic array transducer.

A 100 kN electric Mayes compression rig was used to simulate the vertical force. The wheel section was mounted in the upper loading frame and the rail was clamped to the lower test bed during loading. The rail was free to traverse under the rail to simulate the rolling of the wheel.

The design of the hole in the rail is important as any deflection occurring in the rail section will jeopardise the ultrasonic measurements and could potentially damage the array transducer. It was necessary to statically load the wheel section onto the rail without the array transducer present to measure the deflection in the hole. The transducer was removed from the loading rig and replaced with a digital dial gauge mounted on the solid loading frame bed. The wheel section was incrementally loaded up to 80 kN against the rail and the deflection of the hole face measured to ensure the transducer would not be damaged. A photograph of the test set-up can be seen in Figure 7-6. There was no measureable deflection of the rail so it was determined safe to carry out the test with the array transducer in place.

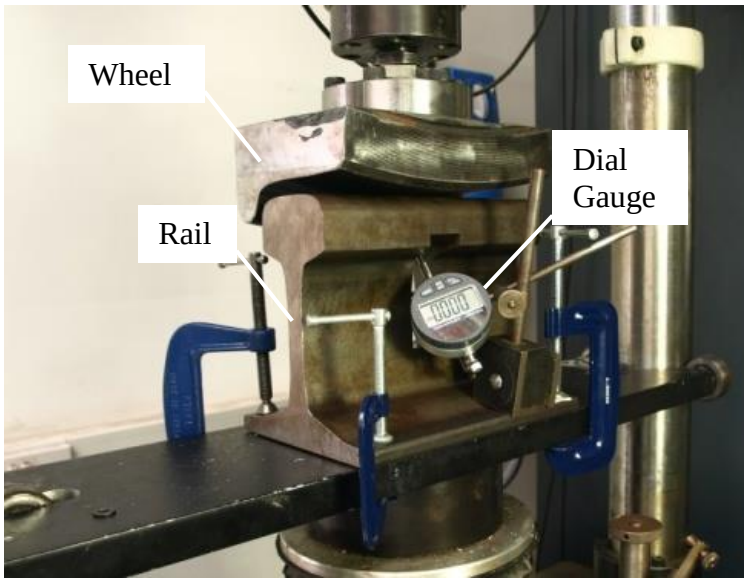

Figure 7-6. The static wheel/rail test set-up with a digital dial guage to measure the displacement of the rail above the hole.

7.3.2 Linear Cross Section Contact Patch Measurement.

The rail was incrementally loaded from 0 to 60 kN in steps of 10 kN. The resultant cross sectional reflection coefficient profiles can be seen in Figure 7-7 below.

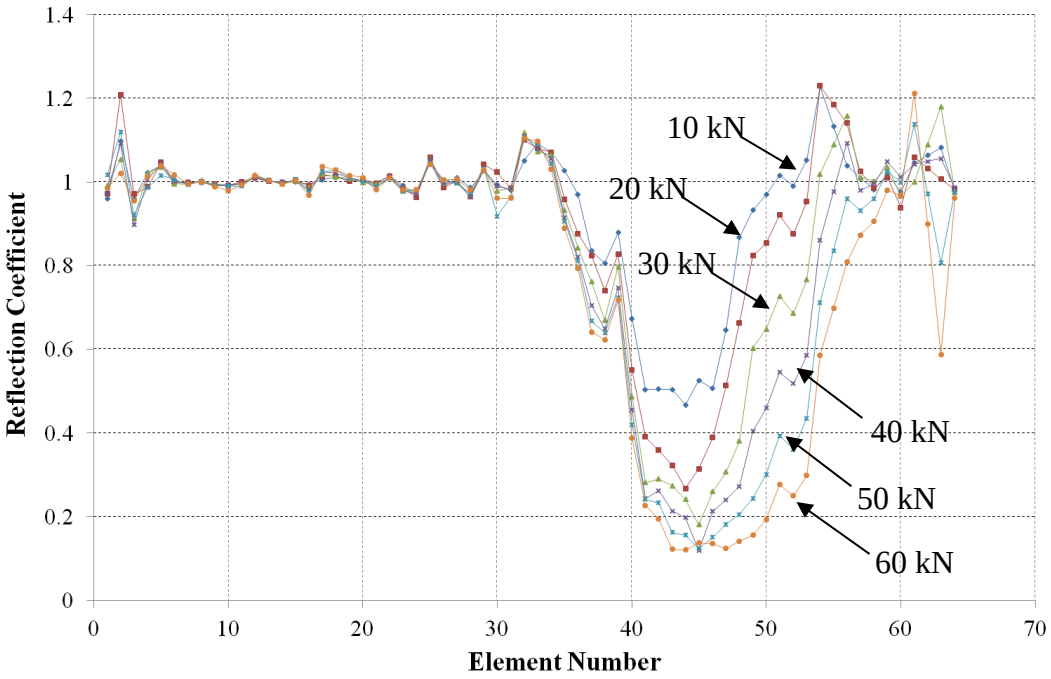

Figure 7-7. The reflection coefficient over the length of the wheel/rail interface.

The interfacial stiffness can be calculated from reflection coefficient using Equation 2-11. Using the relationship between interfacial stiffness and contact pressure discussed in Section 2.3, a cross sectional pressure profile for the wheel/rail contact can be obtained, as shown in Figure 7-8.

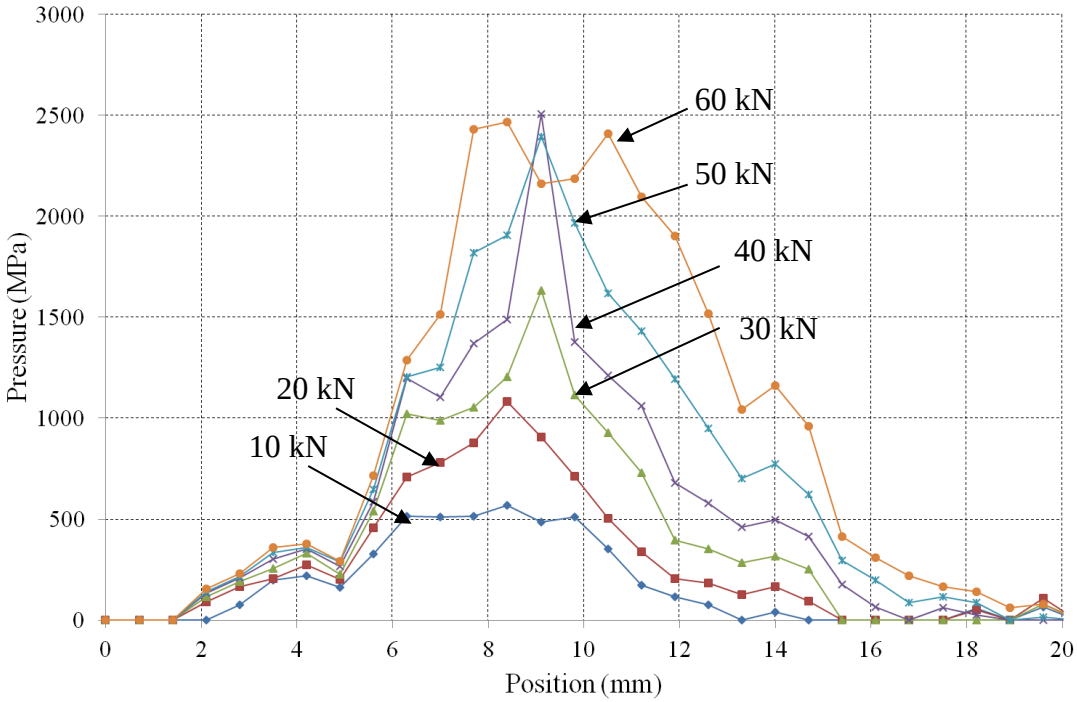

Figure 7-8. Contact pressure plot of the wheel/rail interface for various loads.

7.3.3 Two Dimensional Static Contact Pressure Results

In order to create a two dimensional surface plot, the rail was manually traversed under the fixed wheel at 1 mm steps and re loaded at each step.

Figure 7-9 shows the two dimensional reflection coefficient surface plots at loads of 40 kN shown in (a) and 80 kN shown in (b).

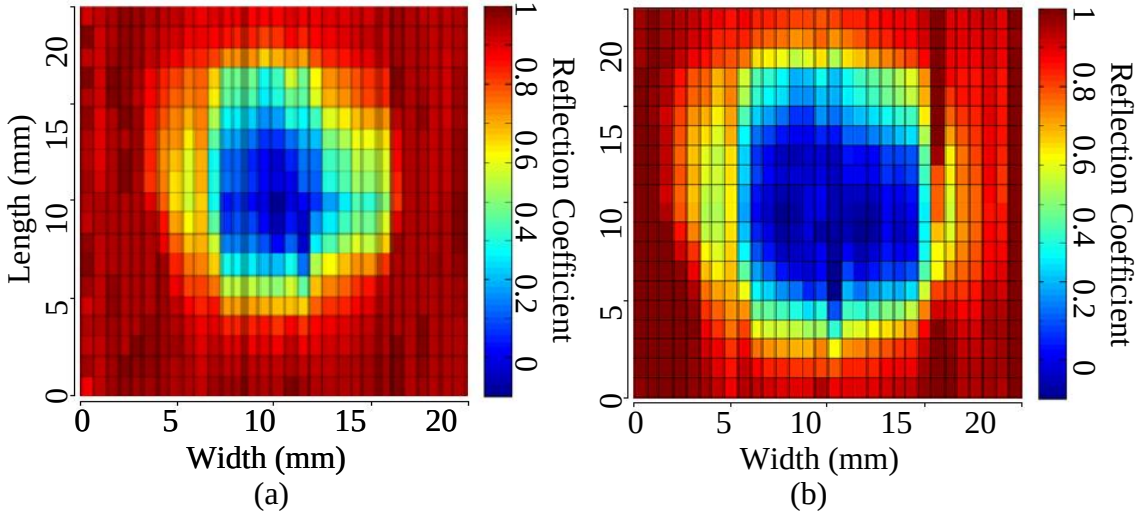

Figure 7-9. Two dimensional reflection coefficient surface plots of the wheel/rail interface at 40 kN shown in (a) and 80 kN shown in (b).

Pressure sensitive film was placed between the contact and the load applied. The results can be seen in Figure 7-10. The measured contact areas from the different methods can be seen in Table 7-1.

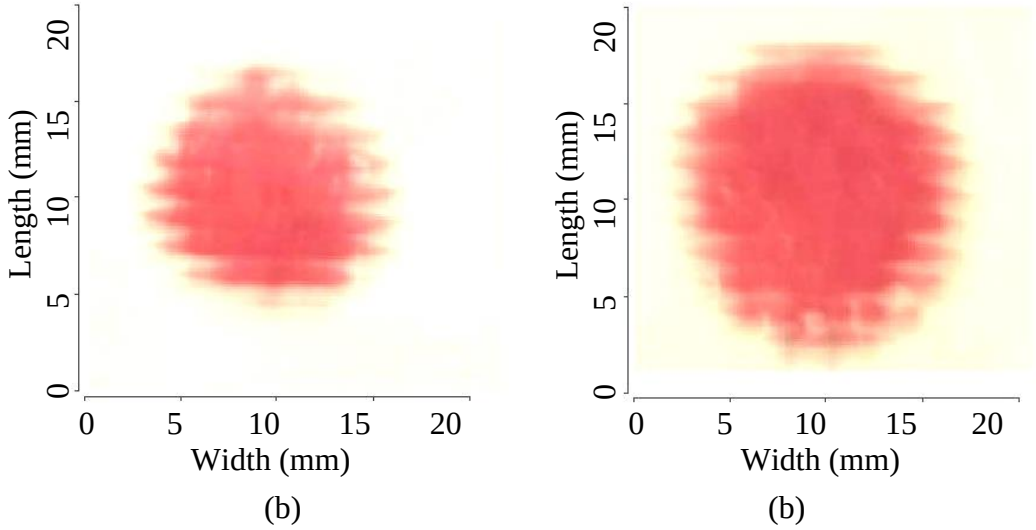

Figure 7-10. The measured contact patch from the pressure sensitive film for an applied load of 40 kN (a) and 80 kN (b).

Contact Geometry Radius (mm)	Loads (kN)	40		80	
		Width	Length	Width	Length
	Ultrasound	5.47	5.98	6.92	7.39
	Pressure Sensitive Film	5.64	6.11	7.01	7.56

Table 7-1. The contact areas from the ultrasonic measurement and the pressure sensitive film.

7.3.4 Discussion of Static Contact Pressure Measurement with an Ultrasonic Array Transducer

This investigation proved that the rail mounted array transducer was a feasible method to measure the wheel/rail contact. It was proven that the hole in the rail did not experience excessive deflection so it was safe to house an array transducer. The resolution of the contact pressure profile was dependent upon the size of the ultrasonic elements, which was fixed at 0.7 mm which is the minimum size a 10 MHz transducer can be made, but also the distance that the rail was moved under the wheel. The ultrasonic contact area measurements were in agreement with the pressure sensitive film. The pressure sensitive film used was not optimised for the pressure range therefore it is not possible to extract pressure values. It is understood that this method of moving the wheel under the rail is not representative of a rolling wheel but is a simplified set-up that only applied normal loads. A rolling wheel on a rail will display a different stress distribution due to the more complex tangential forces acting on the components. The sensors were 7 mm long in the rolling plane, this was accounted for in the contact area measurements by subtracting 6 mm from the centre of the final surface plots to reveal the true contact shape.

7.4 Dynamic Measurement Bench Test

In order to measure a dynamic contact, the author has developed a method to measure various points over a line simultaneously with sufficient resolution to create an image of the wheel passing over the rail. To do this, a number of different ultrasonic elements were used simultaneously. A digital switching system was developed to enable a 64 element ultrasonic array transducer to be used with an 8 channel ultrasonic system as detailed in Section 3.5.2. Due to the large number of transducers, the data analysis also required great care. It is for this reason a bench test was arranged to trial the hardware along with the control and acquisition software.

7.4.1 Experimental Set-up

An initial bench experiment was arranged to test the experimental method. A rolling ball on flat contact was created to measure a simple dynamic rolling contact that is representative of the wheel/rail contact. A 25 mm diameter Nitrile ball was loaded and rolled along an acrylic surface using a bespoke friction measurement test rig shown in Figure 7-11. The lower plate specimen was attached to a worm drive resulting in a linear displacement as the controlled motor was driven.

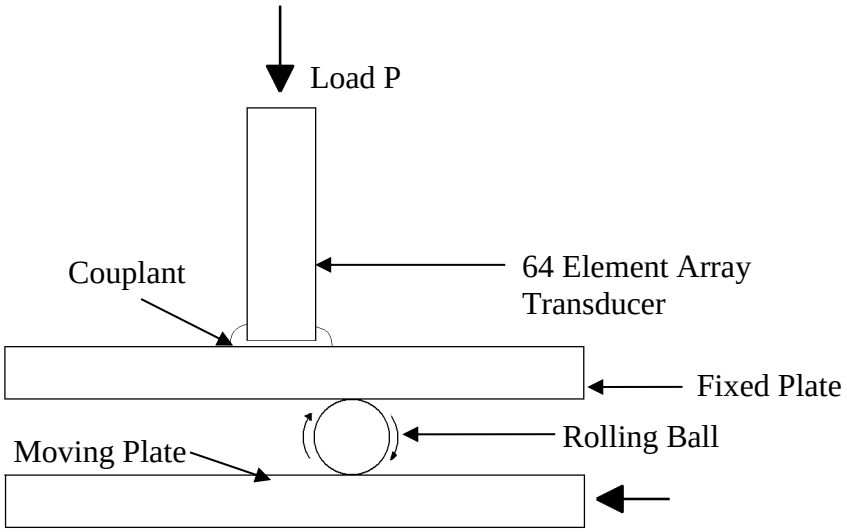

Figure 7-11. A schematic diagram showing the placement of the ultrasonic array transducer and the direction of movement.

All 64 elements of the array transducer were pulsed and the multiplexer was switching at full speed to assess the resolution. A series of tests were undertaken to trial the methodology and establish the limits in switching speed and associated measurement resolution.

7.4.2 Results

Figure 7-12 shows the reflection coefficient surface plots of a 25 mm Nitrile ball rolling between two loaded Perspex plates. Figure 7-12 (a) is the resultant contact plot with an applied load of 0.1 kg and Figure 7-12 (b) was with an applied load of 1 kg. Both tests were conducted with a rolling speed of 0.6 mm/s.

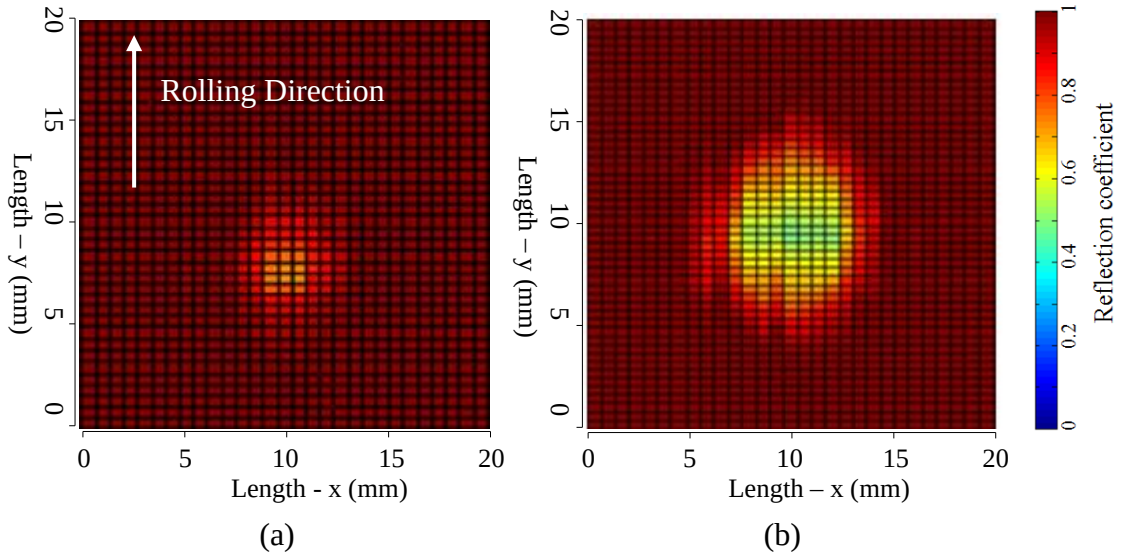

Figure 7-12. Reflection coefficient intensity plot of a Nitrile ball rolling at 0.6 mm/s loaded between two Perspex plates with an applied load of 0.1 kg and 1 kg in figures (a) and (b) respectively.

When no contact occurs, virtually the entire wave is reflected at the solid-air interface, resulting in a reflection coefficient of 1. As the ball passed under the array transducer, part of the energy in the sound wave is transmitted due to the interfacial stiffness. The resultant reflected wave is divided by the reference resulting in a value for reflection coefficient. The resolution of the length measurement in the x-axis was fixed by the size of the elements in the array transducer at 0.7 mm per division. The resolution of the y-axis resolution was dependent on rolling velocity and ultrasonic PRF. If the PRF remained constant and the rolling speed is increased, the resolution in the y axis would decrease proportionately.

The size of the contact patch was validated using a camera mounted in place of the array transducer. The contact patch was evident on the Perspex surface. This can be seen in Figure 7-3.

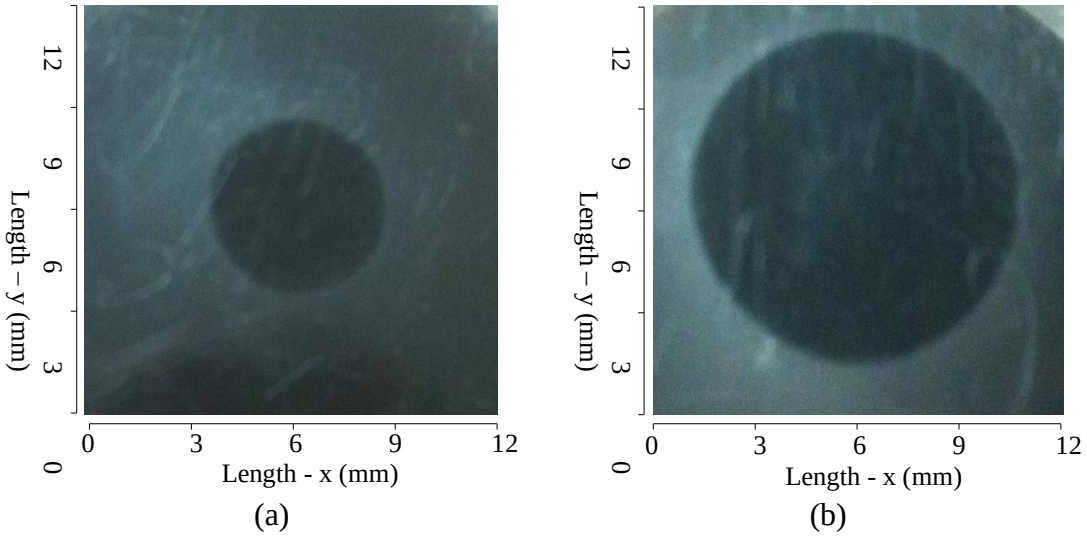

Figure 7-13. A photograph of the contact area between the 25 mm Nitrile ball and an acrylic plate.

Contact Geometry Radius (mm)	Loads (N)	0.981		9.81	
		Width (x)	Length (y)	Width (x)	Length (y)
	Ultrasound	2.45	2.50	4.90	5.24
	Camera	2.57	2.63	4.78	4.92

Table 7-2. The contact areas from the ultrasonic measurement and the camera.

7.4.3 Discussion of Dynamic Measurement Bench Test

The methodology and the bespoke ultrasonic equipment have been proven to function successfully in this simple bench test arrangement. The slower rolling speeds yield far clearer results due to the increased measurement resolution. It was deemed unnecessary to perform a calibration procedure to relate reflection coefficient to contact pressure as the purpose of this investigation was purely to test the equipment.

7.5 Dynamic Measurement of Wheel/Rail Contact

The aim of this section was to obtain dynamic ultrasonic contact patch measurements of a real wheel rolling over a rail with a rail mounted ultrasonic array system.

7.5.1 Experimental Set-up

To simulate the wheel rolling over the rail, a full scale wheel/rail rig was employed. The rig consisted of a rail mounted on a linear translation bed fixed to a hydraulic actuator. The wheel was normally loaded against the rail using a second hydraulic actuator with the ability to apply loads up to 200 kN. The ultrasonic array transducer was mounted in the rail in the same configuration as in Section 7.3. To simulate rolling, the rail was displaced using the actuator and the friction between the two components caused the free wheel to roll over the rail. Figure 7-14 shows three photographs of the rig with three positions of the rail.

Figure 7-14. The wheel/rail arrangement in different stages of displacement.

The wheel has a diameter of 920 mm and has a worn P8 profile. A 1200 mm UIC60A rail section was used. The maximum throw of the rail results in a 1/3 rotation of the wheel. The load was applied and the rail was displaced 200 mm in one direction whilst taking the ultrasonic measurements. The rail was then returned to the original position causing the wheel to rotate in the opposite direction. The array transducer measurement length is 42 mm so the array transducer measurement window did not cover the entire rail head. Through trial and error, the array transducer was positioned in such a way that meant the entire contact patch was captured.

7.5.2 Results

Figure 7-15 shows the 2D contact pressure patch measurements achieved from the ultrasonic array transducer with a rolling speed of 5 mm/s. (a) shows the measurement with an applied load of 40 kN and (b) shows the measurement with an applied load of 80 kN. The sensors were 7 mm long in the rolling plane; this would result in an overestimation of the contact area in the rolling (y) axis. To account for this, the length of the contact patch was reduced by 7 mm to reveal the true contact area.

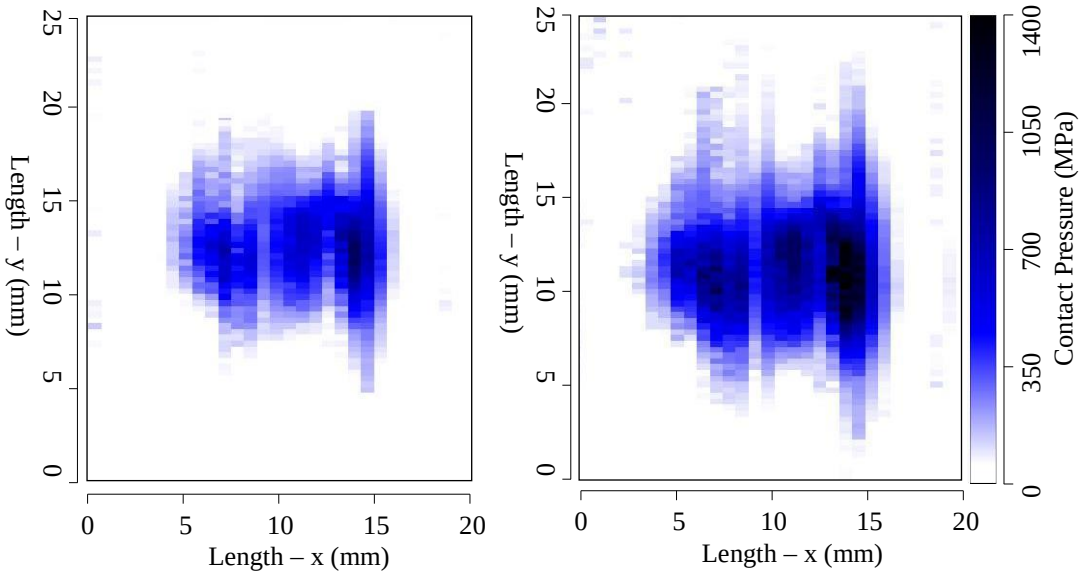

Figure 7-15. Contact patch measurements on a full scale dynamic wheel rail rig using a 10 MHz 64 element ultrasonic array transducer.

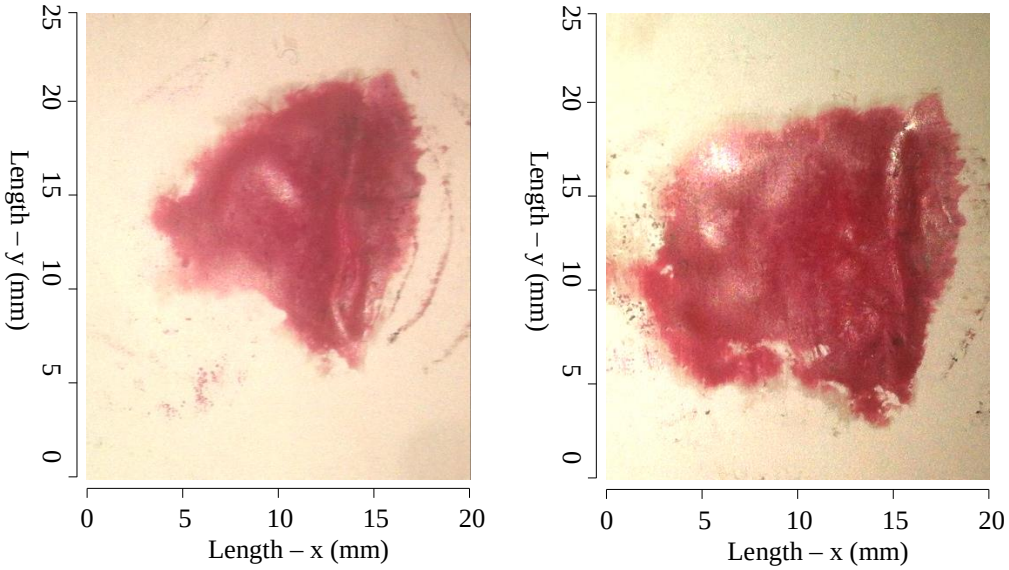

(a) (b)

Figure 7-16. The contact area measurements from the pressure sensitive film with an applied load of 40 kN and 80 kN for (a) and (b) repectively.

To apply this method to measure on the rail network, the ultrasonic pulsing hardware would have to be faster. By using a phased array ultrasonic system, it would be possible to increase measurement speed and resolution, but it would dramatically increase the associated costs and complications in post processing. Figure 7-17 shows the possible number of measurements as the wheel rolls over the rail at various speeds and various pulse repetition frequencies (PRF).

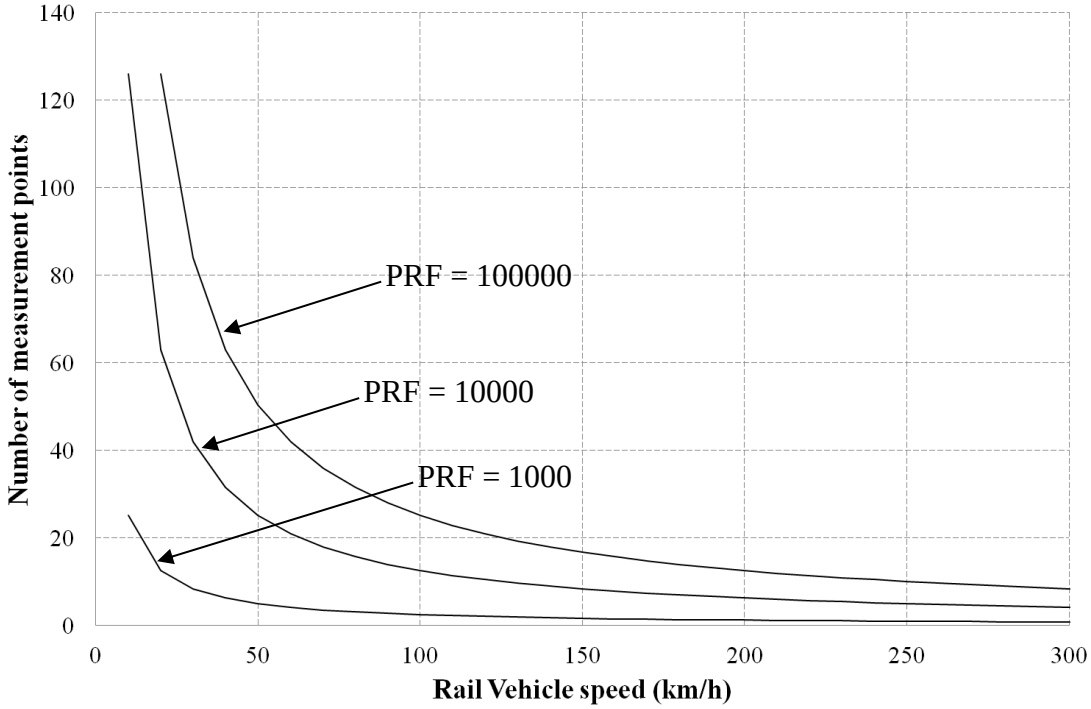

Figure 7-17. A graph showing the number of measuremens as the rail vehicle passes over the array transducer as a function of pulse repatition frequency.

7.6 Discussion of Dynamic Measurement of Wheel/Rail Contact

The introduction to the chapter highlights how important the wheel/rail contact is and how there is a lack of techniques available for the measurement real-time wheel/rail contact distribution. The two dimensional scanning of the static wheel/rail contact showed how the ultrasonic method can be used to measure both contact area and pressure.

The static array transducer measurement proved the ability of the bespoke ultrasonic array system to measure the wheel/rail contact patch. The resolution in the x-axis of the measurement system is a function of element diameter which in this case was fixed at 0.7 mm. The measurement resolution in the y-axis is a function of rolling speed and PRF. This could have been refined, but the resolution was deemed satisfactory for the purposed of this investigation. The resultant contact area measurements were in agreement with the measurements from the pressure sensitive

film. The contact pressure measurements were in agreement with previous measurements of contact pressure. The stiffness values were converted to contact pressure using a previous calibration process involving similar, but not exactly the same specimen which will have resulted in some error.

The dynamic bench test using a Nitrile Ball rolling along a Perspex plate introduced the dynamic measurement. The investigation proved the viability of the bespoke ultrasonic array system. The resolution in the Y-Axis is a function of the ultrasonic pulse repetition frequency and the rolling speed. The limiting factor is the switching speed of the PCi based multiplexer. It is necessary to add a slight delay after switching for the relays to settle, this is known as de-bounce time. The individual channel measurement frequency could have been maximised by reducing the number of active channels, using only those actually measuring the contact.

The measurement on the full scale rig proved successful and dynamic wheel rail measurements where achieved at low rolling speeds. The thickness of the pressure sensitive film will result in a larger contact area being measured. The reason for this is that when there would normally be a thin air gap, the film will still indicate contact due to its inherent thickness. Furthermore, the film has a low friction coefficient which resulted in partial sliding of the wheel as it came into contact with the rail. It was not possible to lock the wheel in position when applying the load like it was in Section 7.3. The pressure sensitive film was not optimised for such high contact pressures so therefore only contact area could be extracted. It was not possible to measure profile information so it is difficult to validate the contact measurement using numerical methods. The results are similar to those measured with the new wheel and rail sample as seen in Sections 7.2 and 7.3.

7.7 Further Work

Cutting a hole in the rail section is not an ideal solution and would not be permitted in a live rail network. It would be possible to mount the sensors at an angle on the outside of the rail head in pitch-catch configuration and achieve a similar result,

although with lower resolution. It would also be possible to mount a series of sensors on the wheel but this would require the use of slip-rings or radio transmission.

One of the main limiting factors of railroad vehicle speeds in the British rail system is the low radius curves. Contact conditions are more severe during curving as the wheel/rail geometry becomes less conformal and contact occurs at the wheel flange. These conditions result in increased slip and resultant wear due to deformation and rolling contact fatigue, [Cannon & Pradier, 1996]. Too much lateral load will result in excessive flange contact and wheel climb that can lead to derailment.

By monitoring the position of the wheel on the rail during railroad vehicle movement, it would be possible to optimise speed with a safety feedback loop system thus preventing too much flange contact. By mounting sensors on the outside of the wheel, it would be possible to create a flange contact detection monitoring system. The transducers would have to be positioned in such a way that the signals could be reflected off the interface at precise locations. To do so might require some removal of wheel material or the use of a wedge to get the correct angle of attack as shown in Figure 7-18. A more in depth feasibility study can be seen in Dwyer-Joyce *et al.* [2012].

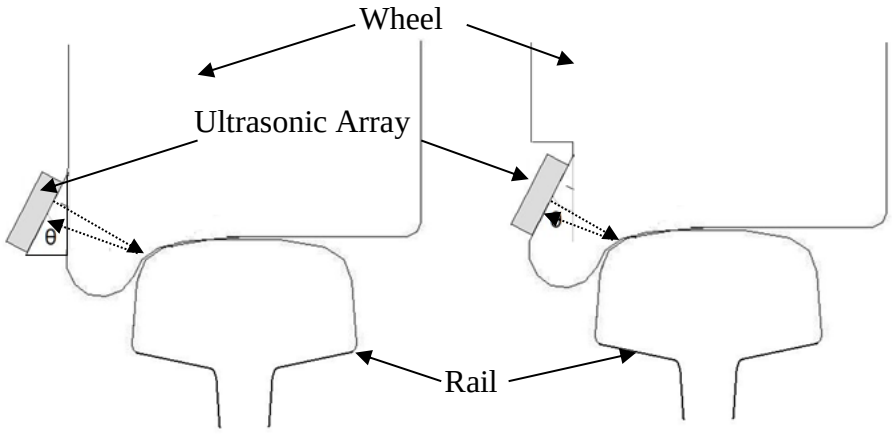

Figure 7-18. A diagram showing the possible options for transducer placement on the wheel for flange detection.

7.8 Conclusions

A method has been developed to characterise rolling contacts using a bespoke low cost ultrasonic array system. This was successfully applied to a simple rolling ball on flat arrangement. A rail mounted sensor was trialled in a static measurement and the results were positive with minimal displacement of the rail head due to the hole.

A full size wheel/rail rig was used to create a loaded wheel/rail interface for inspection. A rail mounted ultrasonic sensor was successfully used to measure the dynamic contact patch evolution. It is also possible to measure the contact pressure distribution with the aid of a calibration procedure. The current system is too slow for full speed rail, but with a commercial phased array system, the measurements would be possible at full speed.

The concept currently requires the removal of a section of the rail which would not be an acceptable solution to use in the field. Possible solutions to this issue have been discussed. Hardware requirements for real-time measurement on the rail network have been determined. A flange detection sensing system has been proposed.

8 DISCUSSION AND CONCLUSIONS

When two machine element components come into contact with one another, they experience complex stress patterns and pressures at the interface. If the components are moving, wear will often result. These are fundamental factors affecting the majority of machine element components. There is a great difficulty in achieving empirical information surrounding dynamic contacting interfaces due to the fact that the contact itself is inaccessible. Traditionally engineers rely on models and modification of the assemblies to install sensors to obtain contact pressure information and disassembling systems to gather wear data. The aim of this work was to investigate the use of ultrasound to measure and monitor contact pressure and wear in real-time. An emphasis was placed on industrial applications and real machine element components as previous ultrasonic contact measurement work has been confined to simple geometries such as ball-on-flat conducted in a laboratory environment. The ultimate aim with all of the techniques was to develop them into tools that can be used, ideally by untrained personnel, to measure and monitor these important factors in real-time in real machine element arrangements to increase understanding of the system for design optimisation and to prevent failure.

The first part of this document explained the fundamental behaviour of components in contact on a micro and macro scale and what happens in a dynamic situation. Methods currently used to measure these factors were discussed and critiqued. The fundamental ultrasonic theory was described as an understanding of this is necessary in order to apply the measurement techniques to new situations with different materials, geometries and arrangements. The options available in terms of measurement hardware were explained to ensure the most appropriate equipment is selected for the specific application.

In order to meet the project aims, new equipment was developed. This thesis has outlined the theory behind the new technology and has described its proper use to ensure future users are able to operate the tools efficiently and recreate them where necessary. A manually switched ultrasonic array system was developed for low

speed or highly repeatable applications, a digitally switched ultrasonic array system was developed for high speed applications and a permanently installable ultrasonic array transducer was developed for long term monitoring applications. The manually switched array system proved to be a successful low cost option for acquiring linear measurements in static applications and could be used for highly repeatable dynamic applications. The low switching speed meant that it was not suitable for single pass contact measurements such as the wheel on rail application. Its development was an important stepping stone paving the way for the digitally switched multiplexing system which was able to switch fast enough to capture these dynamic contacts in a single pass. The system had a maximum global acquisition rate of 750 Hz per channel (if pulsing on 64 elements) which still limits its use for many high speed applications. The permanently installable array transducer was a low cost solution compared to other array transducers on the market. This opened up a host of new measurement opportunities as the device was expendable. By bonding the sensor onto the component, it facilitated linear measurements to be taken over long periods of time and to be used as a monitoring device, rather than just for a single measurement. The device was designed in such a way that meant it could be re-created with any number of elements.

The move away from static tests and laboratory environments has resulted in a requirement for low cost permanently embedded sensors instead of the traditional expensive commercial probes and scanning systems. The author has spent a substantial amount of time developing a wide range of low cost sensors through a process of trial and error investigating numerous piezo-materials, sensor sizes, sensor shapes, cable and termination types, soldering methods, backing and bonding techniques. The different sensor configurations have then been trialled in numerous environments including high temperature, high vibration and general industrial wear and tear. Numerous different ultrasonic hardware arrangements were trialled and developed in order to establish the optimum configuration.

The longer test timescales have required new methods to account for the numerous external factors (including material stresses and strains, electrical noise, electronic hardware and temperature) that affect the measurements. To apply these

measurement techniques for monitoring of dynamic applications, most of the processing algorithms that have been developed in this work have been designed to work in real-time, rather than relying on traditional post processing methods.

The measurements proposed in this thesis have required a number of bespoke hardware solutions to be invented as there are no financially viable commercial solutions available. Furthermore, to interface this hardware with a control and acquisition system has required custom software to be created. Bearing these developments in mind, the time constraints have meant that the author would have preferred to carry out more exhaustive experimental work to explore the techniques in depth and the associated errors of the measurement systems and techniques. Numerous other researchers are initiating in depth studies using the methods developed in this work so this document has been tailored to serve as a manual in the hopes that the foundations laid here will be built upon resulting in fully developed, industry ready measurement systems.

8.1 Wear Measurements

A method of measuring wear in real-time using a time-of-flight based ultrasonic technique was applied to a pin-on-disk tribometer. It was found that the measurement was heavily influenced by temperature and this resulted in inaccurate measurements. A referencing method was devised to automatically account for these temperature effects. The other wear measurement methods used during the test could not be relied on as a tool for validation and error calculations as each method was measuring a different wear attribute. The displacement measurement should have provided the best method for comparison but the experimental set-up was not very reliable and the contact experienced a high level of vibration similar to that in many actual machine element components. Methods in which to apply the technique to machine elements were discussed and a number of alternative referencing methods were introduced.

A further method to measure wear was proposed to virtually eliminate the effects of temperature by placing a reference feature very close to the wearing interface. The wear measurement was then reliant upon the frequency content of the reflected waveforms. This method was trialled in a controlled test in which fixed steps of material were removed using a surface grinder. The technique was then applied to a specific material combination pair in a pin-on-disk tribometer. The measurement algorithm showed great promise in the controlled experiment, but discrepancies were seen in results calculated from different dip numbers when they should have been identical. Some of this error will have been introduced in extracting the frequency index from the frequency domain plot, but it is evident that due to the complex multi-dimensional nature of waveform propagation, this frequency feature method needs further investigation.

8.1.1 Applications

The non-invasive measurement of wear has a wealth of applications spanning across a wide range of industries. Virtually all dry sliding components and failed lubricated contacts are subject to wear and currently there are very few tools available to help manage this process. When machinery has to be stopped and potentially disassembled to carry out the wear measurements, the ultrasonic method would be applicable and will often quickly provide a return on the investment. Furthermore if wear leads to costly failure, the use of the proposed methods as an alarm system would be of great benefit. The fact that the systems are often completely non-invasive and retro-fittable means integrating them into active mechanical systems is a relatively simple process.

Having a constant, real-time wear measurement makes it possible to relate wear to the operating parameters. The following are some example applications for the technology:

- Tribometers
- Engine piston rings and liners
- Engine valve and valve seats
- Mechanical seals
- Journal bearings
- Cams and followers
- Cutting tools
- Bushings and gears
- Conveyor chutes

8.1.2 Limitations

The wear measurement technique is highly dependent on temperature as the both the acoustic velocity and thermal expansion affects the time-of-flight measurements. There are numerous ways to compensate for these effects, but an understanding of what is happening is crucial to select the most appropriate solution. The referencing method assumed a linear thermal gradient which would have introduced some error. Friction causes flash temperatures at the interface in the region of 200 ºC – 250 °C and this heat will propagate throughout the component, see Stackiowack & Batchelor [2005]. By using a more representative thermal gradient, these errors would be reduced.

The component being measured must be able to support a sound wave or the techniques cannot be applied. By using lower frequency transducers, the method can be applied to highly attenuative materials such as cast iron and some polymers. The components may have to be modified in order to position the transducer is such a way that it can generate a signal and sense the reflected signal. Some of the erroneous results from the frequency feature method have shown that further

investigation is needed in order to understand the multi-dimensional effects that subsurface defects have on wave propagation.

8.1.3 Further Work

Equation 4-2 assumes a linear thermal gradient, in reality this is not the case and will introduce some error in the measurement. A more complex model using a more realistic thermal gradient could be introduced. A more robust timing measurement could be introduced to make the measurement less dependent on operator skill, see Section 2.2.1. There is a great deal of work that could be done to investigate the optimum reference feature profile.

8.2 Contact Measurements

The ultrasonic contact pressure measurement technique was applied to a metal-to-metal seal. The seal was based on the design of subsea pipe end-fittings. A number of different ultrasonic sensor types were mounted on the external surface of the simplified component that was positioned in such a way to make the ultrasonic pressure waves reflect off the contacting interface and return to the same sensor. The large end fitting body was forced onto the lower assembly using an axial loading rig which swaged the seal ring. The results from the ultrasonic measurements were in good agreement with the FE predictions and thus provided validation for the model.

The measurement technique was then applied to an actual end fitting assembly modified to hold internal pressure. The aim of this work was to see what effect internal pressure had on the sealing interface. The seal ring was swaged by tightening the bolts before the rig could then be built up to support an internal pressure. The time gap between the measurement of the initial swaging and the pressure test meant that a single reference measurement taken before assembly had to be used throughout the whole test. This required the use of a permanently embedded ultrasonic array transducer and temperature compensation techniques involving a separate channel to be used to account for any environmental changes that could occur. The swaging results obtained were in agreement with the previous experiment, but unfortunately

part of the contact was outside of the measurement window. The sensors detected a change in shape of the pressure profile during internal pressurisation and the results showed the design was not pressure energised. This was as expected from the FE model. The necessary steps to use the technique as a tool for manufacturing quality control have been discussed.

The technique was then applied to analyse the railroad vehicle wheel/rail interface. Initially a two-dimensional scanning system was used to successfully validate a FASTSIM model. A low cost, high channel count ultrasonic array system was then developed in order to measure dynamic contact patch evolution of a rolling wheel on a rail. The array transducer was mounted in the head of a small section or rail, the wheel was manually loaded onto the rail and then traversed across the rail face repeating the loading cycle at 1 mm increments. From this, a contact patch measurement was creating by stacking the linear contact pressure scans up next to one another. The results were in agreement with the measurement using a pressure sensitive film.

The technique was tested with a rolling ball-on-flat contact. The results proved the method successful with this simplified arrangement. A full-scale wheel/rail rig was employed to simulate a railroad vehicle wheel rolling on a rail. The array transducer was again mounted in the rail head and the wheel rolled over the surface. The measurements were in agreement with the statically loaded pressure sensitive film. Modification of the rail in such a way would not be allowed in the active rail network so other routes have been discussed.

8.2.1 Applications

The non-invasive measurement of contact area and pressure has numerous applications across most engineering industries. The main applications are research and condition monitoring. In any application where a high contact pressure is critical, an actual measurement of the interface can confirm and validate calculations and models that would otherwise carry associated risks. With this knowledge, factors of

safety can be significantly reduced saving costs without jeopardising reliability. With a non-invasive empirical measurement technique such as this, engineers are able to design far more complicated components and systems that would not be possible if the design has to rely on calculations and models. The associated factors of safety due to compound errors could make the design unfeasible from cost and size restrictions.

In terms of monitoring contacts, there are a number of applications in which a constant non-invasive measurement of contact pressure would be valuable. In any sealing system where failure would be catastrophic, a constant measurement of the contact pressure could be used to prevent failure by automatically shutting the system down is the pressure drops. With real-time knowledge of the contact area and pressure of critical interfaces, it is possible to push machinery to its limits to maximise productivity without the risk of failure.

8.2.2 Limitations

The position of the sensors is critical to the success of the measurement. To be able to reflect the sound wave off the interface at the exact point of interest, care must be taken when positioning the transducer. This might require modification of the component making it no-longer a non-invasive technique. Some materials cannot support a pressure wave (highly attenuative etc.), in which case it would not be possible to use the ultrasonic method.

To obtain reliable empirical contact pressure measurements, a calibration procedure is required. This procedure requires the use of the same materials in question with the same surface finish. When loading finished components for the first time, the surfaces experience plastic deformation. This fundamentally changes the structure of the interface and therefore the calibration must replicate this for the relationship between contact pressure and interfacial stiffness for it to be valid. This has been investigated by Dwyer-Joyce *et al.* [2001] who identified a shakedown effect in subsequent loading cycles. Other errors can be introduced if the contact becomes contaminated. This work in this thesis has concentrated on dry solid-solid contact. When a lubricant is introduced into the interface, it results in a mixture of two

stiffness regimes; solid/solid contact and solid/liquid/solid contact. This means that the reflection coefficient is a mixture of both regimes and therefore it is not possible to simply perform a calibration procedure to relate interfacial stiffness to contact pressure.

It is imperative that the measurement window is smaller than the contact patch being measured. If the measurement window contains partial contact, the result is often an increase in the reflected amplitude, resulting in a reflection coefficient greater than one. Previous work has not been able to explain this phenomenon so the results when this happens have thus far been ignored as they result in a negative stiffness.

8.2.3 Further Work

The author was not able to investigate the sensitivity of the measurement to the changes in surface finish from the sliding. In doing so, it would be possible to accurately calculate the errors associated and therefore the accuracy of the technique. Investigations using smaller active elements would yield higher accuracy results, as would the use of equipment with a higher pulse repetition frequency for rolling contacts. For the railroad vehicle wheel/rail contact measurement, it would be interesting to explore the options suggested to measure contact pressure, position and shape without any modifications of the rail. Further work investigating the mixture of solid/solid and solid/liquid stiffness regimes could enable the method to be used in a wider range of applications. Further work investigating an increase in reflection coefficient above 1 would be of great interest.

During the author's research, a number of other experimental investigations were conducted that were not presented in this thesis. These included fluid film, wear and contact pressure measurements on a block-on-ring set-up, measurements of stiffness measurements in a fretting contact, see Mulvihill *et al.* [2013], and numerous investigations into the contact pressure of different bolted joint contacts under dynamic conditions, see Marshall *et al.* [2012].

8.3 Conclusions

The following conclusions have been drawn from this body of work.

- Studies in recent years have shown the capability of ultrasonic reflectometry in the characterisation of inaccessible interfacial phenomena such as contact pressures, contact areas and lubricant film thickness measurements.

- For simple geometries, piezoelectric elements can be used to measure such phenomena with confidence that the measurement area is the same size as the element.

- For complex geometries, the time-domain response must be studied to ensure the correct echo is being processed.

- Care must be taken when selecting ultrasonic apparatus to ensure the minimum requirements are satisfied.

- Coupling between the ultrasonic transducer is an important parameter. Bonding the transducer in place allows for a single reference measurement to be valid over a long period of time making it a suitable option for condition monitoring.

- Using ultrasonic array systems can result in line scans that traditionally would have required an immersion system.

- It is possible to use industrial array transducers with low channel count ultrasonic systems by introducing a multiplexer.

- Low cost permanently installed array systems allow linear measurements to be taken over long periods of time making it a suitable option for condition monitoring.

- Consideration must be given to factors that may influence the reference measurement including temperature, hardware, electrical noise and material stress.

- The ultrasonic time-of-flight method of thickness gauging is very sensitive to temperature. It is possible to use this method to measure a change in thickness and thus wear in real-time but referencing must take place to account for temperature effects.

- There are numerous industrial applications for a non-invasive wear measurement system.

- The resonant dip method shows potential for the measurement of wear by placing a frequency feature near the running surface of the component. Further work needs to be done to understand the wave propagation as it reaches the frequency feature to develop optimal designs that result in clear dips in the frequency response.

- A permanently embedded ultrasonic array is capable of measuring and monitoring the contact pressure profile of a metal to metal seal during swaging and during the pressurising of the internal sealed system.

- An ultrasonic immersion transducer and scanning system is capable of measuring the 2D contact pressure distribution of a contact. This was applied to a modified rail vehicle wheel and rail section.

- A commercial ultrasonic array is capable of measuring the contact pressure profile of a rolling contact. This was applied to a simplified rolling contact and the interface between a rail vehicle wheel and rail.

9 PUBLICATIONS ARISING FROM THIS WORK

9.1 Conference Publications

Brunskill, H, B. Zhou, L. Lewis, R. Marshall, M, B. Dwyer-Joyce, R. S. (2012) *Dynamic Characterisation of the Wheel/Rail Contact using Ultrasonic Reflectometry***.** Proceedings of the 9th International Conference on Contact Mechanics and Wear of Rail/Wheel Systems, (CM2012), Chengdu, China, August 27-30, 2012

Brunskill, H. Lewis, R., Dwyer-Joyce, R, S. (2012). *The Dynamic Characterisation Machine Element Components*. Proceedings of the 9th Annual Tribo-Uk, 14th-15th March2012, Southampton, UK

Brunskill, H., Harper, P. Lewis, R. (2013). *The Real-Time measurement of wear using Ultrasonic Reflectometry.* Proceedings of the World Tribology Congress 2013, Torino, Italy, September 8 – 13, 2013

Fernando, U., Nott, P., Graham, G., Roberts, A., Sheldrake, T. Brunskill, H. Zhou, L.& Lewis, R. (2012). *Experimental Evaluation of the Metal-to-Metal Seal Design for High-Pressure Flexible Pipes*, Proceedings of the Offshore Technology Conference, 30 April-3 May 2012, Houston, Texas, USA

Nowell, D., Mulvihill, D, M., Brunskill, H. Dwyer-Joyce, R, S. (2013). M*easurement and Modelling of Interface Stiffness in Frictional Contacts***.** Proceedings of the World Tribology Congress 2013, Torino, Italy, September 8 – 13, 2013

M.B. Marshall, R. Lewis, L. Zhou, H.P. Brunskill. (2014) *Dynamic measurement of railroad vehicle wheel/rail contact pressure*. Proceedings of Railways 2014, Corisca, France, April 8-11, 2014.

9.2 Journal Publications

Dwyer-Joyce, R, S.,Yao, C., Lewis, R., Brunskill, H. (2013). *An ultrasonic sensor for monitoring wheel flange/rail gauge corner contact.* Proceedings of the Institution of Mechanical Engineers, Part F: Journal of Rail and Rapid Transit March vol. 227 no. 2 188-195

Marshall, M, B. Lewis, R. Howard, T., Brunskill, H. (2012). *Ultrasonic measurement of self-loosening in bolted joints*. Proceedings of the Institution of Mechanical Engineers, Part C: Journal of Mechanical Engineering Science July 2012 vol. 226 no. 7 1869

Mulvihill, D, M., Brunskill, H., Kartal, M, E. Dwyer-Joyce, R, S. & Nowell, D. (2013) *A Comparison of Contact Stiffness Measurements Obtained by the Digital Image Correlation and Ultrasound Techniques.* Experimental Mechanics, February 2013, Springer us, 0014-4851

Roda, A, R. Marshall, M, B., Brunskill, H, B. & Lewis, R. (2011). *Experimental and numerical modelling of wheel–rail contact and wear*. Wear, Volume 271, issues 5-6, 22 June 2011, Pages 911–924

10 REFERENCES

ASTM G77 – 05. (2010). *Standard Test Method for Ranking Resistance of Materials to Sliding Wear Using Block-on-Ring Wear Test.* West Conshohocken, PA, USA: ASTM International.

Bhushan, B., Niklas, A., Hogmark, S., & Jacobson, S. (2000). *Modern Tribology Handbook.* Florida: CRC Press.

Birring, A, S., Kwun, H. (1989) *Ultrasonic Measurement of Wear*, Tribology International, Volume 22, Issue 1, February Pages 33–37

Blitz, J. (1963) *Fundamentals of Ultrasonics.* London, England: Butterworths.

Cannon, D, F., & Pradier, H. (1996) *Rail Rolling Contact Fatigue - Research by the European Rail Research Institute.* Wear, Vol. 191, ppl-13.

Cartz, L., (1995). *Nondestructive Testing.* Russell Township, OH, USA: ASM International.

Chang, W, R., Etsion, I., & Bogy, D, B. (1987). *An elastic–plastic model for the contact of rough surfaces*, ASME J. Tribol. 109 (2) 257– 263

Chapman, W, A, J. (1964). *Workshop Technology*, Part 1, London, England, Edward Arnold.

Chiang, C., Graham, A, B., Messana, M, W., Provine, J., Buchman, D, T, O'Brien, G, J., Kenny, T, W. (2011). *Capacitive absolute pressure sensor with independent electrode and membrane sizes for improved fractional capacitance change, Solid-State Sensors, Actuators and Microsystems Conference.* Transducers, 16th Internationale, 5-9 June 2011, 894 - 897

David, J., & Cheeke, N. (2002). *Fundamentals and Applications of Ultrasonic Waves.* Florida, UA: CRC press

Degarmo, E, P., Black, J, T., & Kohser, R, A. (2011). *DeGarmo's Materials and Processes in Manufacturing*. Hoboken, NJ, USA: John Wiley & Sons.

Drinkwater, B, W., Dwyer-Joyce, R, S., & Harper, P. (XXXX). *On-line measurement of lubricant film thickness using ultrasonic reflection coefficients.* CP700, Review of Quantitative Nondestructive Evaluation Vol. 23, ed. by D. O. Thompson and D. E. Chimenti American Institute of Physics P.984 - 991

Dwyer-Joyce, R. S., Drinkwater, B. W., and Quinn, A.M., (2001), *The Use of Ultrasound in the Investigation of Rough Surface Interfaces,* ASME Journal of Tribology, Vol. 123, pp. 8-16. (ISSN 0742-4787)

Dwyer-Joycea, R, S., Drinkwater, B, W., & Donohoea, C, J. (2002) *The Measurement of Lubricant Film Thickness using Ultrasound*, Proc. R. Soc. Lond Vol. 459 no. 2032 957-976

Dwyer-Joyce, R.S., Drinkwater, B.W., & Donohoe, C.J., (2003). "The Measurement of Lubricant--Film Thickness Using Ultrasound", Proceedings of the Royal Society of London, Series A: Mathematical, Physical and Engineering Sciences, Vol.459 (2032), pp 957-976.

Dwyer-Joyce, R.S., Harper, P., & Drinkwater, B.W. (2004). *A method for the measurement of hydrodynamic oil films using ultrasonic reflection.* Tribology Letters, 17(2), 337-348.

Dwyer- Joyce, R, S. (2005). *Application of NDT in Tribology*, J04304 # IMechE Proc. IMechE Vol. 219 Part J: J. Engineering Tribology

Dwyer-Joyce, R, S. (2011). Ultrasonic Measurement for Film Thickness and Solid Contact in Elastohydrodynamic Lubrication. Journal of Tribology, 133 (3). 031501.

Dwyer-Joyce, R, S., Yao, C., Lewis, R., & Brunskill, H. (2012). *An ultrasonic sensor for monitoring wheel flange/rail gauge corner contact*. Proceedings of the Institution of Mechanical Engineers, Part F: Journal of Rail and Rapid Transit March 2013vol. 227 no. 2 188-195

Electric Power Research Institute. (1995) *Bolted Joint Maintenance & Application Guide.* Rockville, MD, USA: NMAC

Etsion, I., & Bogy, D, B. (1987). *An elastic–plastic model for the contact of rough surfaces*, ASME J. Tribol. 109 (2) 257– 263

Fernando, U, S., Nott, P., Graham, G., Roberts, A, E., Sheldrake, T., Brunskill, H., Zhou, L., Lewis, R. (2012). *Experimental Evaluation of the Metal-to-Metal Seal Design for High Pressure Flexible Pipes*. Proceedings of OTC 2012, Houston, Texas, USA, 30 April–3 May 2012.

Gallego-Juarez, J, A. (1989). *Piezoelectric ceramics and ultrasonic transducers. J. Phys. E: Sci. Instrum. 22 (1989) 804-816.*

Harper, P. (2008). *Measurement of film thickness in lubricated components using ultrasonic reflection, University of Sheffield*. (PhD thesis, University of Sheffield, Sheffield, United Kingdom).

Hetènyi, M., & Mc Donald, J, P, H. (1958) .*Contact stresses under combined pressure and twist*. J . Appl. Mechanics, September 1958, 396 - 401.

Hodgson, K. (2002). The Use of Ultrasound to Invesitatio Engineering Contacts, University of Sheffield. (PhD thesis, University of Sheffield, Sheffield, United Kingdom).

Hutchings, I, M. (1992). *Tribology — Friction and Wear of Engineering Materials*. Edward Arnold, London.

Hyo-Sok Ahn, H., & Kim, D. (2001) *In situ evaluation of wear surface by ultrasound.* Wear. Vol. 251, 1193–1201. 0043-1648/01

Imaginant inc. (2011) *JSR DPR 500 Dual pulser receiver operator manual*. Pittsford, NY, USA: Imaginant inc.

Jackson, R, L., & Green, I. (2005). *A finite element study of elasto-plastic hemispherical contact*, ASME J. Tribol. 127 (2) 343–354.

Johnson, J, B., & Marston. (1894). *A. Frictions rollers discussion on paper.* No. 722. Trans. of ASCE, XXXI I , 271-277.

Kalker, J. (1982). *Fast Algorithm for the Simplified Theory of Rolling Contact*. Vehicle System Dynamics, V 01. 11, pp 1-13.

Kasolang, S. (2007). *An ultrasonic Investigation of Various Aspects of Hydrodynamic Lubrication in a Journal Bearing, University of Sheffield*. (PhD thesis, University of Sheffield, Sheffield, United Kingdom).

Kažys R. (1996). *Delay time estimation using the Hilbert transform.* Matavimai. 1996. Vol.3. P.42-46.

Kendall, K., & Tabor, D. (1971). *An ultrasonic study of the area of contact between stationary and sliding surfaces.* Proceedings of the Royal Society, Vol. 323.

Kik, W., Piotrowski, J. (1996). *A fast, approximate method to calculate normal load at contact between wheel and rail and creep forces during rolling. Proceedins* of the Second Mini Conference on Contact Mechanics and Wear of Wheel/Rail System, Ed. Zabory, TU Budapest (1996).

Kobayashi, M. Jen, C-K,. Moisan, J-F., Mrad, N., Nguyen, S, B. (2007). I*ntegrated ultrasonic transducers made by the sol–gel spray technique for structural health monitoring. Smart Mater.* Struct. 16 (2007) 317–322 doi:10.1088/0964-1726/16/2/009

Kräutkramer, J., & Kräutkramer, H. (1969). *The ultrasonic testing of materials.* Berlin, Germany: Springer-Verlag.

Makoto, I., Takikawa, M., & Ying JIN. (2001). *Gauge Face Wear Caused with Vehicle/Track Interaction.* Railway Technical Research Institute, 2-8-38 Hikari-cho, Kokubunji-shi, Tokyo 185-8540, Japan, WCRR2001

Mang, T., Bobzin, K., & Bartels, T. (2010). *Tribological Materials, in industrial Tribology: Tribosystems, Friction, Wear and Surface Engineering, Lubrication.* Weinheim, Germany: Wiley-VCH Verlag GmbH & Co.

Marshall., M, B., Lewis, R., Drinkwater, B, W., & Dwyer-Joyce, R, S. (2004). *An ultrasonic approach for contact stress mapping in machine joints and concentrated contacts.* S05603 # IMechE J. Strain Analysis Vol. 39 No. 4

Marshall, M, B. (2005). *An Ultrasonic Investigation of Real Engineering Contacts, University of Sheffield.* (PhD thesis, University of Sheffield, Sheffield, United Kingdom).

Marshall, M, B., Lewis, R., Dwyer-Joyce, R, S., Olofsson, O., & Björklund, S. (2005). *Measuring Wheel/Rail Contact Stresses using Ultrasound.* - Paper from 14th International Wheelset Congress, 17-21 October, Orlando, USA.

Marshall, M, B., Lewis, R., Dwyer-Joyce, R, S., Olofsson., & Björklund, S. (2006). *Experimental Characterization of Wheel-Rail Contact Patch Evolution*. Journal of Tribology, 2006 by ASME JULY 2006, Vol. 128 / 493

Marshall, M, B., Zainal, I., & Lewis, R. (2010). *Influence of the Interfacial Pressure Distribution on Loosening of Bolted Joints.* J. Strain, 734, doi: 10.1111/j.1475-1305.2010.00734.x

Mason, W, P. & Thurston, R, N. (1976) *Physical Acoustics* (XII). Waltham, MA, USA: Acedemic Press Inc.

Mills, R., Avan, E, Y., & Dwyer-Joyce, R, S. (2013). *Measuring lubricant films at the piston-cylinder contact: An overview of current technologies with focus on ultrasound*. SAE Technical Papers, 2.

Mukesh, A, B., Dhananjay, V., Bhatt, Kishore N Mistry, N. (2013). *Measurement of Oil Film Thickness between Piston Ring and Liner Using Strain Gauge*., Industrial Lubrication and Tribology, Vol. 65 Iss: 5

Namas, T. F., & Dogruel, M. (2008). *A feasible and accurate technique for determining the time-of-flight in ultrasonic distance measurements.* ELMAR, 50th International Symposium. Page(s): 337 - 340

NDT Resource Centre. (2012), *Radiated Fields of Ultrasonic Transducers.* Retrieved March 2012 from http://www.ndt-ed.org/EducationResources/CommunityCollege/Ultrasonics/EquipmentTrans/radiatedfields.htm

NDT Resource Centre. (2012). *PiezoTransducers.* Retrieved July 2012 from http://www.ndt-ed.org/EducationResources/CommunityCollege/Ultrasonics/EquipmentTrans/piezotransducers.htm

Novelline, R., (1997). *Squire's Fundamentals of Radiology* (5th ed.). Cambride, MA, USA: Harvard University Press.

Olympus NDT Inc. (2006). *Ultrasonic Transducers Technical Notes*. Waltham, MA, USA: Olympus NDT Inc

Pau, M., Aymerich., & F., Ginesu, F. (2001). *Measurements of nominal contact area in metallic surfaces: a comparison between an ultrasonic method and a pressure sensitive film*. Wear, Vol. 249, pp. 533-535.

Polycarpou, A., & Etsion, I. (1999). *Analytical approximations in modeling contacting rough surfaces,* ASME J. Tribol. 121 (2) 234–239.

Poole, W. (1987). *The Measurement of Contact Area between Opaque Objects under Static and Dynamic Rolling Conditions*. Proceedings of Contact Mechanics and Wear of the Wheel/rail System, University of Rhode Island, Waterlooville Press, pp59-72.

Queiros R., Girao, P.S., Cruz Serra, A. (2006). *Cross-correlation and sine-fitting techniques for high resolution ultrasonic ranging.* IMTC Instrumentation and Measurement Technology Conference. Sorento. P. 552-556.

Railway Technical Web Page (2012). *Railway Statistics for Britain.* Retrieved June 2012 from http://www.railway-technical.com/statistics.shtml

Reddyhoff, T., Dwyer-Joyce, R, S., & Drinkwater, B, W. (2004).*Operating Limits for Acoustic Measurement of Rolling Bearing Oil Film Thickness*. Tribology Transactions, 47:3, 366 – 375, 10.1080/05698190490455410

Reddyhoff, T., Kasolang, S., Dwyer-Joyce, R, S., & Drinkwater, B, W. (2005). *The phase shift of an ultrasonic pulse at an oil layer and determination of film thickness.* Proc. IMechE Vol. 219 Part J: J. Engineering Tribology. 10.1243/135065005X34044

Reddyhoff, T. (2006). *Ultrasonic Measurement Techniques for Lubricant Films, University of Sheffield*. (PhD thesis, University of Sheffield, Sheffield, United Kingdom).

Rose, J, L. (2004). *Ultrasonic waves in solid media*. Cambridge, England: Cambridge University Press.

Rovira, A., Roda, A., Marshall, M, B., Brunskill, H., & Lewis, R. (2012) *Experimental and numerical modelling of wheel-rail contact and wear.* Wear, Volume 271, Issues 5–6, 22 June 2011, Pages 911–924

Stachowiak, G, W., Batchelor, A, W. (2005). *Engineering Tribology* (3rd Revised edition). Oxford, England: Butterworth-Heinemann Ltd.

Stancu-Niederkorn, S., Engel, U., & Geiger, M., (1993), A New Method for Investigating the Relation Between Real Contact Area and Friction in Bulk Metal Forming Processes, Wear, 43, 381–386.

Silk, M, G. (1984). *Ultrasonic Transducers for non-destructive Testing*. Bristol, England: Adam Hilger Ltd.

Svilainis, L., Dumbrava, V. (2008). *Analysis of the interpolation techniques for time-of-flight estimation.* ISSN 1392-2114 Ultragarsas (Ultrasound), Vol. 63, No. 4.

Tattersall, A, G. (1973). *The ultrasonic pulse-echo technique as applied to adhesion testing.* J. Phys. D: Appl. Phys. ***6*** *819 doi:10.1088/0022-3727/6/7/305*
Timoshenko, S., & J, N, Goodier. (1951). *Theory of Elasticity*. New York, USA: McGraw-Hill.

Thompson, D, O., & Chimenti, D, E. (1995) *Review of Progress in Quantitative Nondestructive Evaluation*. (Vol. 14). New York, USA: Plenum Press.

Toupin, R, A., & Bernstein, B. (1961). *Sound Waves in Deformed Perfectly Elastic Materials. Acoustoelastic Effect*. J. Acoust. Soc. Am. **33**, 216 (1961);

Tverdokhlebov, A. (1983). *On the acoustoelastic effect.* J. Acoust. Soc. Am. 73, 2006.

Vigoureux, P., & Booth, C, F. (1950a) *Quartz Vibrations and their applications*, London, England: H.M.S.O.

Vigoureux, P. (1950b). *Ultrasonics.* London, England: Chapman and Hall ltd.

Zhang, J., Drinkwater, B, W., Dwyer-Joyce, R, S. (2005). *Calibration of the ultrasonic lubricant-film thickness measurement technique.* Measurement Science and Technology, Vol 16, Issue 9, ISSN 0957-0233, pg 1784